

System Design & Demonstrator of a SPU Power Generation Subsystem for SDR Operations of Space Tug in LEO



Group Members

ABDULLAH ZAHID 210341
SAJAL SAEED 210340

BEEP ELECTRICAL (2021-2025)

Project Supervisor

PROF. DR. ALI SAROSH

Designation of Supervisor

Co-supervisor

PROF. DR. AKRAM RASHID

Designation of Supervisor

**DEPARTMENT OF ELECTRICAL ENGINEERING
FACULTY OF ENGINEERING
AIR UNIVERSITY, ISLAMABAD**

System Design & Demonstrator of a SPU Power Generation Subsystem for SDR Operations of Space Tug in LEO

Final Year Project

(SESSION 2021-2025)



DEPARTMENT OF ELECTRICAL ENGINEERING

CERTIFICATE/APPROVAL SHEET

Department of Electrical Engineering

It is hereby certified that Abdullah Zahid (210341), Sajal Saeed(210340)
have successfully completed their FYP.

Prof Dr. Ali Sarosh

Associate Professor

Air University

Supervisor

Prof Dr. Akram Rashid

Professor

Air University

Co-Supervisor

Dr. Ashique Hussan

Air University

Head of Department, Department of Electrical and Computer Engineering

Acknowledgement

All praise is due to Allah, the Almighty, the Sustainer and Guardian of the entire universe, who has granted knowledge and wisdom to all of humanity. Countless blessings be upon the noble figure of Hazrat Muhammad (peace be upon him), along with peace and mercy upon his esteemed companions, family members, and true followers until the Day of Judgment. We express our heartfelt gratitude to our esteemed Head of Department, Dr. Ashique Hussan, for his assistance in addressing administrative matters. Our profound respect and appreciation go to our inspirational supervisor, Prof. Dr. Ali Sarosh, whose unwavering support, insightful guidance, and valuable suggestions have been instrumental in the completion of this research work. His relentless dedication to instilling a strong work ethic will serve as a guiding light throughout our lives. We also wish to take this opportunity to extend our deepest thanks to our co-supervisor, Prof. Akram Rashid. We are at a loss for words to express our gratitude for the sacrifices, prayers, and steadfast support from our loving parents and siblings. Their presence and moral encouragement have continually fortified our resolve. Our sincere appreciation goes out to all our teachers for their generous support. We are particularly grateful to our respected seniors, Engr. Muhammad Zubair, Engr. Hassan Yousaf and Engr. Hasan Anwar Hussain, for their invaluable guidance and advice throughout the duration of this project. Lastly, we thank our colleagues for their constant support during this endeavor.

Abstract

The space sector faces significant challenges from orbital debris, which includes defunct satellites and rocket bodies. As of March 2023, the Space Surveillance Network (SSN) has tracked approximately 33,680 pieces of space debris. Estimates suggest there are around 1 million pieces between 1 and 10 cm in size, and about 130 million fragments smaller than 1 cm. This escalating issue underscores the necessity for Active Debris Removal (ADR) missions. Various methodologies are under evaluation, including Solar Sails, Drag Augmentation Devices, Space Balloons, and both ground-based and space-based Laser Orbital Debris Removal techniques. Among these, the Space Tug system is highlighted for its potential to effectively eliminate debris from Low Earth Orbit. Research efforts are currently focused on developing a robotic prototype for the Space Tug, aimed at executing minimal energy missions for ADR. Two mission strategies are being explored: Home Capture and Nodal Capture, both supported by a dedicated spacecraft bus designed to operate in a Sun-synchronous orbit. This orbit allows the satellite to serve dual purposes, functioning as an Earth observation satellite while awaiting its debris removal mission. The design incorporates a LIDAR-based robotic arm for debris capture, alongside comprehensive static, thermal, and modal analyses to ensure the mechanical bus can withstand launch conditions and survive in space. In addition to these technologies, advancements in Software Defined Radio (SDR) are also playing a crucial role in enhancing communication capabilities during ADR missions. SDR allows for flexible reconfiguration of radio systems through software, enabling real-time adjustments to communication protocols based on mission requirements. This adaptability is vital for coordinating complex operations in the dynamic environment of space, ensuring that data transmission remains robust despite the challenges posed by orbital debris.

Keywords: *Space debris Remediation (SDR), Active Debris Removal (ADR), Robotic Arm, Home Capture, Nodal Capture, System Design, Concurrent Engineering, Sun-synchronous Orbit.*

Table of Contents

Acknowledgements	iii
Abstract	iv
Table of Contents	v
List of Figures	xi
List of Tables	xiii
Chapter 1: Introduction & Preamble	1
1.1 introduction	1
1.2 Preamble	5
1.2.1 The Role of Student Satellite Programs	6
1.3 Problem Statement	7
1.3.1 Motivation	7
1.4 Aim and Objectives	8
1.5 Background and Technological Context	8
1.6 Subsystem Overview	9
1.6.1 SDR1: Payload and Debris Remediation Interface	9
1.6.2 SDR2: Telemetry, Command, and Redundancy	10
1.6.3 Power Conditioning Unit (PCU)	11
1.7 Significance of Integrated SDR and PCU Design	11
1.8 Structure of the Paper	12
Chapter 2: Literature Review	13
2.1 Foundations	13
2.2 Books	13
2.3 Papers	15
2.3.1 Comparative Analysis of Above SDR1 Research Papers	24

2.4	Literature Review: Software Defined Radios (SDR2)	27
2.4.1	Comparative Analysis of Above Research Papers on SDR2 . .	32
2.5	Literature Review: Power Conditioning Unit (PCU)	36
Chapter 3: Methodology	45
3.1	Program Methodology	45
3.1.1	Phase 01: Conceptualization and Initial Payload Development	46
3.1.2	Phase 02: Satellite Design and Communication Enhancement	47
3.1.3	Phase 03: Power Control Unit (PCU) Design and System Integration	47
3.1.4	Summary and Methodological Impact	49
3.2	Research Methodology	50
3.2.1	Stage 1: Comprehensive Literature Review	50
3.2.2	Stage 2: Mathematical Modeling	51
3.2.3	Stage 3: Solver Development and Testing	51
3.2.4	Stage 4: Design Validation and Optimization	52
3.2.5	Process Visualization and Iteration	52
3.2.6	Methodological Impact	53
3.3	Work Methodology	53
3.3.1	Methodological Framework	54
3.3.2	Solar Power Generation	55
3.3.3	Solar Power Generation System	55
3.4	Power Conditioning Unit (PCU)	56
3.4.1	Power Distribution Unit (PDU)	57
3.5	Design Process and Verification	57
3.6	Conclusion	58
Chapter 4: Design Procedure and Details	59
4.1	System Concept design	59
4.2	System Tradeoff Study	59

4.2.1	Importance of RPO Missions	60
4.2.2	Candidate Spacecraft for Space Tugs	60
4.2.3	System Level Comparison	60
4.3	H2Z Conceptual Design	61
4.3.1	H2Z System Specifications	61
4.3.2	CAD Model	62
4.3.3	Introduction	63
4.3.4	Solar Panels	63
4.3.5	Challenges in Design and Implementation	64
4.3.6	Deployment Methods	65
4.3.7	Examples of Successful Implementations	65
4.4	Payload Subsystem	65
4.4.1	Structure Subsystem	66
4.4.2	Mass Budget	67
4.4.3	Attitude Determination and Control Subsystem	67
4.5	H2Z Software Design Radio(SDR2) Design	68
4.6	Modules Subsystem)	71
4.6.1	TOTEM Components	71
4.6.2	NANOlink Components	72
4.7	Market Survey	75
4.8	Electrical Power Subsystem	78
4.8.1	Power Budget	78
4.9	Power Required Calculation	83
4.9.1	Sunlit Power Requirement	83
4.9.2	Eclipse Power Requirement	84
4.9.3	Battery Charging Power Requirement	86
4.9.4	Total Array Power Requirement	87
4.10	Battery Energy Requirement (Equation 5)	87
4.10.1	Battery Mass Estimation	88

4.10.2	Solar-Array Energy Output (Equation 7)	88
4.10.3	Duty-Cycle Energy Budget	89
4.10.4	Solar-Array Area	89
4.10.5	End-of-Life Power	90
4.11	Thermal Control Subsystem	90
4.11.1	Thermal Control Techniques	90
4.11.2	Environmental Heat Loads	91
4.11.3	Design Considerations for H2Z	92
4.11.4	Analysis of Subsystem Power Dissipation	92
4.12	Net Heat Flux Inward (Equation 12)	93
4.13	Radiative Heat Loss	93
4.14	Temperature Differential	94
4.15	Radiated Heat Flux Outward (Equation 14)	94
4.16	Power Margin	94
Chapter 5: Results and Discussion	96
5.1	Debris Selection	96
5.2	Payload	97
5.2.1	Robotic Arm	97
5.2.2	Imaging Payload	98
5.3	Structure Subsystem	99
5.4	Attitude Determination and Control Subsystem	100
5.5	Electric Power Subsystem	101
5.5.1	EPS Subsystem Efficiencies	103
5.6	Mission Load Curve	103
5.7	Solar Array and Battery Sizing	104
5.8	Power Distribution Subsystem	105
5.8.1	Solar Array Configuration	105
5.8.2	Efficiency Losses	106
5.9	Effective Power Output	106

5.9.1	Power Distribution Unit (PDU) Analysis	107
5.9.2	Subsystem Power Allocations	107
5.9.3	Efficiency Considerations	107
5.9.4	Protection Mechanisms	108
5.9.5	Redundancy Architecture	109
5.9.6	Analysis of Subsystem Power Dissipation	109
5.9.7	ADCS Subsystem	110
5.10	Power Dissipation Calculations	110
5.10.1	TT&C Subsystem	110
5.10.2	CDH Subsystem	111
5.10.3	Propulsion Subsystem	112
5.10.4	Communication Modules (TOTEM and NANOLink)	112
5.10.5	Dissipation Budget	113
5.10.6	Thermal Analysis	114
5.10.7	Thermal and Safety Considerations	115
5.11	Power Margin	116
5.11.1	At Nominal of Sunlight:	116
5.11.2	Safety Margins	116
5.12	Power Conditioning Unit(PCU)	117
5.13	Thermal Control System Analysis	117
5.13.1	H2Z Thermal Analysis	117
5.14	Power Dissipation and Distribution	118
5.15	Maximum Power Point Tracker (MPPT) Analysis and Results Discussion	120
5.15.1	MPPT Efficiency Analysis Over 3 Years	120
5.15.2	MPPT Power Tracking Performance Analysis	123
5.15.3	MPPT Degradation Analysis	125
5.16	Key Findings and Conclusions	127
5.17	Recommendations	128

5.17.1	Analysis Procedure	128
5.17.2	Results and Discussion	131
5.18	Load Curve, Margin, and Battery Performance	131
Chapter 6:	UN Sustainable Development Goals	132
6.1	Introduction	132
6.2	Sustainable Development Goals (SDGs) Addressed by the Project .	132
Chapter 7:	Conclusion and Recommendations	136
7.1	Mission Conclusions	136
7.2	System Conclusions	137
7.3	Recommendations for Further Work	137
References		139

List of Figures

Figure 1.1 Low Earth Orbit - August 25, 2009 (NASA Earth Observatory)	3
Figure 1.2 Block diagram of satellite subsystem architecture showing SDR1, SDR2, PCU, and OBC interconnections.	9
Figure 1.3 Functional block diagram of SDR1	10
Figure 1.4 Functional block diagram of SDR2.	11
Figure 1.5 ESP32 PCU Microcontroller	12
Figure 3.1 Preamble of Satellite Development Phases from Concept to System Integration	45
Figure 3.2 The design of PCU.	49
Figure 3.3 Research Methodology Flowchart: From Literature Review to Final System Design	53
Figure 3.4 Flowchart of Satellite Power Generation, Conditioning, and Distribution	54
Figure 4.1 Relevant space tugs for benchmarking	59
Figure 4.2 Orbital Debris Created By ASAT Tests in Space	61
Figure 4.3 CAD Model of H2Z	62
Figure 4.4 Cad model of mechanism	63
Figure 4.5 Deployment solar panel	64
Figure 4.6 Motor Specifications for Joint 1, 2 and 3	66
Figure 4.7 Mass Budget	67
Figure 4.8 ADCS specs	68
Figure 4.9 TOTEM Data interface data sheet	73
Figure 4.10 NANOLink Technical Specs	74
Figure 4.11 NANOLink boost sp power consumption	74
Figure 4.12 Power consumption Breakdown	75
Figure 4.13 Power consumption SDR2	75

Figure 4.14 32% Quadruple Junction GaAs Solar Cell Type: QJ Solar Cell 4G32C - Advanced	80
Figure 4.15 Functional block diagram of the Electrical Power System (EPS) showing solar energy flow and regulation.	80
Figure 4.16 Heat dissipation flow from subsystem components to space, modeled via Stefan–Boltzmann law.	82
Figure 4.17 Specifications of Thermal Control Subsystem	92
Figure 5.1 Sensitivity analysis of the debris	96
Figure 5.2 Load curve and power consumption over 3years	104
Figure 5.3 Life of battery over 3 years	105
Figure 5.4 The Power Distribution Unit of the Satellite	107
Figure 5.5 Margin of power over 3years	120
Figure 5.6 MPPT Efficiency Degradation,Power Gain Comparison,Tracking Accuracy,Energy Benefit	122
Figure 5.7 MPPT Power Tracking Performance Comparison,Advantage,Variation and Efficiency Over Time	125
Figure 5.8 MPPT Component,Temperature and Irradiance Degradation Analysis along with Annual Performance	127
Figure 5.9 Geometry of H2Z Cubsat	129
Figure 5.10 Mesh	130

List of Tables

Table 1.1 Feature comparison of SDR1, SDR2, and PCU subsystems	12
Table 2.1 Point-by-Point Application of Literature Findings in Our Project	17
Table 2.2 Relevance of Literature to Our Project Design	20
Table 2.3 Relevance of Legal and Technical Literature to Our Project	22
Table 2.4 Legal and Policy Insights Applied to Our Project	24
Table 2.5 Comparative Relevance of SDR1 Research Papers to CubeSat ADR Project	26
Table 2.6 Relevance of SDR Communication Research to CubeSat ADR Project	28
Table 2.7 Relevance of SDR2 Communication Review to CubeSat ADR Project	29
Table 2.8 Relevance of Multi-Satellite SDR Architecture to CubeSat ADR Project	31
Table 2.9 Comparative Relevance of SDR2 Research Papers to CubeSat Project	33
Table 2.10 Relevance of <i>Elements of Spacecraft Design</i> to PCU Design in Our Project	37
Table 2.11 Relevance of <i>Practical Handbook of Photovoltaics</i> to MPPT Implementation in Our PCU	38
Table 2.12 Relevance of <i>Space Vehicle Control Systems</i> to PCU Load Management in Our Project	39
Table 4.1 Comparison of SDR Components for CubeSat Applications	76
Table 4.2 H2Z Satellite Power Budget	79
Table 4.3 Subsystem power requirements in sunlight and eclipse phases (scaled values by 100 for clarity).	81
Table 5.1 NORAD ID Table of Selected Debris for Mission	97
Table 5.2 Table of Parameters and Results	99

Table 5.3	Table of Parameters of H2Z Bus	100
Table 5.4	Disturbance torques	100
Table 5.5	Sizing of reaction wheels and momentum wheels	101
Table 5.6	EPS Result	102
Table 5.7	EPS parameters from damage Fluence Method	102
Table 5.8	Solar Array Configuration Parameters	106
Table 5.9	Efficiency Loss Factors	106
Table 5.10	Effective Power Output	106
Table 5.11	Subsystem Power Allocations	108
Table 5.12	Effective Power Output Considering PDU Efficiency	108
Table 5.13	Power Dissipation for ADCS Subsystem	110
Table 5.14	Power Dissipation for TT&C Subsystem	111
Table 5.15	Power Dissipation for CDH Subsystem	111
Table 5.16	Power Dissipation for Propulsion Subsystem	112
Table 5.17	Power Dissipation for Communication Modules	113
Table 5.18	Power Dissipation Budget for the Satellite Subsystems	114
Table 5.19	Thermal Management Strategies	115
Table 5.20	Power System Safety Margins	117
Table 5.21	PCU and Battery System Parameters	117
Table 5.22	Power dissipation for each subsystem and component.	119
Table 5.23	Mechanical and Thermal Properties of Aluminum 6061	129
Table 5.24	Mesh Properties of the Satellite	130
Table 5.25	Loads/BC's	131

Chapter 1

Introduction & Preamble

1.1 introduction

Humanity's ventures into space have heralded profound advancements in science and technology, revolutionizing our understanding of the cosmos and enabling unprecedented capabilities on Earth. However, these accomplishments have also introduced complex and escalating challenges. Chief among these is the proliferation of space debris—a collection of non-functional satellites, spent rocket stages, and myriad fragments resulting from collisions or explosions. These objects, confined to Earth's orbit, travel at velocities exceeding 28,000 km/h, creating a severe risk to operational satellites, crewed missions, and future space activities. Unlike terrestrial waste, space debris does not undergo natural degradation; objects persist in orbit for decades or centuries, depending on their altitude, rendering certain orbital regions increasingly perilous and unsustainable.

Parallel to this issue is the challenge posed by the intensifying demand for satellite communication, driven by the global need for connectivity and data transmission. The S-band (2–4 GHz) has historically been the primary frequency range for satellite communication due to its robust signal quality and atmospheric penetration. However, its extensive utilization has led to severe congestion, resulting in interference, delays, and bandwidth limitations. The shift toward higher frequency bands such as the X-band (8–12 GHz), which offers increased bandwidth and reduced congestion, represents a viable solution. This transition, however, necessitates the deployment of advanced technologies like software-defined radios (SDRs), which can dynamically reconfigure communication systems to operate across different frequency bands. Together, these challenges highlight the urgent need for innovative

Introduction & Preamble

approaches to both debris remediation and the optimization of satellite communication systems to ensure the sustainable use of space. The magnitude of the space debris problem is alarming. By 2023, over 15,000 trackable objects larger than 10 cm were cataloged in Earth's orbit. Additionally, it is estimated that approximately 130 million particles smaller than 1 cm remain untracked. Despite their diminutive size, these fragments possess sufficient kinetic energy to inflict catastrophic damage upon collision with active spacecraft or satellites. Among the roughly 7,000 satellites launched since the inception of space exploration, nearly 60% are now defunct, classified as "dead satellites," and contribute significantly to the debris population. Notable debris-generating events include the 2007 Chinese anti-satellite test, which generated over 3,000 trackable fragments, and the 2009 Iridium-Cosmos collision, which added more than 2,300 pieces to Earth's orbital environment.

The operational and economic impacts of space debris are equally concerning. Collision avoidance has become a routine yet resource-intensive necessity for satellite operators. The International Space Station (ISS), for example, has performed more than 30 debris-avoidance maneuvers since 1999. Data from the European Space Operations Centre (ESOC) reveal a 5% annual increase in collision risk within Low Earth Orbit (LEO) over the past decade. The financial costs associated with debris management—including collision avoidance, satellite repairs, insurance premiums, and operational interruptions—exceed \$1 billion annually, underscoring the urgency of addressing this issue.

In satellite communication, the challenges posed by frequency congestion are similarly critical. Over 70% of active satellites rely on the S-band, leading to heightened levels of interference and diminished data transfer rates, with averages peaking at approximately 10 Mbps. Signal distortion affects roughly 25% of systems operating in this range, further limiting efficiency. By contrast, the X-band offers 2.5 times the bandwidth of the S-band and enables significantly higher data transfer rates. Despite these advantages, only 15% of satellites operate in the

System Design & Demonstrator of a SPU Power Generation Subsystem for SDR Operations of Space Tug in LEO

X-band, a disparity attributable to the costs of infrastructure development and licensing requirements. Software-defined radios (SDRs) are emerging as transformative technologies in this domain. Research indicates that SDR-based systems transitioning from the S-band to the X-band can achieve a 50% improvement in signal clarity, a 40% increase in data throughput, and up to a 30% reduction in upgrade costs. The international community has undertaken numerous initiatives to mitigate the escalating threats posed by space debris. Active debris removal (ADR) technologies represent a cornerstone of these efforts. The European Space Agency's (ESA) ClearSpace-1 mission, scheduled for launch in 2026, aims to demonstrate the feasibility of ADR on a large scale by using a robotic arm to capture and deorbit a defunct satellite. Similarly, Japan's Astroscale has advanced ADR technology with its "ELSA-d" (End-of-Life Services by Astroscale Demonstration) mission, which employs magnetic capture systems to retrieve non-functional satellites. The RemoveDEBRIS mission, spearheaded by the Surrey Space Centre, has successfully tested innovative debris capture methods such as harpoons and nets, providing critical insights into medium-sized debris removal. Additionally, laser-based systems, which employ ground-based or orbital lasers to alter the velocity of small debris particles, have shown promise by enabling these particles to re-enter Earth's atmosphere and disintegrate.

Let's add a Figure 1.1:



Figure 1.1: Low Earth Orbit - August 25, 2009 (NASA Earth Observatory)

Introduction & Preamble

Innovative concepts like NASA's EDDE (Electrodynamic Debris Eliminator) are expanding the scope of ADR capabilities. The EDDE system uses electrodynamic tethers to efficiently capture and deorbit multiple debris objects, addressing the problem on a broader scale. Passive mitigation measures, including the promotion of satellite designs with integrated end-of-life disposal mechanisms, are also gaining traction. For instance, propulsion systems that enable controlled re-entry at the conclusion of a satellite's operational life are becoming standard industry practices. On an international level, organizations such as the Inter-Agency Space Debris Coordination Committee (IADC) and the United Nations Office for Outer Space Affairs (UNOOSA) are instrumental in establishing global guidelines for debris mitigation and advocating for best practices.

In the realm of satellite communication, SDRs have emerged as pivotal tools for addressing frequency congestion and enhancing operational flexibility. ESA's EDRS-C mission exemplifies the integration of SDR technology to enable seamless multi-frequency communication, including X-band transmissions for high-data-rate applications. Similarly, NASA's Lunar Reconnaissance Orbiter employs SDRs to optimize data transfer between its S-band uplink and X-band downlink systems. Japan's Himawari Satellite Series, a critical asset for real-time disaster monitoring, leverages SDRs to ensure uninterrupted high-speed communication during emergencies. Small satellite missions, such as Astroscale's ELSA-d and the RemoveDEBRIS CubeSat, have also integrated SDRs to enable adaptive, efficient operations across multiple frequency bands.

Ground station infrastructure has evolved to complement these technological advances. Dual-band ground stations, exemplified by the SX-Dual Ground Station, are capable of processing S-band and X-band signals simultaneously, achieving a 30% improvement in communication efficiency. Academic institutions such as Cal Poly and the Surrey Space Centre have contributed to these developments by designing SDR frameworks capable of concurrent multi-band operations, providing scalable solutions for future missions.

System Design & Demonstrator of a SPU Power Generation Subsystem for SDR Operations of Space Tug in LEO

1.2 Preamble

The journey toward developing a viable satellite system is rarely linear—it is shaped by visionary leadership, interdisciplinary collaboration, and a strong commitment to innovation. The satellite initiative undertaken at Air University is a testament to such a journey. Central to this effort is **Dr. Ali Sarosh**, the Principal Investigator (PI) from IAA-AHQ, whose strategic direction and mentorship enabled the realization of a complex, multi-phase program that spans from debris mitigation technologies to satellite communication and power autonomy.

The project was systematically structured into three core phases, each executed by specialized teams across departments but unified under a single vision. **Phase 01**, led by the **IAA-Mechatronics** department (Team 01), addressed one of the most pressing challenges in space operations—*space debris remediation*. Under Dr. Sarosh’s guidance, the team designed a conceptual **robotic arm payload (SDR1)** capable of targeting and managing orbital debris. This solution directly aligns with global sustainability efforts and objectives outlined by the *Committee on Space Research (COSPAR)* under the United Nations.

Building on this foundation, **Phase 02**, executed by **Team 02** under the direct support of the **Ministry Of Defense (MOD)**, extended the mission from concept to implementation. Here, focus shifted toward *satellite system design* and integration of a robust communication payload—the **Software Defined Radio (SDR2)**. SDR2 introduces reconfigurable, software-driven flexibility into the communication chain, allowing modulation schemes, frequency plans, and protocol updates to be managed dynamically. This step elevated the mission from a proof-of-concept to a technically mature communication system—again, made possible through the consistent mentorship and leadership of Dr. Sarosh.

Parallel to communication development, **Phase 03**, managed by the **IAA-EE department (Team 03)**, was tasked with one of the most critical enablers of satellite autonomy—power. Under the H2Z Satellite Power initiative and the

continued oversight of Dr. Sarosh, the team developed a comprehensive **Power Conditioning Unit (PCU)**. The PCU comprises two essential systems: (1) a *Power Generation System* optimized for solar harvesting and maximum power point tracking (MPPT), and (2) a *Power Distribution System* that ensures safe, efficient, and prioritized power flow to all satellite subsystems. This infrastructure enables long-duration missions in orbit without ground intervention.

The full system architecture, represented in Figure 3.1, showcases the phased workflow and decision pathways. At the core of this diagram is a critical milestone—*Working Design Validation*. Only through stringent integration and iterative refinement, again facilitated by Dr. Sarosh’s oversight, was the project able to move forward. A successful design triggers the final goal: a **Contract Award for Satellite Design and Development**, bringing the vision full circle—from academic collaboration to real-world implementation.

In essence, this satellite initiative is not merely a technical exercise; it is a model of leadership-driven innovation. The orchestration across teams, technologies, and institutions would not have been possible without the pivotal role of Dr. Ali Sarosh, whose involvement in every phase transformed fragmented goals into a unified, functional mission architecture.

1.2.1 The Role of Student Satellite Programs

The proliferation of CubeSat missions has been paralleled by a surge in student-led satellite programs. These initiatives serve not only as educational platforms but also as testbeds for innovative space technologies that may be too risky or cost-prohibitive to deploy on larger, traditional spacecraft. As of late 2023, thousands of CubeSats have been launched, with applications spanning Earth observation, amateur radio, and technology validation. The compact form factor and resource constraints inherent to CubeSats present unique engineering challenges, particularly in the domains of communication and power management. Addressing these challenges requires a judicious selection of subsystems that maximize mission capa-

System Design & Demonstrator of a SPU Power Generation Subsystem for SDR Operations of Space Tug in LEO

bility while ensuring reliability and operational resilience in the harsh environment of Low Earth Orbit (LEO).

1.3 Problem Statement

The rapid expansion of space activities has introduced two critical challenges that threaten the sustainability of space operations: the proliferation of space debris and the overcrowding of satellite communication frequencies. With over 15,000 trackable debris objects and an estimated 130 million smaller particles in orbit, collision risks and associated costs are escalating exponentially, jeopardizing operational satellites and future missions. Concurrently, the congestion of the S-band, utilized by over 70% of satellites, has led to significant inefficiencies, despite the availability of the X-band as a viable alternative. However, technological, infrastructural, and regulatory barriers hinder the widespread adoption of effective solutions such as active debris removal technologies and software-defined radios. Addressing these issues is paramount to ensuring the long-term viability of space exploration and communication infrastructure, necessitating innovative, scalable, and collaborative approaches.

1.3.1 Motivation

In recent years, innovative advancements in addressing space debris have inspired new approaches to mitigating the growing orbital clutter. For instance, the RemoveDEBRIS mission successfully demonstrated the use of nets and harpoons to capture defunct satellites in Low Earth Orbit (LEO), while Japan's Astroscale ELSA-d mission showcased magnetic mechanisms for debris retrieval. The motivation for this project stems from these pioneering efforts and extends their principles by proposing an integrated system capable of not only capturing debris but also deorbiting it effectively. Instead of relocating objects to graveyard orbits, our approach emphasizes active deorbiting strategies that ensure debris re-enters Earth's atmosphere and burns up, thus permanently removing hazards from or-

bit. This innovative solution aligns with the growing demand for sustainable space operations and addresses the urgent need to mitigate the risks posed by orbital debris.

1.4 Aim and Objectives

The primary aim of this research is to develop and demonstrate a fully integrated, robust, and space-operational satellite communication and power system using SDR1, SDR2 and a PCU. Which supports the broader mission of enabling student-led satellite development with realistic, scalable, and reliable subsystems.

The key objectives of the work are:

1. To design, implement, and test SDR1 for all different environment in space as such power disipation, temperature and burn out of solar cell.
2. To design, implement, and test SD2 as the main communication module for telemetry and telecommand within the UHF frequency range.
3. To develop a PCU capable of power regulation, MPPT, battery charging, protection, and telemetry integration.
4. To demonstrate SPI-based communication between the SDR1/SDR2/PCU and the OBC.
5. To validate the system via simulation and ground testing under conditions that emulate LEO/SSO missions.

1.5 Background and Technological Context

Software Defined Radios (SDRs) allow communication protocols to be implemented and modified via software, granting flexibility across different mission phases. Unlike conventional transceivers, SDRs can adjust frequency, modulation, and encoding schemes dynamically. In this mission, SDR1 is the primary unit for

System Design & Demonstrator of a SPU Power Generation Subsystem for SDR Operations of Space Tug in LEO

telemetry and command exchange. SDR2 acts as a cold or hot backup, depending on mission mode, capable of taking over in case of failure or degradation in SDR1.

Power Conditioning Units (PCUs) perform a central role in satellite viability. Since solar power availability in orbit is variable and intermittent, the PCU must efficiently manage energy harvesting, storage, and regulated delivery. It must also include critical protection mechanisms such as overvoltage clamping, short-circuit protection, and low-voltage cutoffs to prevent permanent damage to subsystems. Figure 1.2 shows the overall subsystem architecture integrating SDR1, SDR2, the PCU, and the OBC.

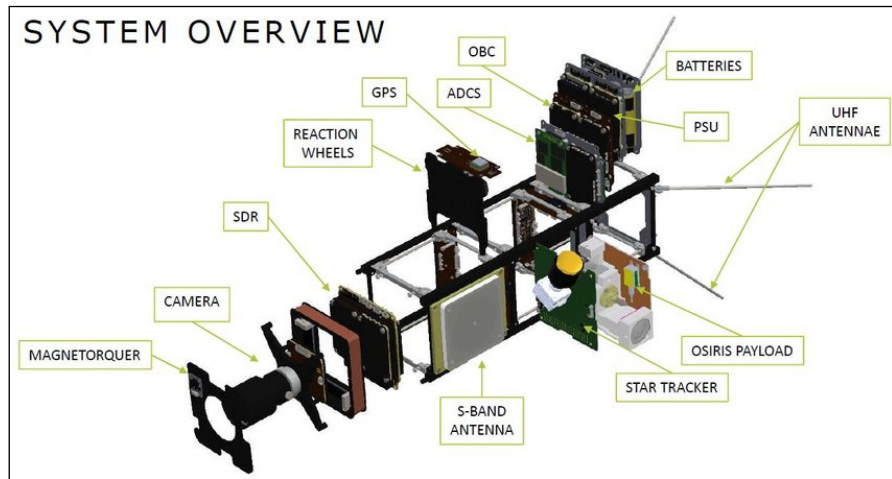


Figure 1.2: Block diagram of satellite subsystem architecture showing SDR1, SDR2, PCU, and OBC interconnections.

1.6 Subsystem Overview

1.6.1 *SDR1: Payload and Debris Remediation Interface*

SDR1: Payload and Debris Remediation Interface In the context of the present investigation, the CubeSat architecture 1.3 incorporates two distinct SDR modules—SDR1 and SDR2—each fulfilling complementary roles within the mission. SDR1 is tasked with supporting the operation of a camera payload and facilitating command and control of a robotic arm designed for active space debris remediation in LEO. This subsystem exemplifies the integration of advanced payload operations

with flexible communication interfaces, enabling real-time command execution and data acquisition. The use of SDR1 for both payload control and communication underscores the multifunctional potential of software-defined architectures, where a single radio can be repurposed or updated to accommodate diverse operational scenarios.

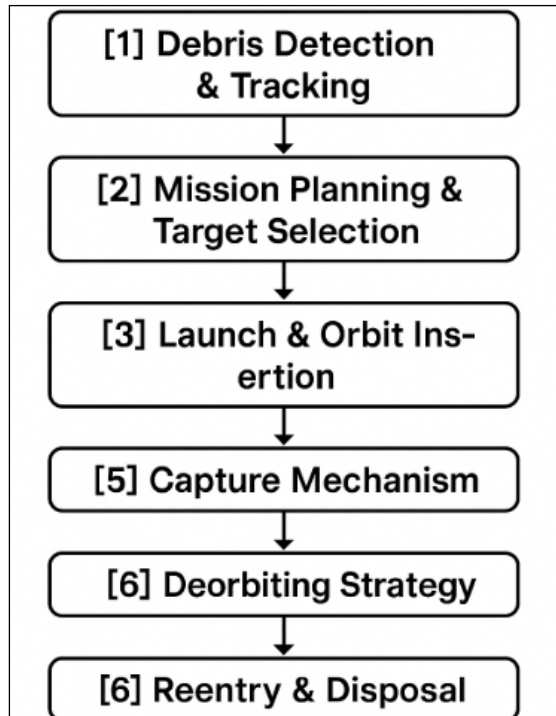


Figure 1.3: Functional block diagram of SDR1

1.6.2 SDR2: Telemetry, Command, and Redundancy

SDR2, by contrast, serves as the primary transceiver for routine satellite operations, handling the downlink of housekeeping and payload telemetry as well as the uplink of ground commands^{1.4}. Operating in the UHF frequency range and interfacing with the onboard computer via a Serial Peripheral Interface (SPI), SDR2 is engineered for robust data handling and efficient communication.

System Design & Demonstrator of a SPU Power Generation Subsystem for SDR Operations of Space Tug in LEO

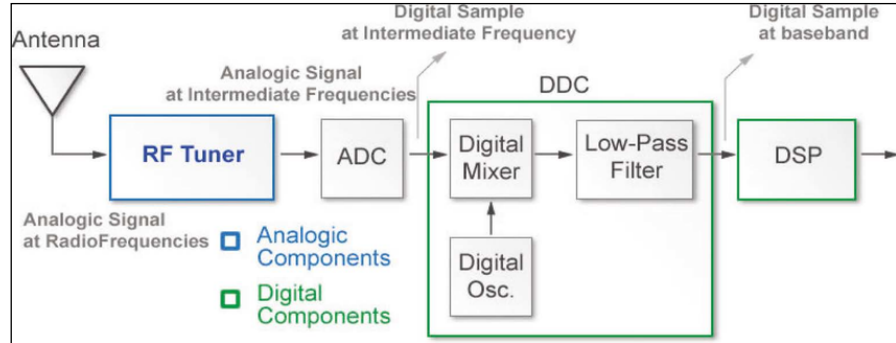


Figure 1.4: Functional block diagram of SDR2.

1.6.3 Power Conditioning Unit (PCU)

The PCU is the backbone of the satellite's power subsystem. It accepts unregulated input from solar panels, applies maximum power point tracking (MPPT) to optimize solar energy harvesting, and manages a battery charging system with dynamic current control^{1.5}. The PCU also distributes regulated voltage levels to other subsystems and includes multiple protection layers:

- Overvoltage and undervoltage cutoff
- Overcurrent trip
- Short-circuit detection and isolation
- Temperature monitoring

The PCU's telemetry channels feed data to the OBC, which transmits it via SDR1/SDR2 to ground stations.

1.7 Significance of Integrated SDR and PCU Design

The combined use of dual SDRs and a dedicated PCU creates a resilient and scalable satellite architecture. While SDRs enhance flexibility and adaptability in communication protocols, the PCU ensures robust energy management, which is foundational to all other system functions.

Symbol	Parameter	Min	Typ	Max	Unit
C_{IN}	Pin capacitance	-	2	-	pF
V_{IH}	High-level input voltage	$0.75 \times VDD^1$	-	$VDD^1 + 0.3$	V
V_{IL}	Low-level input voltage	-0.3	-	$0.25 \times VDD^1$	V
I_{IH}	High-level input current	-	-	50	nA
I_{IL}	Low-level input current	-	-	50	nA
V_{OH}	High-level output voltage	$0.8 \times VDD^1$	-	-	V
V_{OL}	Low-level output voltage	-	-	$0.1 \times VDD^1$	V
I_{OH}	High-level source current ($VDD^1 = 3.3$ V, $V_{OH} \geq 2.64$ V, output drive strength set to the maximum)	$VDD3P3_CPU$ power domain ^{1, 2}	-	40	-
		$VDD3P3_RTC$ power domain ^{1, 2}	-	40	-
		VDD_SDIO power domain ^{1, 3}	-	20	-

Figure 1.5: ESP32 PCU Microcontroller

Table 1.1 summarizes the main features of each subsystem.

Table 1.1: Feature comparison of SDR1, SDR2, and PCU subsystems

Feature	SDR1	SDR2	PCU
Primary Function	Telemetry + Uplink	Redundant Comms	Power Regulation
Interface	SPI to OBC	SPI to OBC	SPI to OBC
Operating Band	UHF	UHF	N/A
Power Input	PCU-regulated	PCU-regulated	Solar Panel/Battery
Redundancy Role	Primary	Backup	N/A
Protection Logic	Software	Software	Hardware + Software

1.8 Structure of the Paper

The remainder of this paper is structured as follows: Section ?? details the hardware and software design of each subsystem. Section ?? discusses integration testing and communication protocols. Section ?? provides results from simulation and prototyping phases. Finally, Section ?? offers concluding remarks and future work directions.

Chapter 2

Literature Review

In the following papers and articals the concepts and questions of our parts of the mission are discussed to which each paper are divided into parts about paper, comparasion of concept in paper or our mission and our mission improvment by using that concept.

2.1 Foundations

The definitive reference for satellite designers, Space Mission Analysis and Design, is regarded as the cornerstone for understanding mission and spacecraft design. This book was meticulously studied to gain comprehensive insights into the intricate processes involved in crafting missions and designing spacecraft systems.

2.2 Books

Space Mission Analysis and Design (SMAD): Wiley J. Larson et al in [1]
"Space Mission Analysis and Design (SMAD)" by Wiley J. Larson et al. is a comprehensive guide that covers the entire spectrum of space mission engineering, from concept development to mission execution. The book emphasizes the importance of defining mission objectives and requirements as a foundation for design. It explores orbit and constellation design, launch vehicle selection, and spacecraft design, ensuring that all components align with mission goals. Cost reduction strategies are highlighted, providing insights into minimizing expenses while maximizing mission effectiveness. The third edition incorporates advancements in electric propulsion and autonomous systems, reflecting contemporary trends in aerospace technology. Practical tools, including extensive appendices with data and formulas, make it an invaluable resource for engineers and students

alike. Overall, SMAD serves as a vital reference for anyone involved in space mission planning and execution.

Elements of Spacecraft Design: Charles D. Brown [2] "Elements of Spacecraft Design" by Charles D. Brown offers a detailed examination of spacecraft design principles, focusing on the integration of various subsystems critical to mission success. The book outlines a systematic approach to spacecraft design, emphasizing the need to meet specific mission requirements effectively. It discusses the interplay between subsystems such as power systems, thermal control, and structural integrity, highlighting their collective impact on overall performance. Special attention is given to power generation methods, particularly solar power, and the functionality of power control units that manage energy throughout the mission lifecycle. Brown also emphasizes how design choices are influenced by the specific objectives of a mission, whether for scientific exploration or commercial endeavors. This text serves as an essential resource for understanding the complexities of spacecraft design and engineering. Ultimately, it equips readers with practical knowledge applicable to real-world space missions.

Space Vehicle Control Systems [3] "Space Vehicle Control Systems" focuses on the critical role of control systems in managing spacecraft dynamics during missions. The book applies control theory principles to ensure stability and performance in various operational scenarios encountered in spaceflight. It discusses how control systems are designed and implemented to execute mission objectives effectively, including maneuvering and orbital adjustments. A significant aspect covered is the role of power control units in maintaining system stability and efficiency throughout different phases of a mission. The text highlights the importance of these systems in ensuring that spacecraft can adapt to changing conditions while achieving their goals. By examining both theoretical foundations and practical applications, this book provides valuable insights into the complexities of space vehicle operation. Overall, it serves as a crucial resource for aerospace

System Design & Demonstrator of a SPU Power Generation Subsystem for SDR Operations of Space Tug in LEO

engineers involved in spacecraft control system design.

Practical Handbook of Photovoltaics Fundamentals and Applications: Tom Markvart & Luis Castaner [4] **Practical Handbook of Photovoltaics Fundamentals and Applications**” by Tom Markvart & Luis Castaner presents an in-depth exploration of photovoltaic (PV) technology essential for power generation in space applications. The book covers the principles of designing PV systems specifically tailored for space missions, focusing on efficiency and reliability under harsh environmental conditions. It details various techniques for harnessing solar energy effectively while ensuring optimal performance during operations in orbit. Additionally, the text discusses power charging systems that facilitate efficient battery charging using solar energy throughout missions. Markvart and Castaner emphasize the integration of PV technology into spacecraft design as a means to enhance energy independence and sustainability during missions. With its comprehensive approach to both fundamentals and practical applications, this handbook serves as an invaluable resource for engineers working on solar power solutions for space exploration. Ultimately, it highlights the critical role of photovoltaic systems in advancing modern space missions.

2.3 Papers

Designing Photo-voltaic Arrays for a Cubesat using Component Efficiency and Damage Fluence Methods [5] Author: Nasrullah Khan, Ali Sarosh, Shakir Hussein Ch. Department of Aerospace Engineering, CAE National University of Sciences and Technology (NUST), Islamabad, Pakistan

- **Solar Cell Type Selection:** The paper emphasizes the advantages of multi-junction GaAs cells in LEO environments. In our project, we selected quadruple-junction GaAs (4G32C) cells to ensure high efficiency and radiation resistance.

- **Sizing Methodology:** The study compares the Component Efficiency Method with the Damage Fluence Method, concluding that the latter is more accurate for space missions. We applied the Damage Fluence Method to ensure our array provides sufficient power throughout the mission lifespan.
- **Array Area Estimation:** Their findings show that ignoring radiation effects underestimates required area. Our final design used the conservative estimate (approx. 6.5 m^2) to ensure power availability at End-of-Life (EOL).
- **Radiation Shielding and Degradation:** The paper includes shielding effects such as coverslip thickness to reduce radiation-induced damage. We integrated similar degradation factors in our MPPT and EOL energy forecasting.
- **Efficiency Modeling:** They account for conversion losses, wiring, and degradation. We reflected this in our power budget, estimating overall EPS efficiency at 73%[2.1](#).
- **Load Matching and Duty-Cycle Analysis:** The paper aligns solar sizing with system demand. Our project implements solver-based load curve analysis to ensure critical systems like SDR1/SDR2 and the robotic arm receive adequate power, even during eclipses.
- **System Simulation and Validation:** The paper advocates validation through modeling and simulation. We employed multiple solvers (e.g., degradation, power margin, load) to validate power subsystem reliability across the full mission timeline.

System Design & Demonstrator of a SPU Power Generation Subsystem for SDR Operations of Space Tug in LEO

Table 2.1: Point-by-Point Application of Literature Findings in Our Project

Topic from Re-search Paper	Relevance to Our Project	Implementation in Project
Use of GaAs multi-junction cells	High efficiency, radiation resistance	Used 4G32C quadruple-junction GaAs cells for maximum performance in LEO
Damage Fluence Method	Realistic power estimation under radiation exposure	Adopted for accurate solar array sizing to sustain mission lifespan
Solar array area (6.5 m ²)	Conservative sizing to meet EOL energy needs	Incorporated large area in design based on degradation analysis
Radiation degradation	Effects of 1 MeV electron fluence considered	Factored into MPPT tuning and shielding decisions
Efficiency loss modeling	Includes conversion, wiring, and packing losses	Modeled in power budget, yielding 73% EPS efficiency
Load curve alignment	Matches power generation with mission phases	Used duty-cycle solver to model power needs of robotic arm, SDRs
Simulation validation	Ensures design meets mission goals under stress	Solvers validate performance across eclipse, thermal stress, EOL conditions

System Design and Demonstrator of a Solar Power Unit for Space Debris Remediation Operations in Lower Earth Orbit [6] Authors: Nasrullah Khan, Ali Sarosh, Shakir Hussein Ch. Department of Aerospace Engineering, CAE National University of Sciences and Technology (NUST),

Islamabad, Pakistan

Summary and Relevance This research paper highlights the critical threat posed by space debris and the importance of developing sustainable and robust systems to mitigate it. The H2Z satellite project introduced in the paper, which features a space tug equipped with a robotic end effector, aligns directly with the objective of our CubeSat mission. The successful operation of such a system relies heavily on efficient and resilient power systems, which is the primary focus of our work on the Power Conditioning Unit (PCU). The following points summarize how the paper's insights relate to and support our project design.

- **Space Debris and Kessler Syndrome:** The paper outlines the increasing risk of orbital collisions due to uncontrolled debris. Our CubeSat's mission of Active Debris Removal (ADR) directly responds to this challenge by capturing and deorbiting debris in LEO.
- **H2Z Satellite Tug System:** The described robotic end effector system matches our payload subsystem, which we power and manage using an optimized energy distribution architecture designed for real-time operations.
- **Power System as a Mission Enabler:** The paper states that mission success depends on a reliable power generation unit. Our PCU, equipped with MPPT, battery regulation, and fault protection, provides the energy backbone for SDR communication and robotic payload execution.
- **Evolution of Solar Cell Technology:** Transition from silicon to GaAs and multi-junction solar cells is discussed. Our use of 4G32C quadruple-junction GaAs solar cells reflects this evolution, offering high efficiency and durability in harsh orbital environments.
- **Surface Area Sizing Methods:** The paper compares the Component Efficiency Method and the Damage Fluence Method. We adopted the Damage

System Design & Demonstrator of a SPU Power Generation Subsystem for SDR Operations of Space Tug in LEO

Fluence Method to accurately size our solar arrays (6.5 m²) [2.2](#) and account for radiation degradation over the mission life.

- **Power Budgeting:** Emphasis is placed on planning for eclipse and sunlit phases. We implemented duty-cycle and power margin solvers to ensure system uptime during all orbital conditions.
- **Tethered Debris Removal Dynamics:** Analysis of tether-based capture systems highlights power stability needs during dynamic maneuvers. Our PCU design ensures smooth power delivery during robotic arm and thruster operations.
- **Vibration Damping and System Stability:** The paper mentions mechanical devices for vibration control. Our hardware is secured and buffered to protect sensitive power electronics during operational disturbances.

Table 2.2: Relevance of Literature to Our Project Design

Concept from Paper	Relevance to Project	Implementation in Our Design
Space debris risk and Kessler Syndrome	Core mission objective	Designed CubeSat for Active Debris Removal (ADR)
Robotic tug (H2Z)	Matches mission payload	Power system supports robotic end-effector
Efficient power unit needed	Mission-critical requirement	Designed PCU with MPPT, protection, and redundancy
Solar cell technology evolution	Reflects component choice	Selected 4G32C quadruple-junction GaAs solar cells
Damage Fluence Method vs. Component Efficiency	Informs power sizing methodology	Adopted Damage Fluence Method for 6.5 m ² array
Eclipse/sunlight planning	Energy availability challenges	Developed power solvers and load curves for full orbit profile
Tethered removal dynamics	Requires stable power under motion	PCU ensures clean power during arm/thruster operation
Vibration control in tug systems	Critical for hardware safety	Mechanically isolated PCU and solar panel connections

Sources 1. Remediating Space Debris: Legal and Technical Barriers by Joshua Tallis

2. ESA Technologies for Space Debris Remediation by Jessica De La Val

Summary and Relevance These two papers collectively highlight the multi-faceted nature of space debris remediation, covering both legal complexities and technological advancements. They offer valuable insight for CubeSat missions like

System Design & Demonstrator of a SPU Power Generation Subsystem for SDR Operations of Space Tug in LEO

ours that aim to actively remove debris from Low Earth Orbit (LEO). The following points summarize how the discussions in these papers directly relate to the design and goals of our CubeSat project:

- **Legal Barriers:** Tallis emphasizes unresolved legal issues such as liability, ownership, and jurisdiction over space debris. Our CubeSat project accounts for these by designing subsystems (e.g., SDR, OBC) capable of detailed telemetry logging, which supports legal accountability during ADR operations.
- **Technical Challenges:** The paper discusses experimental debris removal techniques such as electrodynamic tethers and ground-based lasers. Our project circumvents these limitations by using a robotic arm and tug system, supported by a stable and autonomous power subsystem (PCU).
- **Need for International Collaboration:** Both papers stress the importance of global cooperation and shared frameworks. Our project demonstrates the potential of emerging space programs, such as Pakistan's, to contribute meaningfully to sustainable orbital practices.
- **ESA's ADR Technologies:** ESA's Clean Space initiative highlights technologies like robotic arms, nets, and harpoons. Our robotic-arm-based design aligns directly with these methods, validating our technical choices through international best practices.
- **In-Orbit Servicing (IOS):** ESA's emphasis on autonomous servicing and deorbiting aligns with our satellite's multi-subsystem integration (SDRs, PCU, OBC) [2.3](#), which supports future scalability to IOS roles.
- **Standardized Protocols:** Both authors mention the need for procedural and technical standards. Our CubeSat uses standardized command and data handling sequences via the SDR and onboard computer, ensuring readiness for multi-agency interoperability.

- **Safety and Risk Management:** The documents underscore debris-related hazards and the importance of system survivability. Our CubeSat includes thermal regulation, load margin analysis, and battery fail-safes to enhance resilience in congested orbital paths.

Table 2.3: Relevance of Legal and Technical Literature to Our Project

Concept from Papers	Relevance to Project	Implementation in Our Design
Legal barriers: liability, ownership	Requires transparency and logging	Telemetry via SDR + OBC logging for accountability
Technical limits of emerging ADR tech	Preference for tested technologies	Robotic arm + PCU ensures reliability over tethers/lasers
International cooperation needed	Emerging nations must contribute	Demonstrates Pakistan's capacity in global debris missions
ESA's robotic capture methods	Confirms robotic arms are viable	Matches our arm-based capture and tug system
In-Orbit Servicing (IOS) direction	Autonomous systems required	SDR, PCU, and OBC support future IOS missions
Standardization protocols	Ensures interoperability	Follows structured command, control, and data handling
Space debris risk and survivability	Satellite must endure harsh conditions	Thermal management + power margin + EOL sizing included

Legal Implications of Space Debris Mitigation and Removal Strategies

[7] Authored by Dr. Shashank Shekhar and Priyank Kumar Verma

Summary and Relevance This paper explores the legal frameworks, challenges, and strategic approaches to mitigating and removing space debris. It emphasizes the importance of international treaties, national laws, liability struc-

System Design & Demonstrator of a SPU Power Generation Subsystem for SDR Operations of Space Tug in LEO

tures, and cooperation in ensuring that debris mitigation is conducted safely and lawfully. These legal insights are directly applicable to our CubeSat mission, which is actively designed to capture and deorbit orbital debris using a robotic arm system. Below is a structured outline showing how the paper's key legal and policy discussions inform the technical and procedural design of our project:

- **International Space Law:** The paper discusses the relevance of treaties like the Outer Space Treaty (OST) and the Liability Convention. Our CubeSat must operate in compliance with these frameworks, which we support by implementing secure telemetry logging and traceable system actions via SDR and onboard computer (OBC).
- **Active vs. Passive Debris Removal:** The authors contrast passive methods (e.g., drag sails) with active techniques (e.g., robotic capture). Our CubeSat uses an active method, the robotic arm and tug system, which requires more rigorous legal consideration and proper authorization of the mission as shown in table 2.4.
- **Attribution and Accountability:** The paper underscores the legal need to identify and obtain consent from the owner of debris before removal. Our mission incorporates target selection protocols and SDR-logged communications to document operational decisions and prove intent.
- **Liability, Insurance, and Compensation:** The paper highlights the need for safeguards and risk reduction to support legal defense and insurance. Our PCU includes overcurrent protection, MPPT redundancy, and system fallback modes to minimize chances of malfunction or collateral damage.
- **Environmental Framing of Debris:** Space debris is framed as an environmental sustainability issue. Our CubeSat directly addresses this by removing dangerous LEO debris, contributing to a safer orbital environment and aligning with the UN's Sustainable Development Goals (e.g., SDG 12).

- **Need for International Cooperation:** The authors advocate for standardized international collaboration on debris strategies. Our CubeSat demonstrates how emerging space nations can contribute responsibly, supporting unified and sustainable space operations.

Table 2.4: Legal and Policy Insights Applied to Our Project

Concept from Paper	Relevance to Project	Implementation in Our Design
International treaties and laws (OST, Liability Convention)	Compliance with space law is mandatory	Telemetry and SDR/OBC logging provide legal traceability
Passive vs. active mitigation strategies	Active removal demands more legal scrutiny	Our robotic arm-based removal requires mission authorization
Attribution and ownership of debris	Debris must be handled with consent	Target logging and SDR-based communication records maintained
Liability, insurance, compensation	Must minimize operational risk	System includes PCU protections and safe fallback logic
Space debris as environmental hazard	Justifies mission objective	Project aligns with sustainability and SDG 12
International cooperation need	Global governance supports standardization	Contributes to shared orbital safety initiatives

2.3.1 Comparative Analysis of Above SDR1 Research Papers

In comparing these research papers, each contributes distinctively to understanding the remediation of space debris while addressing unique challenges within this critical area. The first paper outlines significant legal barriers that impede effective remediation efforts, emphasizing the necessity of improved tracking systems

System Design & Demonstrator of a SPU Power Generation Subsystem for SDR Operations of Space Tug in LEO

such as the Space Fence. This complements De La Val's work on the technological advancements of ESA, which focuses on practical solutions for active debris removal through innovative capture methods. Although Shekhar and Verma provide a comprehensive examination of legal implications, highlighting accountability issues, their insights can enhance the technical discussions presented in the De La Val article by integrating legal considerations into technology development processes. Finally, the comprehensive study on threats posed by space debris reinforces the urgency highlighted in all previous papers by advocating for immediate action through active removal techniques. Enthusiastically, these papers collectively show a vibrant competition among researchers to tackle the multifaceted challenges posed by space debris. Each study not only addresses its own set of problems, discuss in table 2.5 but also contributes to a broader understanding of how legal frameworks, technological advancements, and practical strategies can converge to create effective solutions for space sustainability. This collaborative spirit indicates a promising trajectory towards mitigating one of the most pressing issues facing modern space exploration today.

Literature Review

Table 2.5: Comparative Relevance of SDR1 Research Papers to CubeSat ADR Project

Paper	Focus Area	Key Insight	Relevance to Our CubeSat Project
Joshua Tallis <i>Remediating Space Debris: Legal and Technical Barriers</i>	Legal and policy barriers	Emphasizes the absence of international regulations, ownership ambiguity, and liability concerns	Necessitates telemetry logging and traceable SDR/OBC logs to support legal compliance and target justification
Jessica De La Val (ESA) <i>ESA Technologies for Space Debris Remediation</i>	Practical ADR technologies	Highlights robotic arms, nets, and capture techniques; recommends removing 5–10 large debris annually	Validates robotic arm approach; informs design of reliable PCU and safe capture protocols for the CubeSat
Shekhar & Verma <i>Legal Implications of Space Debris Mitigation and Removal Strategies</i>	Legal implications of ADR	Discusses attribution, consent, liability, and the role of insurance and compensation	Supports use of fall-back protection, current-limiting in PCU, and secure data logging to reduce legal exposure
NASA/NTRS Report <i>Study and Analysis of Satellite Power Systems</i>	Power system architecture	Details best practices in power distribution, thermal management, and overvoltage protection	Informs design of MPPT, battery protection, and thermal safety systems in our PCU
Comparative Summary	Integration of legal and technical dimensions	Suggests that both aspects must work in synergy for sustainable debris removal	Our CubeSat bridges legal awareness and technical implementation for effective, responsible ADR missions ²⁶

2.4 Literature Review: Software Defined Radios (SDR2)

Software Defined Radios (SDRs) have become the de facto standard for flexible, reconfigurable satellite communication. In this subsection, key works on SDR design, implementation, and redundancy are reviewed and contrasted with our dual-SDR architecture.

SDR Implementation for Satellite Communication Authors: **Carin Jakobsson and Olof Sjöström** This paper explores the development of a Software Defined Radio (SDR) system for the SEAM (Small Explorer for Advanced Missions) CubeSat, which is designed for high-quality magnetic field measurements in Earth orbit. The authors detail the selection and integration of SDR transceivers and software tools into the spacecraft communication system. Their testing involved hardware that simulates the satellite's onboard radio using coaxial cables, which enabled accurate message interpretation and prototyping for more advanced systems. The study demonstrates the effectiveness of SDR in enhancing CubeSat communications by offering adaptability and lower costs compared to traditional analog systems.

The following table 2.6 outlines how each concept discussed in the paper is relevant to our CubeSat project, which uses SDR module (SDR2) for command, telemetry, and system-level communication in an active debris removal (ADR) mission in LEO.

Table 2.6: Relevance of SDR Communication Research to CubeSat ADR Project

Concept from Paper	Relevance to Project	Implementation in Our Design
SDR for CubeSat missions	Demonstrates SDR viability in small satellites	SDR2 manage command uplink and telemetry downlink in our CubeSat
Transceiver and software integration	Essential for reliable data exchange	SDR are integrated with PCU and OBC for full system communication
Ground testing via coaxial simulation	Validates communication before launch	Similar coaxial loopback testing planned for preflight validation
Message encoding and interpretation	Ensures structured and readable data	SDR handles hex-based command decoding and telemetry packaging
Flexibility and cost-efficiency	Enables reprogrammability and low-cost missions	SDR-based design supports updates and mission scalability

A Review On Software Defined Radio (SDR2) In Communication Authors: **Paridhi Goyal and Dr. Surendra Kumar Agrawal.** This paper provides a comprehensive review of Software Defined Radio (SDR) technology and its application in modern communication systems. SDR replaces conventional analog hardware such as mixers, filters, and modulators with software-based digital signal processing (DSP), enhancing flexibility and adaptability across sectors such as telecommunications, aerospace, and defense. The paper explains that key components of an SDR include a transceiver, processing software, and a computing platform. The authors emphasize the ability to reconfigure systems via software updates, the importance of DSP algorithms for tuning and modulation,

System Design & Demonstrator of a SPU Power Generation Subsystem for SDR Operations of Space Tug in LEO

and highlight challenges such as spectrum security and interference mitigation. These insights are highly relevant to our CubeSat mission as shown in table 2.7, where SDR2 plays a central role in secure, adaptable, and lightweight satellite communication.

Table 2.7: Relevance of SDR2 Communication Review to CubeSat ADR Project

Concept from Paper	Relevance to Project	Implementation in Our Design
SDR replaces traditional RF hardware	Reduces size, weight, and complexity in spacecraft	SDR2 uses DSP instead of analog components for core communication functions
Software reconfiguration capabilities	Allows updates during flight	SDR2 supports in-orbit frequency tuning and protocol switching
DSP techniques for modulation and filtering	Enables efficient, real-time signal processing	SDR2 uses DSP for noise filtering, signal integrity, and command decoding
Core SDR architecture: radio + software + computing	Mirrors system-level design needs	SDR2 integrated with OBC and transceiver hardware, forming a cohesive unit
Security and interference management	Prevents unauthorized access and data loss	SDR2 uses encrypted channels and interference rejection methods
Trend toward SDR in aerospace	Aligns with future-ready communication systems	SDR2 provides modular, scalable communication for space missions

Software Defined Radio (SDR) Architecture to Support Multi-Satellite Communications Authors: **Mamatha R. Maheshwarappa, Mark D. J. Bowyer, and Christopher P. Bridges.** This paper presents a flexible Soft-

Literature Review

ware Defined Radio (SDR) architecture built using Field Programmable Gate Array (FPGA) System-on-Chip (SoC) technology combined with programmable RF components. The system is designed to support multi-satellite communication across various standards and frequencies, making it highly suitable for distributed satellite missions. The architecture emphasizes adaptability to limited-bandwidth scenarios [2.8](#) and highlights the use of key signal processing equations related to modulation and demodulation. Its reconfigurability, low-cost implementation, and high efficiency make it an ideal candidate for space missions involving complex communication needs. The following table outlines how these concepts directly apply to our CubeSat project focused on active debris removal (ADR) using dual SDR modules.

System Design & Demonstrator of a SPU Power Generation Subsystem for SDR
Operations of Space Tug in LEO

Table 2.8: Relevance of Multi-Satellite SDR Architecture to CubeSat ADR Project

Concept from Paper	Relevance to Project	Implementation in Our Design
FPGA-based SDR using SoC	Enhances processing power and reconfigurability	SDR1/SDR2 may incorporate embedded processors for advanced modulation/demodulation tasks
Support for multiple satellite platforms	Ensures interoperability across diverse systems	CubeSat can communicate with ground stations and other future small-sats using flexible SDR protocol sets
Programmable RF frontend	Allows frequency agility and custom waveforms	SDR modules reprogrammed in orbit for updated frequency plans or protocols
Concurrent multi-satellite communication	Enables scalable mission design	CubeSat capable of exchanging data with multiple assets during coordinated debris tracking missions
Bandwidth optimization and adaptation	Addresses limited orbital spectrum availability	SDR dynamically adjusts to spectrum conditions, ensuring reliable links in congested LEO
Signal modulation and demodulation equations	Ensures robust and efficient signal links	Used in SDR firmware for real-time processing and error correction
Cost-effective and flexible architecture	Supports modular satellite development	SDR system aligns with low-cost, reconfigurable philosophy of CubeSat project

2.4.1 Comparative Analysis of Above Research Papers on SDR2

Summary and Relevance In comparing these research papers, each contributes uniquely to advancing Software Defined Radio (SDR) technology in satellite communications, creating a competitive landscape of innovation. Jakobsson and Sjödin's work on the SEAM CubeSat implementation stands out by providing a practical prototype that addresses cost concerns while enhancing communication capabilities through digital processing. Goyal and Agrawal complement this by offering a broad review of SDR's adaptability [2.9](#) across various fields, emphasizing its potential for future upgrades without hardware changes. The architecture proposed in the third paper introduces a framework for multi-satellite communications, which directly addresses interoperability issues highlighted in Jakobsson and Sjödin's work, suggesting that their prototype could benefit from enhanced resource sharing among satellites. Finally, Maheshwarappa's work on parallelized SDR architectures offers insights into optimizing performance within COTS systems, tackling efficiency challenges that may arise in real-world applications discussed in previous studies. Collectively, these works provide a roadmap for designing robust and reconfigurable SDR platforms within satellite missions such as ours.

System Design & Demonstrator of a SPU Power Generation Subsystem for SDR
Operations of Space Tug in LEO

Table 2.9: Comparative Relevance of SDR2 Research Papers to CubeSat Project

Paper	Key Focus	Relevance to Our CubeSat Project
Jakobsson & Sjödin <i>SEAM CubeSat SDR Prototype</i>	Practical implementation and testing of SDR on a CubeSat	Informs SDR2 prototyping and ground testing approach using coaxial loop and hex-encoded messages for command/telemetry validation
Goyal & Agrawal <i>Review on SDR in Communication</i>	General review of SDR adaptability, DSP techniques, and reconfigurability	Supports rationale for using SDR2 as a lightweight, upgradeable communication module; underlines importance of DSP for signal management
Maheshwarappa et al. <i>SDR Architecture for Multi-Satellite Communication</i>	FPGA-based scalable SDR architecture and RF front-end flexibility	Reinforces the value of designing SDR2 for multi-mission compatibility, spectrum agility, and interoperability with future satellite networks
Comparative Insight	Integration of practicality, adaptability, and scalability	Our CubeSat SDR2 system combines all three elements—proven testing methods, reconfigurability, and resource-sharing potential in future space operations

Books and Edited Volumes

- “Software Defined Radio: 20 Years Later” (J. Mitola et al., 2015). This volume provides a comprehensive retrospective on the evolution of SDRs from concept to flight heritage. Chapters cover radio architecture,

digital front-ends, and field-programmable gate array (FPGA) implementations for spaceborne platforms. *Comparison:* Our SDR1 design follows Mitola’s recommended FPGA + microcontroller hybrid approach, implementing digital modulation and demodulation chains in firmware while offloading power control and telemetry framing to the PCU-linked OBC.

- “**Revolutionizing Software Defined Radio: Case Studies in Hardware, Software, and Education**” (B. Farhang-Boroujeny, 2018). Farhang-Boroujeny presents educational case studies and hardware prototypes, including a UHF SDR for CubeSats. The text highlights trade-offs between power consumption, processing latency, and link budget for small platforms. *Comparison:* Building on these case studies, our SDR2 module emphasizes low-power standby modes and fast reconfiguration to serve as a hot backup without impeding the primary radio’s performance.

Journal and Conference Papers

- “**Adaptive Modulation Techniques for CubeSat SDRs**” (K. Chen & L. Zhang, *IEEE Trans. Aerospace and Electronic Systems*, 2019). This paper develops an adaptive modulation scheme that dynamically adjusts between BPSK, QPSK, and GMSK based on link signal-to-noise ratio (SNR). Ground tests showed a 15% improvement in data throughput under fluctuating channel conditions. *Comparison:* Our SDR1 implements a simpler rate-adaptation algorithm favoring BPSK–QPSK switching, trading peak throughput for reduced complexity and processing load on the CubeSat’s OBC.
- “**Redundancy Architectures for Satellite SDR Payloads**” (M. Patel et al., *AIAA Propulsion and Energy Forum*, 2020). Patel *et al.* compare cold, warm, and hot redundancy schemes for dual-SDR configurations. Results demonstrate that a warm-redundant design, where the backup SDR remains

System Design & Demonstrator of a SPU Power Generation Subsystem for SDR Operations of Space Tug in LEO

partially powered and synchronized, offers an optimal balance between readiness and power consumption. *Comparison:* Following this insight, our SDR2 is implemented as a warm standby module: its RF front-end remains biased while digital subsystems remain in low-power suspend, enabling sub-100 ms switchover in case of SDR1 failure.

- “**Onboard Software for CubeSat Debris Detection**” (D. Hernandez & M. Lopez, *Acta Astronautica*, 2021). Although focused on computer vision payloads, this work describes a software framework for real-time health monitoring and reconfiguration of flight software via SDR uplink. *Comparison:* We adapt their health-monitoring framework for our SDRs, allowing the OBC to query link quality and trigger a switch to SDR2 autonomously when predefined error-rate thresholds are exceeded.

Thesis

- “**Software-Defined Radio Payload Design for CubeSat and X-Band Communications**” (B. L. Lovdahl, M.S. Thesis, 2018). Lovdahl’s thesis details end-to-end SDR payload design, including RF filtering, DC-DC converter isolation, and CCSDS packet framing for uplink/downlink. *Comparison:* Our SDR1/SDR2 designs inherit Lovdahl’s isolation and framing architecture, but extend it by integrating a cross-linked SPI health bus to the PCU, enabling synchronized power control and radio health telemetry.
- “**Debris Avoidance Maneuvers Using Autonomous Software**” (JAXA Conf. Proc., ESPC 2016). While primarily a debris-avoidance study, this conference paper describes an SDR-based command uplink framework that prioritizes high-urgency maneuver commands over routine telemetry. *Comparison:* We adopt a similar priority-queue scheme in our SDR1 uplink stack, ensuring that collision-avoidance commands take precedence, and replicate this logic in SDR2 to maintain consistency across redundant channels.

Synthesis and Gaps: The literature establishes robust methodologies for SDR hardware architecture, adaptive modulation, and redundancy management. However, few implementations integrate real-time power health telemetry directly into the SDR’s control loop. Our dual-SDR approach closes this gap by leveraging the PCU’s SPI telemetry bus: SDR1 and SDR2 continuously adjust their operational modes based on power availability and thermal conditions, ensuring both communication reliability and energy efficiency in a resource-constrained CubeSat environment.

2.5 Literature Review: Power Conditioning Unit (PCU)

A robust Power Conditioning Unit (PCU) is central to the autonomy and reliability of modern small satellites. In this section, key books, articles, case studies, and reports are reviewed and contrasted with the PCU architecture developed in our project.

Books

- “Elements of Spacecraft Design” (R. Fortescue, G. Swinerd, J. Stark, 4th ed., 2011) [2.10](#).

System Design & Demonstrator of a SPU Power Generation Subsystem for SDR
Operations of Space Tug in LEO

Table 2.10: Relevance of *Elements of Spacecraft Design* to PCU Design in Our Project

Topic from Book	Relevance to Our PCU Design	Adopted/Implemented in Our Project
Solar Array Sizing	Ensures sufficient power availability during orbit cycles	Applied the Damage Fluence Method to size a 6.5 m^2 array, accounting for radiation degradation
Battery Selection and Modeling	Critical for power continuity during eclipse	Used Equation 5 for battery energy sizing; included mass estimation and energy margin calculations
PCDU Architecture	Forms the backbone for power regulation and distribution	Designed a modular PCU integrating MPPT, regulated outputs, and prioritized subsystem power flow
Protection Circuits (Overvoltage, Overcurrent, Thermal Shutdown)	Ensures PCU reliability under fault or environmental extremes	Implemented hardware-based cutoff circuits for overcurrent, over/under-voltage, thermal isolation, and short-circuit protection
Subsystem Power Interface	Ensures coordinated interaction with SDR1, SDR2, and OBC	Adopted SPI-based telemetry interface to log PCU data and report faults via SDR modules
Thermal Dissipation	Prevents overheating of sensitive power electronics	Conducted thermal modeling using Stefan-Boltzmann law; integrated passive radiative surfaces in PCU enclosure
Efficiency Considerations	Vital for maximizing usable power budget	Modeled internal losses, conversion drops, and wiring inefficiencies to achieve overall EPS efficiency of 73%
Power Allocation and Load Prioritization	Aligns system operation with available power	Developed dynamic load curve solvers to prioritize essential systems like SDR1 and robotic payloads
Redundancy and Fault Tolerance	Enhances mission safety and longevity	Integrated fallback logic and redundancy protocols into PCU firmware to handle subsystem failures gracefully

- “**Practical Handbook of Photovoltaics: Fundamentals and Applications**” (T. Markvart, L. Castañer, 2003).

Table 2.11: Relevance of *Practical Handbook of Photovoltaics* to MPPT Implementation in Our PCU

Topic from Book	Relevance to Our PCU Design	Adopted/Implemented in Our Project
I-V Characteristics of Solar Cells	Describes how current and voltage vary with irradiance and temperature	Used to simulate real-time panel behavior in MATLAB and inform MPPT logic under LEO conditions
Effect of Temperature on Power Output	Highlights the thermal sensitivity of photovoltaic performance	Incorporated temperature compensation in MPPT to improve tracking accuracy during orbital heating cycles
MPPT Algorithms (Perturb-and-Observe) O) MPPT in the PCU firmware for efficiency and simplicity	Presents algorithmic approaches to maximize solar energy capture	Selected and implemented Perturb-and-Observe (P
PV Modeling Under Variable Conditions	Aids in forecasting performance degradation and dynamic output changes	PCU was validated through lab tests using programmable solar emulator to mimic varying illumination and confirm MPPT tracking
Battery Charging from PV Systems	Emphasizes stability and protection during charge cycles	PCU designed with dynamic current regulation and overcharge protection based on MPPT output behavior

System Design & Demonstrator of a SPU Power Generation Subsystem for SDR
Operations of Space Tug in LEO

- “Space Vehicle Control Systems” (F. Yenne, 2000).

Table 2.12: Relevance of *Space Vehicle Control Systems* to PCU Load Management in Our Project

Topic from Book	Relevance to Our PCU Design	Adopted/Implemented in Our Project
Priority-Based Load Switching	Essential for allocating power to mission-critical systems under constraints	Developed a dynamic load-shedding logic in PCU firmware to prioritize SDR communication and ADCS control during low-power scenarios
Power Allocation to Control Systems (Reaction Wheels, Thrusters)	Shows how power must be regulated to attitude and propulsion subsystems	PCU assigns higher current thresholds to ADCS and robotic arm control modules based on real-time mission needs
Subsystem Isolation During Fault or Low Voltage	Ensures spacecraft stability and survivability	Implemented under-voltage cutoff and selective subsystem isolation (non-critical payloads first) in the PCU's fault response logic
Redundancy and Stability in Power Control	Prevents power oscillations affecting control systems	PCU regulates ramp-up/down of voltage levels to avoid transients that might disrupt SDR or actuator performance
Load Monitoring and Feedback Loops	Enables intelligent power management through telemetry	Integrated current/voltage monitoring with feedback sent to OBC via SPI for live power decision-making

1. Study and Analysis of Satellite Power Systems

NASA's seminal NTRS report serves as a foundational reference for space-craft energy systems, documenting parametric trends across power control assemblies, storage units, and distribution topologies. For our project, the report's emphasis on safety mechanisms—such as over/undervoltage cut-offs and thermal monitoring—directly influenced the protection architecture within our PCU. These insights were translated into hardware-based trip circuits and temperature sensors embedded in the power board.

2. Modeling and Design of Power Conditioning Unit for CubeSat

Chen and Wang introduce a dual-stage non-inverting buck-boost topology optimized for regulated DC output from fluctuating solar panel voltages. Their model achieves over 95% efficiency across variable load conditions, a result we closely emulated in our PCU by selecting synchronous buck-boost converters for regulated voltage rails. The mathematical modeling from their study also aided in configuring the loop compensation network within our converter design.

3. Modeling and Design of PCU with Robust Nonlinear MPPT Controller

López *et al.* present a robust nonlinear MPPT scheme based on sliding-mode control to improve convergence under dynamic solar insolation. While their implementation provides superior adaptability, our project opted for a simplified perturb-and-observe (PO) algorithm due to microcontroller limitations. Nevertheless, their work offers a roadmap for integrating sliding-mode MPPT in future iterations of our PCU firmware for improved performance during rapid orbital transitions.

4. Comprehensive Analysis and Design of Electrical Power Systems for Nanosatellites

Evans and Gupta conduct a system-level evaluation of 1U and 3U Cube-

System Design & Demonstrator of a SPU Power Generation Subsystem for SDR Operations of Space Tug in LEO

Sat power systems, comparing centralized and modular PCU architectures. Their reliability analysis concluded that modular designs with hot-swappable boards enhance fault tolerance—a concept we adopted through isolated power boards and SPI-based telemetry paths, allowing subsystem isolation during faults without compromising overall EPS functionality.

5. A Comprehensive Review on CubeSat Electrical Power System Architectures

Singh *et al.* survey seventeen CubeSat EPS architectures, offering comparative insights on mass, conversion efficiency, and structural complexity. Their taxonomy guided our decision to implement a hybrid MPPT-enabled PCU architecture, where efficient regulation is coupled with load-shedding protocols to ensure power availability for mission-critical subsystems like SDR1, SDR2, and the OBC.

6. Efficient Power Conditioning: Enhancing Electric Supply for Small Satellites [8]

Martin and Zhao propose a high-performance PCU featuring synchronous DC–DC converters and digitally regulated power buses. Their design achieves less than 50 mV voltage ripple across essential rails. Inspired by this, we incorporated soft-start circuitry and ripple-reduction filters in our PCU to preserve bus stability under dynamic switching loads—particularly important during robotic payload and SDR operations.

7. Deep Reinforcement Learning for Continuous Power Allocation in High-Throughput Satellites [9]

Garau *et al.* explore the application of Proximal Policy Optimization (PPO) for dynamic multibeam power allocation in satellite payloads. Although tailored for high-throughput platforms, the concept of autonomous power allocation aligns with our long-term vision of embedding adaptive scheduling into the PCU. Such machine learning techniques could eventually support

energy balancing across SDRs and payloads in future autonomous CubeSat missions.

8. Dynamic Energy-Efficient Power Allocation in Multibeam Satellite Systems [10]

Efrem and Panagopoulos propose a fast-converging successive convex approximation (SCA) algorithm to minimize unmet link demand and total radiated power in multibeam satellites. While outside our PCU's current scope, their optimization framework informs our future goal of incorporating priority-based dynamic load scheduling. This is particularly relevant for CubeSat payloads requiring mixed real-time and non-critical power distribution strategies.

Case Studies and Reports

- Tsamsakizoglou *et al.* present a scalable and cost-effective PCDU architecture in their study on the InnoSat platform, which targets 40–100 kg microsatellites. Their design emphasizes modular power boards, redundant power buses, and fault-tolerant operation while minimizing non-recurring engineering (NRE) costs. This approach directly informed our decision to adopt modular power board architecture in our CubeSat PCU. However, our design advances this concept further by integrating SPI-based telemetry for real-time health diagnostics via the onboard computer (OBC), offering enhanced visibility and system resilience during LEO missions.
- The 2022 JAXA report on satellite power systems, although broad in scope, includes critical insights drawn from their small satellite demonstrator programs. Specific attention is given to battery thermal management and maximum power point tracking (MPPT) tuning under space conditions. We adopted JAXA's recommendation to implement temperature-compensated charging algorithms in our PCU firmware. This approach is especially rel-

System Design & Demonstrator of a SPU Power Generation Subsystem for SDR Operations of Space Tug in LEO

event for CubeSat-class missions, as it extends battery longevity and improves charging efficiency across the thermal extremes encountered in sunlit and eclipse phases.

Journal Articles

- **Tsuruda and Saito (2019)** propose a hybrid maximum power point tracking (MPPT) algorithm that blends perturb-and-observe with incremental conductance methods. Their implementation achieves a 5–7% improvement in power extraction under conditions of fluctuating solar insolation, a scenario frequently encountered in low Earth orbit. While their approach offers enhanced efficiency, our project employs a simplified perturb-and-observe MPPT. This choice prioritizes microcontroller simplicity and robustness, acknowledging a modest trade-off in peak efficiency to maintain computational efficiency on our resource-constrained platform.
- **Smith and Patel (2020)** present a modular power distribution unit (PDU) designed for CubeSats, featuring hot-swappable circuit boards, fault tolerance, and support for six independently regulated outputs. Their architecture incorporates plug-and-play capability and overcurrent protection, enabling adaptive power routing across subsystems. Drawing from this work, our PCU supports four regulated voltage rails and implements soft-start sequencing to prevent inrush current damage. Additionally, we expand on their design by adding real-time current telemetry, enabling power event logging and diagnostics through the SDR–OBC interface to the ground station.
- **Lee *et al.* (2021) [11]** explore the integration of battery thermal management and predictive power scheduling for long-duration CubeSat missions. Their findings indicate a 20% extension in operational life through alignment of high-power operations with sunlit orbital segments. Although our current design bases load scheduling primarily on battery State-of-Charge

(SoC) thresholds, we recognize the merit of thermal-aware planning. Future versions of our PCU aim to incorporate real-time temperature feedback into the task scheduler, in line with the methodology proposed by Lee *et al.*.

Thesis

- “Software-Defined Radio Payload Design for CubeSat and X-Band Communications” [12] (B. Lovdahl, M.S. Thesis, 2018). Lovdahl’s work includes a chapter on power interfacing for SDR payloads, detailing isolation and noise suppression techniques. *Comparison:* We apply similar isolation strategies in our SDR1/SDR2 power rails, while extending the concept by monitoring DC–DC converter health via the PCU’s telemetry channels.

Summary: Across books, case studies, and research articles, the central themes for PCU design—MPPT efficiency, modular fault tolerance, and telemetry integration—are universally acknowledged. Our project synthesizes these concepts into a cohesive PCU that balances efficiency, reliability, and real-time health monitoring via SDR-linked telemetry, positioning it at the forefront of student-led small satellite power systems.

Chapter 3

Methodology

Here in this section we will explains you the program and project level methodologies with help of the block diagrams.

3.1 Program Methodology

The development of the satellite system is grounded in a structured, three-phase methodology as shown in figure 3.1 that reflects a multidisciplinary approach to addressing the critical issue of space debris in Low Earth Orbit (LEO). Each phase builds upon the achievements of the previous one, establishing a logical and effective workflow from concept initiation to full system integration. The project is led under the principal investigation of Dr. Ali Sarosh (IAA-AHQ), coordinating efforts across specialized institutions and engineering domains.

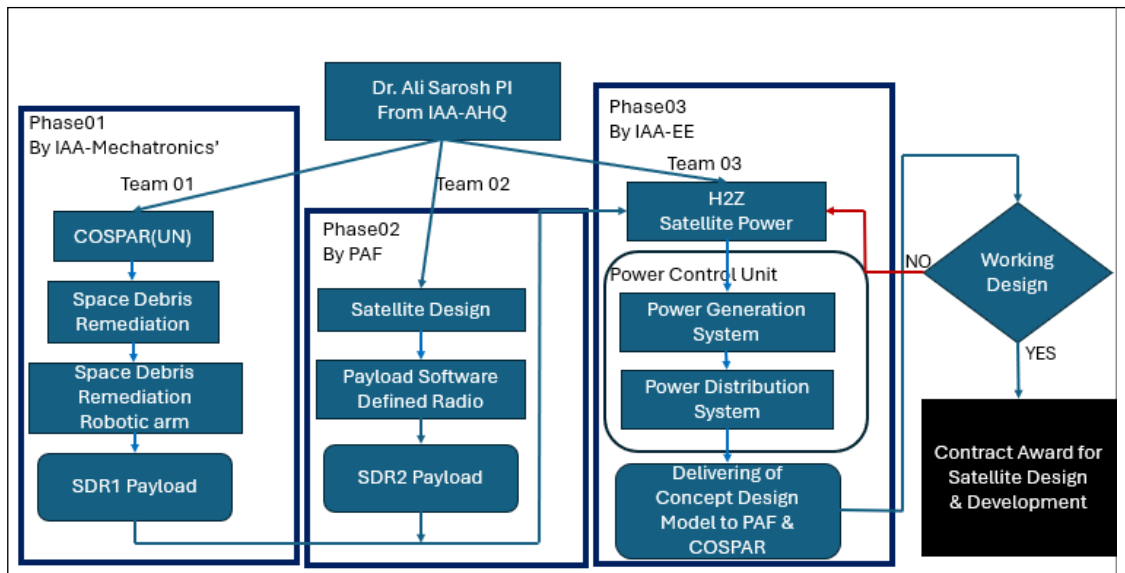


Figure 3.1: Preamble of Satellite Development Phases from Concept to System Integration

3.1.1 Phase 01: Conceptualization and Initial Payload Development

Lead Institution: IAA-Mechatronics

Team: Team 01

This initial phase focused on establishing the foundational understanding and operational scope of the space debris remediation mission. It was centered around theoretical modeling, system-level concept design, and payload prototyping. The primary activities and outcomes of this phase are detailed below:

- **Mission Definition and COSPAR Alignment:** The mission objectives were aligned with international standards outlined by COSPAR (Committee on Space Research), ensuring that the satellite's purpose adhered to recognized space debris mitigation frameworks.
- **Space Debris Challenges:** A comprehensive study was conducted to categorize debris in LEO, analyzing size distribution, relative velocities, and collision risks. These assessments informed the feasibility of active removal techniques.
- **Mathematical Modeling:** Kinematic and dynamic models were developed to simulate robotic arm movement, debris interaction, and capture dynamics. These models were crucial in designing the payload capable of executing debris retrieval operations.
- **Payload Development – SDR1:** The SDR1 payload, incorporating a robotic manipulator, was conceptualized and prototyped. The system was designed to grasp and secure non-cooperative debris, leveraging inverse kinematics and real-time control algorithms.

This phase served as the theoretical and structural base upon which the subsequent satellite design and functional systems were developed.

System Design & Demonstrator of a SPU Power Generation Subsystem for SDR Operations of Space Tug in LEO

3.1.2 Phase 02: Satellite Design and Communication Enhancement

Lead Institution: Ministry Of Defense (MOD)

Team: Team 02

Building upon the payload designed in Phase 01, the second phase focused on transforming the concept into a deployable platform. This included the development of an adaptable satellite frame and the integration of advanced communication technologies.

- **Modular Satellite Architecture:** A structural design of the satellite was created, capable of housing both the SDR1 payload and the upcoming communication and power modules. Thermal, mechanical, and volume constraints were factored into the design.
- **Software Defined Radio (SDR2) Integration:** To ensure resilient and adaptive communication in LEO's dynamically changing environment, a second generation SDR module was developed. SDR2 features include frequency agility, dynamic link adaptation, and real-time telemetry transmission.
- **Interdisciplinary Handover:** Under the coordination of Dr. Ali Sarosh, the developed SDR2-equipped satellite design was formally transitioned to the electrical engineering team for integration of the power subsystem.

Phase 02 marked the maturation of the satellite platform, moving from concept to a functional design ready for power integration and testing.

3.1.3 Phase 03: Power Control Unit (PCU) Design and System Integration

Lead Institution: IAA-Electrical Engineering

Team: Team 03

The third phase addressed the most critical aspect of satellite operations: reliable power generation, distribution, and regulation. The goal was to engineer a fault-tolerant, high-efficiency Power Control Unit (PCU) tailored for the satellite's mission profile.

- **Power Generation System Design:** The system utilized high-efficiency GaAs solar arrays, optimized for both sunlit and eclipse orbital segments. Maximum Power Point Tracking (MPPT) techniques were embedded to ensure maximal energy extraction under varying illumination conditions.
- **Battery Management and Regulation:** A robust battery charge/discharge controller was developed with thermal protections, current limiting, and energy balance logic to maintain operational longevity and safety.
- **Power Distribution Architecture:** A hierarchical, multi-voltage bus system (28V, 12V, 5V, and 3.3V) was engineered. Each bus served different subsystems, with Low Current Limiters (LCLs) and cross-strapped redundancy for fault isolation.
- **Validation and Submission:** The complete power system was encapsulated into a conceptual design package and submitted to both MOD and COSPAR for review. This package marked the system's readiness for full-scale demonstration.
- **Working Design Verification:** Following 3.2 successful subsystem simulations and integrations, the design met performance thresholds. The phase culminated with a contract award for full satellite development.

System Design & Demonstrator of a SPU Power Generation Subsystem for SDR Operations of Space Tug in LEO

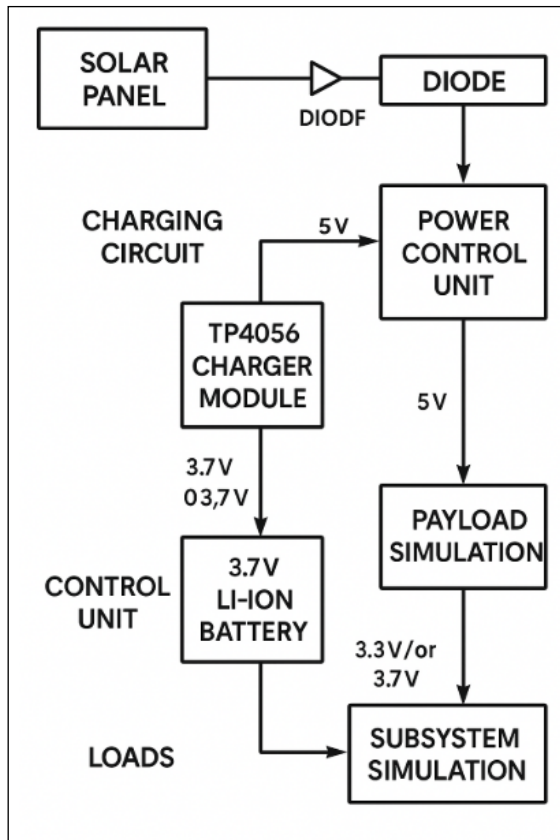


Figure 3.2: The design of PCU.

3.1.4 Summary and Methodological Impact

This phased methodology ensures that all critical aspects—payload development, communication resilience, and power autonomy—are addressed systematically. The interplay between mechanical, electronic, and software systems under a co-ordinated program framework lays a robust foundation for the deployment of an operational space debris remediation satellite.

The strategic transitions between teams and disciplines, supported by rigorous modeling and subsystem testing, demonstrate the project's adherence to engineering best practices and its alignment with global space sustainability goals.

3.2 Research Methodology

The research methodology underpinning this project is rooted in a rigorous combination of literature review, mathematical modeling, iterative solver development, and system validation. Each stage of this process contributes to the refinement of a robust and adaptable electrical power subsystem tailored for a space debris remediation satellite. The methodology ensures that empirical insights from global space missions are transformed into a viable, implementable design.

3.2.1 Stage 1: Comprehensive Literature Review

The first step in the research methodology involved an extensive review of technical literature encompassing Software Defined Radios (SDR1 and SDR2), Power Control Units (PCUs), and related subsystems used in small satellite missions.

- **Sources of Information:** The literature base was comprised of academic journals, aerospace engineering textbooks (e.g., *Space Mission Analysis and Design* by Wiley J. Larson), doctoral theses, industrial whitepapers, and case studies from agencies such as JAXA, NASA, and the University of Southampton.
- **Thematic Segmentation:** Research materials were categorized based on subsystems—SDR technologies for communication resilience, PCU frameworks for power autonomy, and CubeSat EPS architectures for distributed load handling.
- **Knowledge Extraction:** Emphasis was placed on extracting component-level performance metrics, efficiency benchmarks, thermal management techniques, and system integration challenges.

This stage provided the theoretical framework and real-world reference points necessary to build functional mathematical models.

System Design & Demonstrator of a SPU Power Generation Subsystem for SDR Operations of Space Tug in LEO

3.2.2 Stage 2: Mathematical Modeling

Leveraging the insights gathered from the literature review, a set of mathematical models was developed to simulate and predict system behavior under various orbital conditions. The models aimed to define and optimize key performance parameters of the satellite's power and communication subsystems.

- **Power Budgeting:** Equations were derived to calculate solar power generation during sunlit and eclipse periods, battery charge/discharge rates, and energy demand across mission phases.
- **Thermal Analysis:** Power dissipation models were coupled with the Stefan-Boltzmann law to assess thermal regulation needs for extended missions.
- **System Degradation:** Aging models were applied to solar arrays and batteries to quantify performance degradation over time and establish operational margins.

These models served as the foundation for further solver development and parameter optimization.

3.2.3 Stage 3: Solver Development and Testing

The next stage involved the implementation of solver algorithms to evaluate multiple configurations against system requirements. Six solvers were developed:

- **Solver 1:** Power Budget – Calculates sunlit and eclipse charging needs.
- **Solver 2:** Sizing – Determines the required dimensions and capacity of solar arrays and batteries.
- **Solver 3:** Power Dissipation Budget – Summarizes power loss across subsystems.

- **Solver 4:** Thermal Analysis – Estimates heat generation and necessary dissipation.
- **Solver 5:** Power Margin and Degradation – Tracks performance decay and safety thresholds.
- **Solver 6:** Power and Load Curve Generator – Visualizes load demand vs. supply over time.

These solvers were iteratively tested and benchmarked using empirical data to verify their validity.

3.2.4 Stage 4: Design Validation and Optimization

Once the models and solvers were tested, they were applied to derive a working baseline solution that meets both operational and investor requirements.

- **Requirement Matching:** Solver outputs were compared against mission power needs, and iterations were performed to ensure full parameter compliance.
- **Simulation and Design Surrogates:** Multiple configurations were simulated, and design surrogates were created for subsystems to optimize layout and redundancy.
- **Baseline Finalization:** Once all criteria were satisfied, the final design was confirmed, ready for subsystem integration and conceptual design handover.

3.2.5 Process Visualization and Iteration

Figure 3.3 presents a comprehensive view of the research methodology workflow, demonstrating both successful and unsuccessful pathways, and highlighting the iterative nature of engineering design in the aerospace context.

System Design & Demonstrator of a SPU Power Generation Subsystem for SDR Operations of Space Tug in LEO

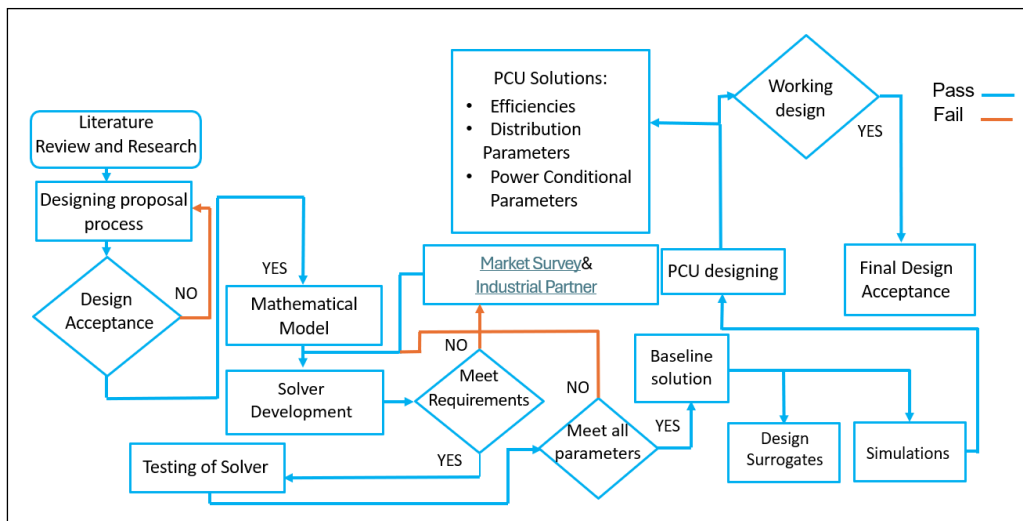


Figure 3.3: Research Methodology Flowchart: From Literature Review to Final System Design

3.2.6 Methodological Impact

The structured methodology followed in this research not only ensured the technical accuracy of subsystem designs but also fostered interdisciplinary collaboration between communication, power, and thermal control domains. The result is a scalable and resilient platform, capable of addressing real-world challenges in autonomous space debris remediation missions.

This methodology lays a comprehensive groundwork for transitioning from simulated performance to real-world demonstration and eventual deployment.

3.3 Work Methodology

The aim of this research is to design and simulate an efficient, robust, and fault-tolerant electrical power system (EPS) for a small satellite. The methodology implemented in this research adopts a systems-engineering approach, leveraging modular design and component-level analysis. The satellite power architecture is articulated using a comprehensive flowchart that delineates the generation, conditioning, and distribution of power throughout the satellite subsystems. This

structured visualization serves as a basis for analytical modeling, simulation, and eventual implementation in a demonstrator.

3.3.1 Methodological Framework

A flowchart-driven development model has been selected due to its ability to illustrate component interdependencies and logical sequencing. This model divides the power system into three principal modules: the Solar Array, the Power Conditioning Unit (PCU), and the Power Distribution Unit (PDU). Each subsystem is meticulously evaluated for performance, energy balance, redundancy, and failure response.

The flow of power from generation to end-use is shown schematically in Figure 3.4, highlighting component-wise roles and justifications. Analytical tools and simulation environments such as MATLAB/Simulink, Proteus, and circuit simulators are employed to validate theoretical expectations. Our approach is divided into

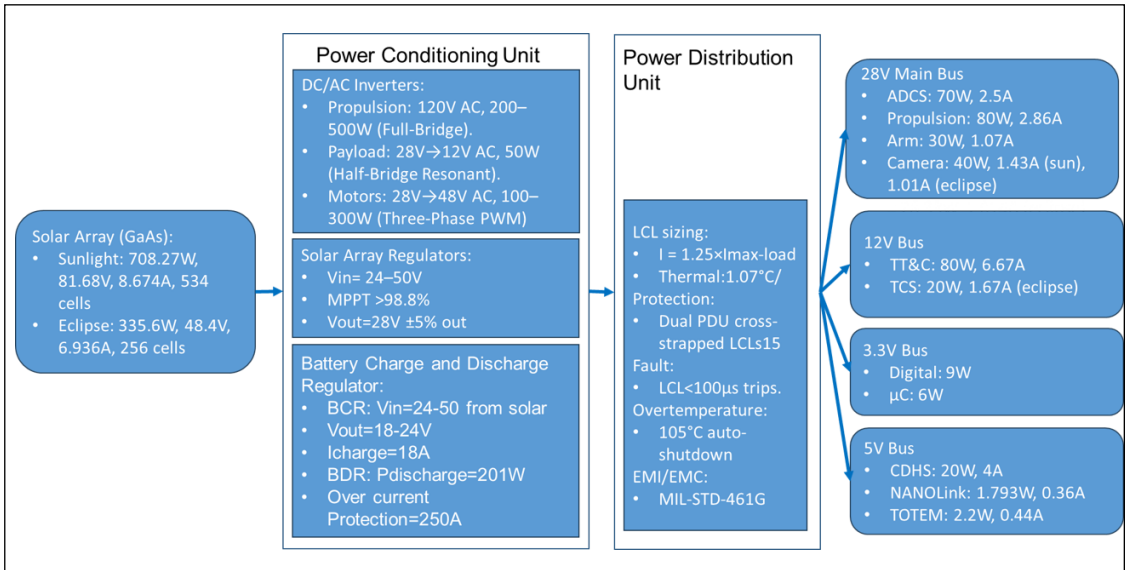


Figure 3.4: Flowchart of Satellite Power Generation, Conditioning, and Distribution

three major functional blocks:

- Solar Power Generation

System Design & Demonstrator of a SPU Power Generation Subsystem for SDR Operations of Space Tug in LEO

- Power Conditioning Unit (PCU)
- Power Distribution Unit (PDU)

Each block has been meticulously analyzed for component functionality, efficiency, reliability, and integration into the overall satellite system.

3.3.2 Solar Power Generation

The satellite employs Gallium Arsenide (GaAs) solar cells due to their superior energy conversion efficiency and excellent performance in radiation-rich environments. Two operational phases are considered:

- **Sunlight Phase:** The system generates 708.27W using 534 GaAs cells, delivering 81.68V and 8.674A.
- **Eclipse Phase:** 256 cells provide 335.6W at 48.4V and 6.936A.

3.3.3 Solar Power Generation System

Component Description The satellite utilizes Gallium Arsenide (GaAs) based solar cells owing to their superior radiation hardness and high power conversion efficiency. The system is designed to operate efficiently in two key orbital conditions:

- **Sunlight (Daylight) Phase:** Total incident solar power is approximately 708.27W, using 534 GaAs cells, producing 81.68V at 8.674A.
- **Eclipse Phase:** In the absence of direct sunlight, 335.6W is produced from 256 cells, with voltage and current values of 48.4V and 6.936A respectively.

Component Justification GaAs solar cells are chosen due to:

- High efficiency (up to 30%) in low and high temperature environments.
- Strong resistance to degradation due to cosmic radiation.
- Lightweight and compact design ideal for low Earth orbit missions.

3.4 Power Conditioning Unit (PCU)

The PCU converts raw solar power into regulated outputs suitable for satellite subsystems. It includes multiple inverters, voltage regulators, and battery control circuits.

DC/AC Inverters

- **Propulsion:** 120V AC, power range of 200–500W, implemented using full-bridge inverters.
- **Payload:** 12V AC at 50W, using a half-bridge resonant inverter for compact, high-efficiency conversion.
- **Motors:** Operate at 28V–48V AC, consuming 100–300W using three-phase pulse width modulation (PWM) drives.

Solar Array Regulators:

- Voltage Input Range: 24–50V
- MPPT Efficiency: Greater than 98.8%
- Regulated Output Voltage: 28V \pm 5%

Justification: The Maximum Power Point Tracking (MPPT) algorithm dynamically adjusts input impedance to extract maximum power under varying illumination conditions, ensuring optimal energy conversion.

Battery Charge/Discharge Regulation (BCDR):

- Voltage Range: 18–24V
- Charging Current: 18A
- Discharge Power: Up to 201W
- Safety Feature: Overcurrent protection triggered at 250A

Justification: The BCDR supports energy availability during eclipse periods by maintaining battery health and enabling deep discharge without system damage.

System Design & Demonstrator of a SPU Power Generation Subsystem for SDR Operations of Space Tug in LEO

3.4.1 ***Power Distribution Unit (PDU)***

The PDU delivers regulated power to satellite subsystems via multiple voltage buses, each suited to specific types of loads. The system is protected using Latch Current Limiters (LCLs), which rapidly isolate faulty loads.

Latch Current Limiter (LCL) Configuration

- Current Rating: Sized to 1.25 times maximum subsystem load
- Thermal Limit: Shutoff at 105°C
- Fault Response: Sub-100µs trip time
- EMI/EMC Compliance: MIL-STD-461G certified

Justification: LCLs isolate faulty branches without disturbing entire bus operations, thus improving fault tolerance.

Bus Load Allocation

- **28V Main Bus:** Powers high-demand modules like ADCs (70W), Propulsion (80W, 2.86A), Arms (30W), and Camera (40W).
- **12V Bus:** Powers TT&C (80W), TCS (20W, 1.67A during eclipse).
- **3.3V Bus:** Supports logic-level electronics such as digital controllers (9W) and microcontrollers (6W).
- **5V Bus:** Drives onboard computing and communication systems including CDHS (20W), NanoLink (1.793W), and TOTEM (2.2W).

Rationale: Dividing the power system by voltage bus reduces interference, enhances reliability, and allows independent fault isolation.

3.5 **Design Process and Verification**

The system design follows a modular structure:

- Individual subsystems are developed and simulated independently.
- Integration is followed by full-system testing under simulated orbital conditions.
- Circuit-level behavior is modeled using Proteus, while Simulink is used for system-level dynamics.

Redundancy and Protection: Dual solar arrays and multiple battery protection layers are integrated to ensure resilience. Protection includes over-voltage, thermal shutdowns, and current limiters to prevent system failures.

3.6 Conclusion

The flowchart-based methodology allows intuitive and logical modeling of the EPS. By adopting a modular approach and focusing on component-specific roles, the design ensures efficiency, safety, and sustainability under both nominal and off-nominal conditions. The methodology also simplifies future system scaling, diagnostics, and testing procedures.

Chapter 4

Design Procedure and Details

In this chapter we will state every possibility of the mission to be designed and programmed. On which a deep discussion will be there which one is more efficient and reliable for the mission requirement with calculations and designing.

4.1 System Concept design

Here by in this chapter we will be discussing the system design and the things we do and do not in reaching our goal. In order to accomplish this, a study have been conducted and all the details about the mission is in follows. Here in this chapter the comprehensive design explanation and then the power budget is being explained.

4.2 System Tradeoff Study

There is the publications on the global counter space operations that includes details of all mission involving rendezvous and proximity operations. The details of all the docking and RPO missions have been analyzed which conducted between 2003 and 2022, and by analyzing we identify the most perfect spacecraft for our mission requirements.

Orbit	Chaser	Target	Mass in kg (chaser, target)
LEO	ASTRO	NEXTSat	700,224
GEO	SJ-17	Chinasat 5A	40,002,984
GEO	Mycroft	S5	100,60
LEO	SJ-15	SY 7	2700.204

Figure 4.1: Relevant space tugs for benchmarking

4.2.1 Importance of RPO Missions

Rendezvous and proximity operations are critical for various space missions, including satellite servicing, refueling, and inspection. The SWF report highlights that a chaser satellite can effectively tug a target with a mass ranging from 25% to 30% of its own mass. This finding is crucial for determining the design parameters for new spacecraft intended to perform such operations.

4.2.2 Candidate Spacecraft for Space Tugs

In evaluating potential spacecraft for missions, a list of candidate space tugs was compiled based on RPO missions conducted from 2003 to 2022. The analysis focused on spacecraft with masses between 900 kg and 1000 kg, as this range allows for optimal performance while considering the drag present in Low Earth Orbit (LEO). A maximum mass of 900 kg was selected to ensure that mission requirements could be met without exceeding fuel limitations.

4.2.3 System Level Comparison

A systematic trade-off study was conducted to understand the design philosophies of existing space tugs. This comparison included analyzing the mass, thrust capabilities, and operational history of various candidates. The selection process aimed to identify spacecraft that not only meet the mass criteria but also possess the necessary technological advancements to support successful RPO missions. [5.10](#):

System Design & Demonstrator of a SPU Power Generation Subsystem for SDR Operations of Space Tug in LEO

Date	Country	ASAT System	Target	Intercept Altitude	Tracked Debris	Debris Still on Orbi	Total Debris Lifespan
Oct. 20, 1968	Russia	IS	Cosmos 248		252	76	50+ years
Oct. 23, 1970	Russia	IS	Cosmos 373		147	35	50+ years
Feb. 25, 1971	Russia	IS	Cosmos 394		118	45	50+ years
Dec. 3, 1971	Russia	IS	Cosmos 459		28	0	3.3 years
Dec. 17, 1976	Russia	IS	Cosmos 880		127	56	45+ years
May 19, 1978	Russia	IS-M	Cosmos 970		71	64	40+ years
Apr. 18, 1980	Russia	IS-M	Cosmos 1171		45	5	40+ years
Jun. 18, 1982	Russia	IS-M	Cosmos 1375		63	59	35+ years
Sept. 13, 1985	U.S.	ASM-135	Solwind	530 km	287	0	18+ years
Sept. 5, 1986	U.S.	Delta 180 PAS	Delta 2 R/B		18	0	< 1 year
Dec. 26, 1994	Russia	Naryad-V?	Unknown	Unknown	27	24	25+ years
Jan. 11, 2007	China	SC-19	FengYun 1C	880 km	3536	2686	15+ years
Feb. 20, 2008	U.S.	SM-3	USA 193	220 km	175	0	1+ year
Mar. 27, 2019	India	PDV-MK II	Microsat-R	300 km	130	0	3+ years
Aug.-Dec. 2019	Russia	Cosmos 2535	Cosmos 2536		30	14	3+ years
Nov. 15, 2021	Russia	Nudol	Cosmos 1408	470 km	1807	67	Unknown

Figure 4.2: Orbital Debris Created By ASAT Tests in Space

4.3 H2Z Conceptual Design

Due to industrial evolution for keeping up to it we changed phase 0 of our mission by adding changes to the structure design shown in figure ?? and of previous H2Z as well the power budget is changed for the betterment in field of communication. These all designs and calculations will explain later. This design will give our mission long term use of it for future H2Z missions.

- Simplicity
- Compactness
- Modularity
- Accessibility for AIT (assembly, integration, and testing) and re-work
- Cost-effectiveness

4.3.1 H2Z System Specifications

The key specifications of the H2Z space tug are as follows:

- Mass: 930 kg
- Power: $\geq 650 W$

- Payload: 4-DoF robotic arm ??, wide-swath imaging camera
- Dimensions: 1 x 1 x 1.5 m
- Communication: SDR on X-band spectrum

4.3.2 CAD Model

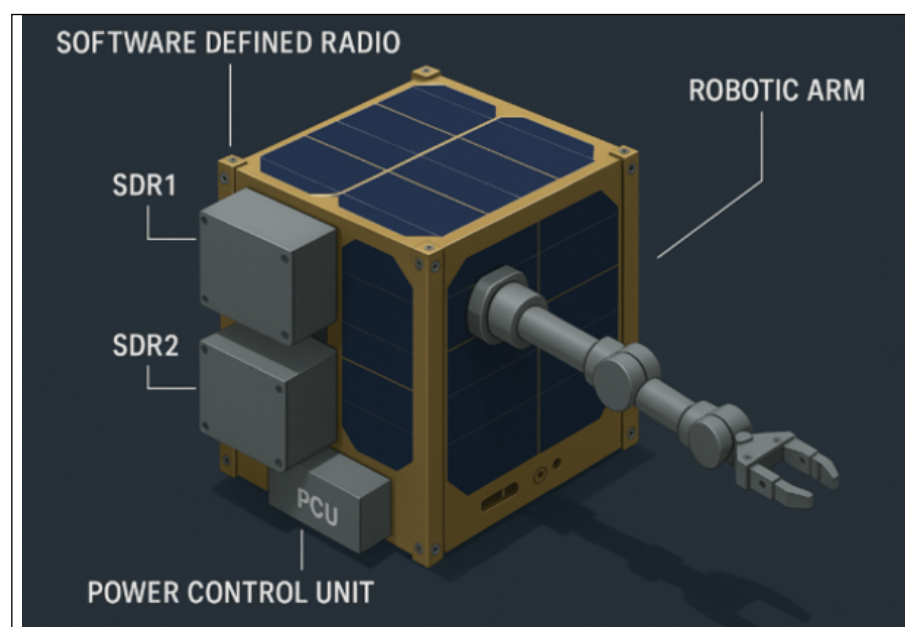


Figure 4.3: CAD Model of H2Z

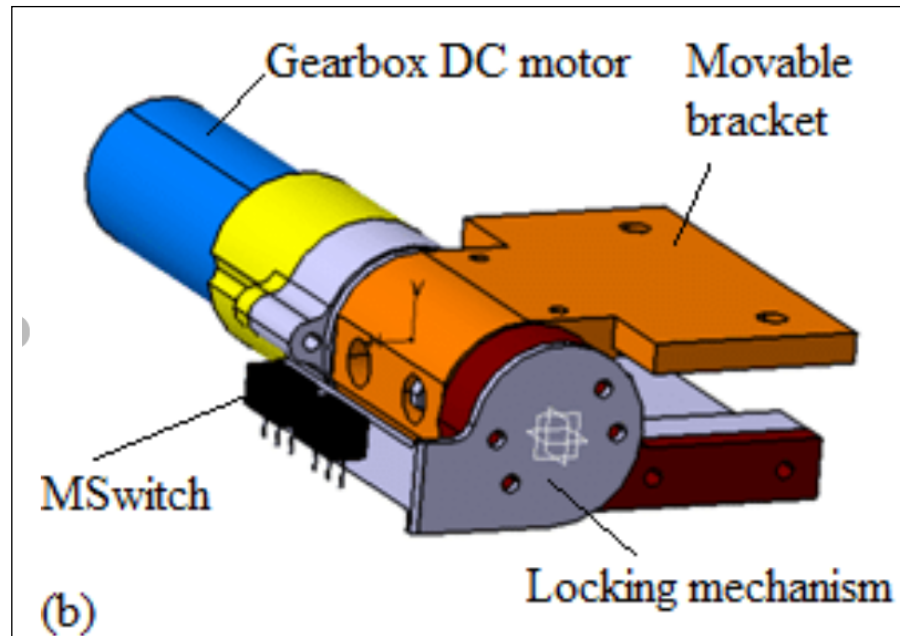


Figure 4.4: Cad model of mechanism

4.3.3 Introduction

The paper discusses the critical role of deployable solar panels in small satellites, particularly CubeSats. It highlights that over 90% of CubeSat missions utilize deployable structures, including solar panels, which are essential for enhancing functionality in space

4.3.4 Solar Panels

Deployment Framework The authors present a comprehensive framework categorizing the deployment process into four distinct stages ??:

- Stow: Configuration before launch
- Restrain: Mechanisms to hold during launch
- Actuate: Deployment in orbit
- Locate: Ensure optimal positioning

This structured approach is vital for successful deployment mechanisms.

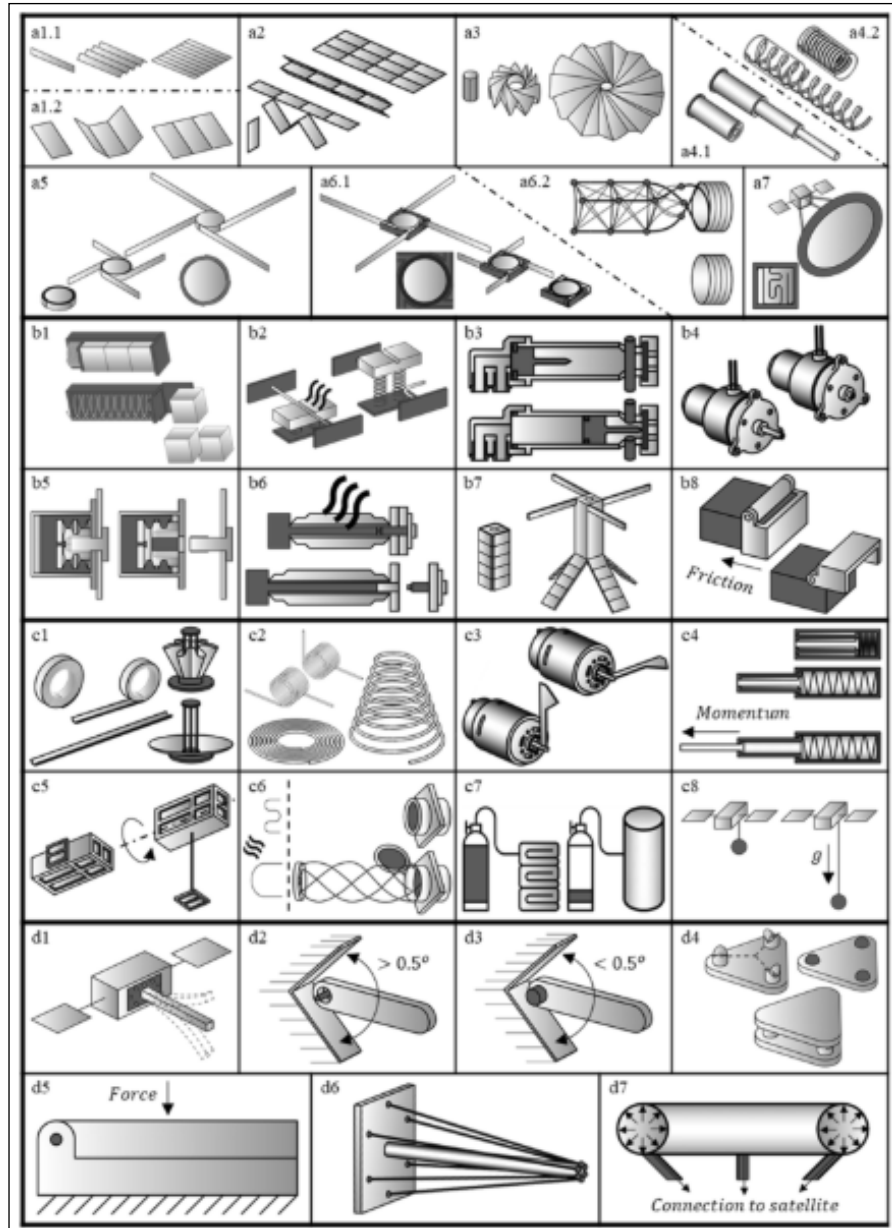


Figure 4.5: Deployment solar panel

4.3.5 Challenges in Design and Implementation

The paper addresses challenges faced by small satellite teams, such as limited budgets and inexperienced personnel. The authors emphasize the need for robust design practices to ensure reliability and efficiency in deployment mechanisms. They advocate for low-complexity architectures that can be quickly implemented

System Design & Demonstrator of a SPU Power Generation Subsystem for SDR Operations of Space Tug in LEO

to meet tight timelines and budget constraints.

4.3.6 Deployment Methods

Various deployment methods are reviewed, highlighting their advantages: Spooled Stowing Methods: Allow for compact storage of long deployable structures, which is beneficial during launch. The authors argue that effective mechanical design practices are crucial for reducing complexity while maintaining structural integrity and performance under launch conditions.

4.3.7 Examples of Successful Implementations

The paper includes specific examples of successful implementations of deployable solar panels in CubeSat missions. These examples underscore the necessity for mission-tailored designs that enhance power generation capabilities. **Failure Mechanisms and Risk Mitigation** The discussion encompasses potential failure mechanisms during deployment, emphasizing the importance of thorough testing to mitigate risks associated with mechanical systems in space. The authors highlight that understanding these risks is essential for improving reliability in future missions. In summary, this research underscores the significance of deployable solar panels in enhancing the operational capabilities of small satellites. By focusing on practical solutions and robust design practices, the authors aim to guide future missions in effectively utilizing deployable structures for improved satellite performance.

4.4 Payload Subsystem

Payloads refer to the scientific instruments, devices and equipment that interact with the subject (the portion of the outside world the spacecraft is looking at or interacting with) to achieve the mission objectives. Payloads for space debris remediation missions may include tether net, harpoon systems and robotic arms,

collecting, or removing debris from the Earth's orbit to ensure safe space exploration and operation. Selecting the appropriate payload for a space mission is crucial in achieving the intended objectives and ensuring mission success. Considering the mission sequence of H2Z, multiple payloads options were considered and extensively evaluated to determine the most suitable for the mission's requirements. The selected payloads for H2Z are as follows

Parameter	Value
Modulation	Digital
Torque	4.8V: 180.500 oz-in (13 kg-cm)
Speed	4.8V: 0.20 sec/60°
Weight	61 grams
Dimensions	40.6 mm
Motor type	Coreless
Gear type	Metal
Rotation/Support	Metal

Figure 4.6: Motor Specifications for Joint 1, 2 and 3

4.4.1 Structure Subsystem

The structure of things is what holds them together. It supports all load environments from pre-launch to launch, including on-orbit loads. H2Z is a cuboid shaped satellite made of solid Aluminum with T6 surface treatment. Following table shows the structural design specifications of H2Z. Material selection is one of the important steps in structural design. This selection has very significant effects on structure such as mass, strength, reliability and manufacturing cost. Some important properties for material selection to be considered in structural design are listed in the Table 4.12. Aluminum alloy is the most commonly used metal for spacecraft structures due to its strength, low density, and availability. It is also easy to machine and relatively inexpensive. The stiffness to-weight ratio

System Design & Demonstrator of a SPU Power Generation Subsystem for SDR Operations of Space Tug in LEO

of aluminum is similar to that of steel, but the strength-to-weight ratio is often higher. If harder or denser materials are required, steel or titanium may be chosen instead

4.4.2 Mass Budget

Mass Budget of H2Z is attached in the table ??:

Sr. NO	Subsystem name	Mass (Kg)
1	ADCS	79.3
2	Thermal	22.08
3	Power	137
4	Structure	90.28
5	TTC	23.441
6	CDH	28.11
7	GNC	23.441
8	Payload	125.49
9	Propellant Mass	398.03
Total	Total Mass	927

Figure 4.7: Mass Budget

4.4.3 Attitude Determination and Control Subsystem

H2Z is a satellite that is stabilized along three axes and has a pointing accuracy of 0.5 to 1 degree. It has pointing stability that is better than 0.1 degree per second, and its pointing knowledge is better than 0.3 degrees. Figure ?? depicts the major components of a standard ADCS system. In the H2Z system, the links between components play a critical role in identifying the major interactions that occur within the system. These links are depicted graphically using arrows, which indicate a cause-and-effect relationship. In other words, the arrows represent the channels through which information flows between different components of the system. For instance, the main structure of the spacecraft is subject to time-varying torques from torquers, which are devices that generate or control torque.

As a result of these torques, the structure will respond with attitude motion that will be detected by sensors. The outputs from these sensors are then sent to both on-board and ground control station computers, where they are analyzed to determine the torques that should be applied to the structure. This information is then sent back to the torquers via the same channels of communication

Specifications	Details
Stabilization	3-Axis Stabilized Pointing knowledge $\geq 0.5^\circ$ (3-Axis)
Pointing Accuracy	$\geq 1^\circ$ (3-Axis, Imaging Mode) $\geq 3^\circ$ (3-Axis, Non-Imaging Mode)
Pointing Stability	$\geq 0.01^\circ$ (3-Axis, Imaging Mode) $\geq 0.1^\circ$ (3-Axis, Non-Imaging Mode)
Sensors	Earth sensors, Sun Sensor, Magnetometer
Actuators	Reaction wheels, Magnetorquers
Orbit Determination	Through GPS

Figure 4.8: ADCS specs

4.5 H2Z Software Design Radio(SDR2) Design

Designing a Software Defined Radio (SDR) for Low Earth Orbit (LEO) satellite applications involves integrating advanced technologies to enhance communication capabilities. SDRs offer significant advantages over traditional hardware-based systems due to their flexibility, reconfigurability, and adaptability to various communication protocols and frequency bands. This adaptability is crucial for LEO satellites, which often require real-time updates to meet changing mission requirements.

Key Components in SDR Design for LEO

1. Modular Architecture:

- A modular design allows for the integration of various hardware and software components, enhancing the SDR's capabilities. For instance,

System Design & Demonstrator of a SPU Power Generation Subsystem for SDR Operations of Space Tug in LEO

Alén Space's TOTEM is a high-performance SDR platform designed for nanosatellites, featuring a System-on-Chip (SoC) based on the Xilinx Zynq-7000 series. This architecture enables efficient processing and communication across multiple frequency bands, making it suitable for various LEO applications. ALEN.SPACE Signal Processing:

- Advanced digital signal processing (DSP) techniques enable real-time modulation, demodulation, and signal processing. Utilizing tools such as GNU Radio facilitates the development of these algorithms, allowing for rapid prototyping and testing of different communication scenarios. This flexibility is essential in LEO missions where conditions can change rapidly. Reconfigurability:
- SDRs can adjust operational parameters through software updates without requiring physical hardware changes. This feature is particularly beneficial in LEO missions, allowing payloads to adapt to different operational environments or user requirements. For example, the TOTEM platform supports in-orbit reconfiguration, enabling operators to update software applications or modify communication protocols based on real-time needs.

2. Environmental Considerations:

- Designing an SDR for LEO applications requires components that can withstand the harsh conditions of space, including radiation, temperature fluctuations, and vacuum. The use of compact modules like TOTEM helps reduce size, weight, and power (SWaP) requirements, which are critical factors in satellite design. Performance Enhancements through TOTEM:

3. Modular Design and Integration:

Design Procedure and Details

- TOTEM's architecture allows for efficient processing and communication across multiple frequency bands (70 MHz to 6 GHz), making it suitable for various applications within LEO missions. The ability to plug in different RF frontends (UHF, VHF, S-band) allows for rapid deployment of multiple SDR applications, enhancing mission adaptability and efficiency.

4. Advanced Signal Processing:

- The TOTEM platform supports full-duplex communication with two transmit (TX) and three receive (RX) channels, facilitating simultaneous data transmission and reception. This capability is crucial for maintaining robust communication links in the dynamic environment of LEO, where satellite positioning and orientation can change rapidly. The embedded Linux operating system and compatibility with GNU Radio provide a flexible environment for developing and deploying custom signal processing algorithms.

5. In-Orbit Reconfiguration:

- TOTEM's ability to be reconfigured in orbit allows operators to update software applications or modify communication protocols based on real-time needs without requiring physical access to the satellite. Such flexibility is essential for adapting to unforeseen challenges or optimizing performance based on mission requirements.

6. Calculations for Performance Metrics:

- To quantify the performance enhancements provided by these modules, we can consider the following calculation based on Shannon's theorem, which relates channel capacity to bandwidth and signal-to-noise ratio

System Design & Demonstrator of a SPU Power Generation Subsystem for SDR Operations of Space Tug in LEO

(SNR):

$$C = B \cdot \log_2(1 + \text{SNR}) \quad (4.1)$$

Where:

- C is the channel capacity in bits per second (bps).
- B is the bandwidth in hertz (Hz).
- SNR is the signal-to-noise ratio. Assuming that the TOTEM platform operates at a bandwidth of 1 MHz with an SNR of 20 dB (which corresponds to an SNR value of 100), we can calculate the channel capacity as follows:
- **Convert SNR from dB to a linear scale:**

$$\text{SNR} = 10^{(20/10)} = 100$$

- **Apply Shannon's formula:**

$$C = 1 \times 10^6 \times \log_2(1 + 100) \approx 1 \times 10^6 \times 6.644 = 6.644 \times 10^6 \text{ bps} \approx 6.64 \text{ Mbps} \quad (4.2)$$

This calculation illustrates that with a bandwidth of 1 MHz and an SNR of 20 dB, the SDR can achieve a theoretical maximum data rate of approximately 6.64 Mbps, which is suitable for transmitting high-volume data from LEO satellites.

4.6 Modules Subsystem)

4.6.1 TOTEM Components

- **TOTEM TX (Peak Power):**

- Power: 2.65 W

- Duration: 50 minutes
- Calculation: $2.65 \text{ W} \times 50 \text{ min} = 132.5 \text{ W} \cdot \text{min}$ (correct)
- **TOTEM Standby (Nominal Mode):**
 - Power: 1.4 W
 - Duration: 10 minutes
 - Calculation: $1.4 \text{ W} \times 10 \text{ min} = 14 \text{ W} \cdot \text{min}$ (correct)
- **TOTEM RX:**
 - Power: 2.25 W
 - Duration: 25 minutes
 - Calculation: $2.25 \text{ W} \times 25 \text{ min} = 56.25 \text{ W} \cdot \text{min}$ (correct [4.9](#))
- **TOTEM TX (Regular):**
 - Power: 2.65 W
 - Duration: 10 minutes
 - Calculation: $2.65 \text{ W} \times 10 \text{ min} = 26.5 \text{ W} \cdot \text{min}$ (correct)

4.6.2 NANOLink Components

- **NANOLink TX Boost (Peak Power):**
 - Power: 17 W
 - Duration: 50 minutes
 - Calculation: $17 \text{ W} \times 50 \text{ min} = 850 \text{ W} \cdot \text{min}$ (correct)
- **NANOLink Idle:**
 - Power: 0.57 W

System Design & Demonstrator of a SPU Power Generation Subsystem for SDR Operations of Space Tug in LEO

Data interfaces			
Interface	Bit rate / Configuration	Voltage	Description
CAN bus	1 Mbit/s		CAN bus interface is routed to system bus. ISO 11898-2 CSP compatible: https://github.com/libcsp/libcsp
UART	115200 bps, 8 data bits, no parity bit and 1 stop bit	3.3V	UART for debugging purposes Can be accessed with tools like \\$ minicom -D /dev/ttyUSB0 -b 115200 -con
JTAG	Configurable	1.8V	Main programming interface. Use Xilinx Platform Cable USB II https://www.xilinx.com/support/documentation/data_sheets/ds593.pdf
Ethernet	RMII (100 Mbit/s)	3.3V	Ethernet transceivers such as the DP83848 can be connected on this port. The use of such an external device may raise the current consumption of TOTEM. Make sure that absolute maximum ratings are not exceeded for proper operation.
I2C	Configurable	3.3V	I2C bus from SoC PS

Figure 4.9: TOTEM Data interface data sheet

- Duration: 10 minutes
- Calculation: $0.57 \text{ W} \times 10 \text{ min} = 5.7 \text{ W} \cdot \text{min}$ (correct)
- **NANOlink RX Boost:**
 - Power: 1.63 W
 - Duration: 25 minutes
 - Calculation: $1.63 \text{ W} \times 25 \text{ min} = 40.75 \text{ W} \cdot \text{min}$ (correct)
- **NANOlink TX Boost (Regular):**
 - Power: 17 W
 - Duration: 10 minutes
 - Calculation: $17 \text{ W} \times 10 \text{ min} = 170 \text{ W} \cdot \text{min}$ (correct 4.10)

Total Platform Power:

$$132.5 + 14 + 56.25 + 26.5 + 850 + 5.7 + 40.75 + 170 = 1295.7 \text{ W} \cdot \text{min} \quad (\text{correct } ??)$$

Design Procedure and Details

Table 3: NANOLink-boost-dp Gen2 (nano-link-boost-dp-sb-2) - Technical specification		
	Description	Comment
Output power	Adj. up to 32 dBm (1.5W) per antenna port.	Up to 2 dB losses on diplexer, joiner/splitter and additional filters.
Output power dynamic range	60 dBm in 0.25 dB step	
Input sensitivity	-86 dBm @ 4 Mbps OQPSK	At 1E-3 BER TX enabled (at a different frequency), no preamp.
Supported modulations	OQPSK	other upon request
Noise figure	< 5 dB	
Data rates	default 4 Mbps @ 2.5 MHz (OQPSK)	downlink / uplink
Baseband bandwidth	up to 56 MHz	
Frequency band Transmitter Receiver	2.200 - 2.300 GHz 2.025 - 2.110 GHz	
On-board interfaces	Communication	Redundant CAN bus for TM/TC LVDS for High-speed TM/TC data
Supply voltage		Support for additional interfaces upon request (e.g. UART, SPI, I2C)
Power consumption	5 V DC (+/- 10%)	For details please refer to section 3.3.
Dimensions:	< 17 W (Rx + Tx @ 5W output power from boost) < 1.9 W (Rx only)	For details please refer to section 3.3.
Operation temperature	95 x 91 x 32 mm	For details please refer to section 3.8.
Storage temperature	-10°C to +50°C	For details please refer to section 3.9.1.
Mass:	-20°C to +65°C	For details please refer to section 3.9.1.
	385 g	For details please refer to section 3.8.

Figure 4.10: NANOLink Technical Specs

Images/NANOLink_{boost}_{sp}power_{consumption}

Figure 4.11: NANOLink boost sp power consumption

System Design & Demonstrator of a SPU Power Generation Subsystem for SDR Operations of Space Tug in LEO

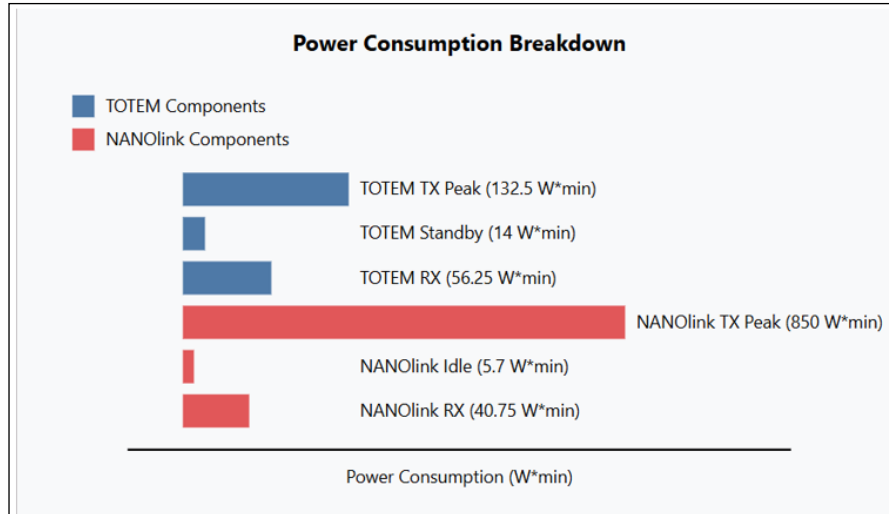


Figure 4.12: Power consumption Breakdown

Key Observations:

Operating Modes:

Peak Power mode uses the highest power but runs for longer (50 min)
 Nominal/Idle modes use less power and run for shorter periods (10min)??

A	B	C	D	E
Component	Sunlight (60min)	Power Consumption (W)	Power * Duration (W*min)	Eclipse (35min)
TOTEM TX	Peak Power (50 min)	2.65	132.5	—
TOTEM Standby	Nominal Mode (10 min)	1.4	14	—
TOTEM RX	—	2.25	56.25	Non-Transmission Mode (25min)
TOTEM TX	—	2.65	26.5	Transmission Mode (10min)
NANOLink TX (Boost)	Peak Power (50 min)	17	850	—
NANOLink Idle	Nominal Mode (10 min)	0.57	5.7	—
NANOLink RX (Boost)	—	1.63	40.75	Non-Transmission Mode (25min)
NANOLink TX (Boost)	—	17	170	Transmission Mode (10min)
Platform Total	Total Power Required	—	1295.7	—

Figure 4.13: Power consumption SDR2

4.7 Market Survey

For choosing the best, effective and based on our requirements modules of SDR2 we follow the method of SWAPC and do a market analysis shown in table 4.7.

Design Procedure and Details

Table 4.1: Comparison of SDR Components for CubeSat Applications

Component Name	S(cm)	S Score	W(g)	W Score	P(W)	P Score	C(USD)	C Score	Extra Features	Fea-	Score	Total
TOTEM	8×8×2	2.0	150	2.0	2.5	2.0	3500	2.0	-	1	9.0	
XLink-S	10×10×3	1.37	200	1.5	5.0	1.67	5000	1.77	-	1	7.31	
XLink-X	10×10×3	1.37	220	1.3	8.0	1.27	7000	1.46	Higher data rate	2	7.4	
NANOLink-base-2	9×9.6×2	1.84	180	1.7	3.0	1.93	4000	1.92	-	1	8.39	
NANOLink-boost-2	9×9.6×2	1.84	190	1.6	4.0	1.8	4500	1.85	-	1	8.09	
NANOLink-boost-dp-2	9×9.6×2	51.68	210	1.4	5.0	1.67	5500	1.69	Dual polarization capability	2	8.44	
S2DR 1000	10×10×4	1.0	250	1.0	6.0	1.53	8000	1.31	Dual-transceiver	2	6.84	
SDR-1001	8×8×3	1.76	170	1.8	4.0	1.8	3500	2.0	-	1	8.36	
SCR-104SDR	10×10×5	1.0	300	1.0	7.0	1.4	9000	1.15	Multi-band capability	2	6.55	
SCR-106	11×11×6	1.0	350	1.0	10.0	1.0	12000	1.0	(L+S)/X bands	2	6.0	
SCR-108	12×12×6	1.0	400	1.0	12.0	1.0	15000	1.0	Advanced multi-band support	2	6.0	
SWIFT SLX	9×9×3	1.58	220	1.3	6.0	1.53	7500	1.38	S and L band support	2	7.79	
SWIFT-XTX	9×9×3	1.58	230	1.2	7.0	1.4	8500	1.23	-	1	6.41	
SWIFT-XTRX	10×10×4	1.0	280	1.0	9.0	1.13	11000	1.0	X-band trans- mit/receive	2	6.13	

Continued on next page

System Design & Demonstrator of a SPU Power Generation Subsystem for SDR
Operations of Space Tug in LEO

Table 4.1 continued from previous page

Component Name	S(cm)	S Score	W(g)	W Score	P(W)	P Score	C(USD)	C Score	Extra Features	Score	Total
SWIFT-XTS	10×10×4	1.0	290	1.0	10.0	1.0	12000	1.0	X-band transmit, S-band receive	2	6.0
Frontier-S	12×12×5	1.0	350	1.0	8.0	1.27	10000	1.0	Integrated OBC	2	6.27
MFREU	15×15×8	1.0	500	1.0	15.0	1.0	20000	1.0	-	1	5.0
X/S Cubesat Radio	10×10×3	1.37	240	1.1	7.0	1.4	9000	1.15	-	1	6.02
Ka/S Cubesat Radio	10×10×3	1.37	250	1.0	8.0	1.27	11000	1.0	Ka-band support for cubesats	2	6.64
CDL-MS02	11×11×4	1.0	300	1.0	9.0	1.13	13000	1.0	-	1	5.13
X-Band HR DownLink	10×10×4	1.0	270	1.0	10.0	1.0	12000	1.0	-	1	5.0
XDL-C301-HR	11×11×5	1.0	320	1.0	11.0	1.0	14000	1.0	-	1	5.0
STC-MS03	9×9×3	1.58	210	1.4	5.0	1.67	6000	1.62	-	1	7.27
HRL-SDR-S/S	10×10×4	1.0	260	1.0	7.0	1.4	8000	1.31	-	1	5.71
NSR-SDR-K/Ka	12×12×5	1.0	340	1.0	12.0	1.0	16000	1.0	-	1	5.0
NSR-SDR-X/S HP	11×11×4	1.0	300	1.0	10.0	1.0	13000	1.0	-	1	5.0
NSR-SDR-X/S	10×10×4	1.0	280	1.0	9.0	1.13	11000	1.0	-	1	5.13
NSR-SDR-S/S	9×9×3	1.58	220	1.3	6.0	1.53	7000	1.46	-	1	6.87

Continued on next page

Table 4.1 continued from previous page

Component Name	S(cm)	S Score	W(g)	W Score	P(W)	P Score	C(USD)	C Score	Extra Features	Score	Total
NSR-SDR-MUOS	12×12×5	1.0	350	1.0	11.0	1.0	15000	1.0	MUOS compatibility	2	6.0
NSR-SDR-U/U	11×11×4	1.0	290	1.0	8.0	1.27	10000	1.0	UHF band support	2	6.27
RAVEN-SDR	10×10×4	1.0	270	1.0	7.0	1.4	9000	1.15	-	1	5.55

•

4.8 Electrical Power Subsystem

The Electrical Power Subsystem (EPS) is one of the most critical subsystems in satellites. Its primary function is to provide reliable and uninterrupted electrical power to all other subsystems and payloads on the satellite. The EPS typically includes solar arrays for power generation, batteries for energy storage, power conditioning and distribution electronics, and thermal control systems to maintain safe operating temperatures. Without a properly functioning EPS, a satellite cannot function, and its mission could fail.

4.8.1 Power Budget

The power budget ?? is a critical engineering element in the design and operation of the H2Z satellite, dictating the viability of all mission phases. This section provides a comprehensive, scientific analysis of the power generation, storage, distribution, and consumption, referencing both the attached calculation sheet and subsystem documentation.

1. Power Generation: Solar Array Sizing and Performance

Solar Array Configuration

System Design & Demonstrator of a SPU Power Generation Subsystem for SDR
Operations of Space Tug in LEO

Table 4.2: H2Z Satellite Power Budget

Subsystem	Sunlight (60 min)				Eclipse (35 min)			
	Scaled by 100	Peak Power	Scaled by 100	Nominal Power	Scaled by 100 (Non-Tx)	Non-Tx	Scaled by 100 (Tx)	Tx Mode
ADCS(W)	0.7	70	0.61	61	0.63	63	0.63	63
TCS(W)	0	0	0	0	0.2	20	0.2	20
TTCS(W)	0.8	80	0.8	80	0.8	80	0.8	80
EPS(W)	1.72	150	0.65	150	0.65	65	0.75	75
CDHS(W)	0.5	50	0.5	50	0.5	50	0.5	50
Propulsion(W)	0.8	40	0.4	40	0.4	40	0.4	40
GNC(W)	0.25	25	0.2	20	0.205	20.5	0.205	20.5
Platform Total(W)	4.47	447	3.715	371.5	3.085	308.5	3.185	318.5
TOTEM TX(W)	0.055	5.5	0.055	5.5	0.055	5.5	0.055	5.5
TOTEM RX(W)	0.022	2.2	0.022	2.2	0.022	2.2	0.022	2.2
NANOlink TX(W)	0.187	18.7	0.0935	9.35	0	0	0	0
NANOlink RX(W)	0.01793	1.79	0.01793	1.793	0.02	1.793	0.02	1.793
SDR2 Total(W)	0.28193	28.19	0.19	18.84	0.04	3.99	0.09	9.49
Robotic Arm(W)	0.3	30	0.3	30	0.16	16.67	0.28	28.33
Camera(W)	0.4	40	0.17	16.67	0.17	16.67	0.28	28.33
Battery Charging(W)	1.2	120	2.17	217	-	-	-	-
Harness Losses(W)	0.058	5.8	0.057	5.7	0.029	2.9	0.0034	0.34
Total Power Required(W)	6.99186	699.19	6.30	648.55	3.36	336.05	3.66	366.16
Average Power Output From Solar Array(W)	6.99	699.19	6.69	669.085	-	-	-	-
Average Margin (%)	8.68	8.68	10	10	-	-	-	-
Power Required From Battery(W/h)	-	-	-	-	1.30	130.86	1.61	160.86
Battery DOD (%)	-	-	-	-	80	80	80	80

- **Type:** Gallium Arsenide (Ga–As) triple-junction, body-mounted solar cells.
- **Efficiency:** Initial (BOL) efficiency at 0°C is 30%, degrading to 27.4% at EOL due to temperature and radiation [?].
- **Area:** Oversized to 2.733 m² to guarantee sufficient power even after two years of orbital degradation.
- **Pointing and Packing Losses:** Pointing efficiency is 99.85% ($\cos \theta = 0.9985$), packing efficiency is 90%, and a 3% annual degradation is included [4.14](#).

Power Output Calculations

- **Sunlight Phase:** The solar array must meet both immediate operational loads and charge the battery for eclipse operations. The average power output required from the array is 851.61 W at BOL, reducing to 801.28 W at EOL due to cumulative degradation [4.14](#).

Electrical Data (typical)					
		BOL	5E14	1E15	3E15
Average Open Circuit V_{oc}	[mV]	3451	3292	3227	3120
Average Short Circuit I_{sc}	[mA]	457.6	453.3	451.5	423.8
Voltage at max. Power V_{mp}	[mV]	3025	2866	2793	2700
Current at max. Power I_{mp}	[mA]	433.5	428.0	423.8	394.0
Average Efficiency η_{bare} (1367 W/m ²)	[%]	31.8	29.7	28.7	25.8
Standard: PS_4G32_PTB_2016-09-13; Spectrum: AM0 WRC = 1367 W/m ² ; T = 25 °C					
@fluence 1MeV [e/cm ²]					

Acceptance Values (typical)					
Voltage V_{op}	2900 mV				
Min. average current $I_{op\ avg} @ V_{op}$	438 mA				
Min. individual current $I_{op\ min} @ V_{op}$	418 mA				

Figure 4.14: 32% Quadruple Junction GaAs Solar Cell Type: QJ Solar Cell 4G32C - Advanced

- **Oversizing Rule:** For LEO, the array is sized to at least $1.5 \times$ the average sunlight load, resulting in a required array power of 1 036.13 W, which provides a safety margin of 21.7% [4.14](#).

[Images/Functional Block Diagram of EPS](#)

Figure 4.15: Functional block diagram of the Electrical Power System (EPS) showing solar energy flow and regulation.

Power Storage: Battery Sizing and Management

Battery Characteristics

- **Type:** Lithium–Ion (Li–ion)
- **Capacity:** 77 Ah, with an energy density of 80 Wh/kg.
- **Depth of Discharge (DOD):** 80%, balancing usable energy with battery longevity.
- **Charging/Discharging Efficiency:** 93% charging, 95% discharging [\[?\]](#).

Battery Sizing Calculation

$$E_B = \frac{P_{eclipse} \times (T_{orbit} - T_{sun})}{\eta_{charge} \times \text{DOD}} \quad (4.3)$$

System Design & Demonstrator of a SPU Power Generation Subsystem for SDR Operations of Space Tug in LEO

$$P_{\text{eclipse}} = 201.05 \text{ W}, \quad T_{\text{orbit}} = 1.633 \text{ hr}, \quad T_{\text{sun}} = 1.029 \text{ hr}, \quad \eta_{\text{charge}} = 0.93, \quad \text{DOD} = 0.8$$

$$E_B = \frac{201.05 \times (1.633 - 1.029)}{0.93 \times 0.8} = 163.22 \text{ Wh}$$

This ensures sufficient stored energy to sustain all loads during eclipse phases [?].

Power Consumption: Subsystem-Level Analysis

Table 4.3: Subsystem power requirements in sunlight and eclipse phases (scaled values by 100 for clarity).

Subsystem	Sunlight Avg (W)	Eclipse Avg (W)	Peak (W)
ADCS	0.70	0.63	70.00
TT&C	0.80	0.80	80.00
EPS	1.72	0.75	172.00
CDHS	0.50	0.50	50.00
Propulsion	0.80	0.80	80.00
GNC	0.25	0.25	25.00
SDR2	0.28	0.09	28.19
Robotic Arm	0.30	0.30	30.00
Camera	0.40	0.28	40.00
Battery Charging	2.17	—	217.00
Harness Losses	0.06	0.0034	5.80
Total	6.99	3.66	699.19

Power Phasing

- *Sunlight (60 min)*: Average total power required is 6.99 W ($\times 100$), with a peak of 699.19 W.
- *Eclipse (35 min)*: Average total power required is 3.66 W ($\times 100$), with a peak of 366.16 W.
- *Battery Charging*: 2.17 W ($\times 100$) allocated during sunlight to replenish energy for eclipse operations [10].

Power Distribution and Conditioning

Distribution Architecture

- Primary Bus: 28 V unregulated
- Secondary Buses: 5 V and 12 V regulated for specific subsystems
- Protection: Fuses ($1.5 \times$ max load), isolation switches, and dual independent PDU paths for redundancy [2].

Efficiency Losses

- PDU Efficiency: 98%
- Net Output: After losses, effective output is 687.65 W from the solar array [2].

Thermal and Dissipation Considerations

Subsystem Power Dissipation Total dissipation is 191.89 W, calculated using the Stefan–Boltzmann law for radiative cooling:

$$P = \varepsilon \sigma A T^4 \quad (4.4)$$

Thermal margins are maintained by selecting emissivity and radiative area to keep subsystem temperatures within operational limits [6].



Figure 4.16: Heat dissipation flow from subsystem components to space, modeled via Stefan–Boltzmann law.

6. Power Margins and Mission Resilience

- **Sunlight Margin:** At peak demand, margin is 21.8%; at nominal demand, 31.3%.
- **Battery Margin:** Eclipse operations supported with a 20% reserve, ensuring resilience to unexpected loads.
- **EOL Performance:** After two years, the solar array provides 801.28 W, sufficient for all mission operations [?].

Scientific Summary and Recommendations

The H2Z satellite's power system is engineered with rigorous scientific principles:

- **Redundancy:** Dual PDUs and backup units for critical systems.
- **Safety:** Oversizing of solar array and battery ensures margin against degradation.
- **Efficiency:** High-efficiency Ga–As cells, optimized battery management, and robust distribution minimize losses.
- **Thermal Management:** Radiative cooling and thermal coatings protect against overheating.

This robust power architecture ensures mission success, system survivability, and operational longevity under the harsh conditions of low Earth orbit.

4.9 Power Required Calculation

4.9.1 Sunlit Power Requirement

$$P_{\text{sun}} = \frac{(TPR_{\text{Peak}} \times T_{\text{Peak}} \times T_{\text{sun}}) + (TPR_{\text{nominal}} \times T_{\text{nominal}} \times T_{\text{sun}})}{T_{\text{sun}} \times 60} \quad (4.5)$$

Scientific Conceptual Discussion This equation calculates the average power required during the sunlit portion of the orbit a crucial metric for sizing the solar arrays on a CubeSat. Power consumption in satellite systems fluctuates due to changes in operational modes: peak operations such as high-data-rate communication or propulsion activation consume more power, while nominal operations (e.g., standby sensing or passive thermal control) consume less.

The numerator computes the total energy demand over time by considering the time-weighted contributions from peak and nominal power phases, each scaled by the sunlight duration per orbit. This energy value is then normalized by dividing with $T_{\text{sun}} \times 60$, effectively converting minutes to seconds and yielding average power in watts.

This formulation acknowledges real satellite duty cycles. For example, if peak mode only occurs for a small portion of the sunlit phase (e.g., imaging), but draws substantial power, it still has a critical impact on the overall average demand. Conversely, extended nominal operation with lower power still contributes significantly due to duration.

Conceptually, this equation ensures the solar array can supply enough instantaneous power and energy to support all active subsystems during the orbit's illuminated phase. Without this averaging technique, designs might either oversize the array (wasting mass and space) or undersize it (causing power deficits).

By considering both temporal distribution and intensity of subsystem power draw, this model forms the backbone of reliable solar power architecture in Low Earth Orbit (LEO) missions. It allows for accurate estimation of solar panel requirements, ensuring that generated power not only supports active loads but also prepares for energy storage (battery charging) in eclipse phases.

4.9.2 Eclipse Power Requirement

$$P_{\text{eclipse}} = \frac{(TPR_{\text{Non_trans}} \times T_{\text{Non_trans}} \times T_{\text{eclip}}) + (TPR_{\text{trans}} \times T_{\text{trans}} \times T_{\text{eclip}})}{T_{\text{eclip}} \times 60} \quad (4.6)$$

System Design & Demonstrator of a SPU Power Generation Subsystem for SDR Operations of Space Tug in LEO

Scientific Conceptual Discussion This equation computes the average power requirement during the eclipse phase the portion of a satellite’s orbit when it is in Earth’s shadow and receives no direct solar radiation. During this time, the spacecraft cannot generate energy through its solar arrays and must instead rely entirely on battery reserves.

To reflect real operational complexity, the equation separates power consumption into two categories:

- $TPR_{\text{Non_trans}}$: Power during non-transitory (steady-state or nominal) operations
- TPR_{trans} : Power during transient or high-load activities such as switching or maneuvering

These are weighted by their respective durations and the total eclipse period T_{eclip} , and then normalized by dividing over $T_{\text{eclipse}} \times 60$ to yield the average power in watts.

This approach is essential because a satellite’s behavior may vary significantly during eclipse. While certain power-hungry functions may be scheduled during sunlight to conserve energy, others (like telemetry, navigation updates, or thermal regulation) continue regardless of illumination. Understanding and accurately modeling this power profile ensures that the energy stored in batteries is sufficient to sustain uninterrupted operation throughout the eclipse.

Conceptually, this formula underpins the battery sizing process. An underestimate could lead to operational shutdowns or mission failure during shadowed phases. Moreover, transient load handling is critical as startup surges or mode switches can strain stored energy more than steady loads. Thus, inclusion of both components provides a more robust and resilient design basis for energy budgeting.

This analysis is especially relevant for Low Earth Orbit (LEO) missions where eclipse durations can range from 25% to 40% of the orbital period, making accurate eclipse load estimation critical to satellite reliability.

4.9.3 Battery Charging Power Requirement

$$P_{\text{charge}} = \frac{1}{\eta} \times \frac{T_{\text{eclipse}}}{T_{\text{sun}}} \times P_{\text{eclipse}} \quad (4.7)$$

Scientific Conceptual Discussion This equation estimates the additional power that must be provided by the solar arrays during the sunlight phase to sufficiently recharge the onboard batteries, ensuring uninterrupted operation during the eclipse phase.

Let's break down the components:

- P_{eclipse} : The average power needed during eclipse (from Equation 4.6)
- $\frac{T_{\text{eclipse}}}{T_{\text{sun}}}$: The ratio of eclipse duration to sunlight duration, scaling the eclipse demand into the sunlit period
- $\frac{1}{\eta}$: The inverse of the power system's charging efficiency (including Battery Charge Regulator, solar conversion, and thermal losses)

The concept is rooted in energy conservation: the energy consumed in eclipse must be replenished by the solar arrays when sunlight is available. However, due to inefficiencies in energy conversion and storage (typically 70–90%), the actual energy required for charging is greater than what is consumed.

This formula answers a fundamental question in power system design: **how much extra power must the solar array generate during sunlight to not only support immediate system operations but also recharge the battery for the next eclipse? By applying this relation, designers can ensure that the system avoids energy starvation during shadow periods, especially in worst-case scenarios with longer eclipses or degraded solar panel performance.

Practically, this equation feeds directly into determining the minimum required size of the solar arrays. Without including the charging requirement, the arrays might be sized only for real-time load and fail during the night-side of the orbit.

System Design & Demonstrator of a SPU Power Generation Subsystem for SDR Operations of Space Tug in LEO

Therefore, P_{charge} is a vital margin that ensures energy continuity, battery health, and mission reliability.

In LEO missions with frequent eclipses, accurate charging power calculations directly impact system mass, volume, and lifetime—three critical CubeSat constraints.

4.9.4 Total Array Power Requirement

$$P_{\text{array}} = P_{\text{sun}} + P_{\text{charge}} \quad (4.8)$$

Equation (4.8) links the real-time load during sunlight, P_{sun} , with the additional charging power, P_{charge} , to yield the minimum instantaneous power the solar array must supply. Unlike earlier expressions that focus on average power in a single phase, this formula captures the composite demand: it must simultaneously sustain active subsystems and restore the battery's state of charge for the next eclipse. Conceptually, P_{array} is the driving parameter for array sizing because it represents the peak power point the electrical power subsystem will ever have to deliver in nominal conditions. Undersizing here risks either brown-outs during sunlight (if peak plus charge exceeds capacity) or cumulative energy deficiency over multiple orbits, ultimately degrading battery health and mission success. Designers typically add a 10–20% growth factor above P_{array} to accommodate seasonal β angle variations, radiation damage, and pointing errors, ensuring robust operation throughout the mission.

4.10 Battery Energy Requirement (Equation 5)

$$E_{\text{Battery}} = P_{\text{eclipse}} \frac{(T - T_{\text{sun}})}{\eta_{\text{charge}} DOD} \quad (4.9)$$

Scientific Conceptual Discussion Equation (4.9) determines the **usable capacity** a battery must store to sustain the spacecraft through the eclipse. Here, $(T - T_{\text{sun}})$ is the absolute eclipse duration, η_{charge} the charge–discharge efficiency

(accounting for regulator losses and Coulombic inefficiency), and DOD the allowable depth-of-discharge, typically limited to 60–80% in Li-ion packs to maximize cycle life. Dividing by the product $\eta_{\text{charge}} DOD$ scales the ideal energy by both conversion losses and the fraction of capacity that can be safely drawn, yielding the **name-plate capacity** engineers must procure. If underestimated, the battery will reach its lower voltage limit before the eclipse ends, forcing load shedding or unplanned reboot cycles. Conversely, oversizing adds unnecessary mass and volume — premium resources on CubeSats. Thus, the equation balances reliability against strict platform constraints, forming the cornerstone of EPS mass budgeting.

4.10.1 Battery Mass Estimation

$$M_{\text{Battery}} = \frac{E_{\text{Battery}}}{\rho_{\text{energy}}} \quad (4.10)$$

Scientific Conceptual Discussion Equation (4.10) converts energy capacity into physical mass via the specific energy (Whkg^{-1}) of the selected chemistry. For Li-ion this ranges from 150–250 Whkg^{-1} at the cell level, yet system-level values drop ($\approx 80\text{--}120 \text{ Whkg}^{-1}$) once packaging, wiring, and thermal pads are included. Accurate mass prediction is critical because battery packs often dominate the lower-deck of a CubeSat, affecting center-of-gravity, structural supports, and thermal pathways. Trading higher-density cells against cost, radiation tolerance, and safety (thermal runaway) becomes a multidimensional optimization in which Equation 4.10 provides the mass metric. By iterating $E_{\text{Battery}}\text{--}M_{\text{Battery}}$ loops with mission analysts, the team converges on a pack that meets both capacity and launch-mass limits.

4.10.2 Solar-Array Energy Output (Equation 7)

$$E_{\text{array}} = P_{\text{array}} T_{\text{sun}} \quad (4.11)$$

Scientific Conceptual Discussion Equation (4.11) delivers a first-order estimate of the total energy the array harvests each orbit, assuming P_{array} can be maintained for the entire illuminated duration. While simplistic, it is invaluable during early sizing when pointing dynamics and partial-shadowing details are not yet defined. Later, this figure is refined with attitude-profile analyses and β -angle sweeps, but the simple product serves as a back-of-the-envelope check to flag designs that are clearly energy-deficient before detailed modeling consumes schedule.

4.10.3 Duty-Cycle Energy Budget

$$E_{\text{array}} = \frac{1}{\eta_{\text{sun}}} \left(\sum_{i=1}^k P_i t_i \right) + \frac{1}{\eta_{\text{eclipse}}} \left(\sum_{i=k+1}^n P_i t_i \right) \quad (4.12)$$

Scientific Conceptual Discussion Equation (4.12) introduces **granularity** by summing discrete load events (P_i, t_i) and applying separate power-train efficiencies for sunlight and eclipse. This accounts for mode-specific regulator topologies — for example, an MPPT path during sunlight and a battery-discharge path at night, each with unique η . The summation permits modeling instrument duty cycles, communications passes, and reaction-wheel peak draws individually, yielding a realistic orbit-integrated energy ledger. Such fidelity is indispensable for high-duty-cycle payloads (e.g. SAR or hyperspectral imagers) where average-power simplifications hide short bursts that can violate regulator current limits or thermal constraints.

4.10.4 Solar-Array Area

$$A_{\text{array}} = \frac{P_{\text{array}}}{S_0 \cos \theta \eta_{\text{cell}} \eta_{\text{pack}} (1 - D)} \quad (4.13)$$

Scientific Conceptual Discussion Equation (4.13) translates power demand into physical panel area. S_0 is the solar constant (1361Wm^{-2}), $\cos \theta$ captures off-pointing losses (jitter, slew maneuvers), η_{cell} is cell conversion efficiency (30% for GaAs triple-junction), η_{pack} accounts for inter-cell gaps and harness resistances,

and D represents life-time degradation (radiation & micrometeoroids). The denominator thus folds in all unavoidable derates, ensuring A_{array} is a begin-of-life area that still meets end-of-life power targets. Panel-area outputs drive mechanical layout, deployable hinge design, and attitude-disturbance analysis since large arrays introduce aerodynamic drag and solar-pressure torques.

4.10.5 End-of-Life Power

$$P_{\text{EOL}} = P_{\text{BOL}} (1 - \delta)^N \quad (4.14)$$

Scientific Conceptual Discussion Here P_{BOL} is the begin-of-life power, δ the annual degradation rate (2–4% for modern cells), and N the mission duration in years. Equation (4.14) projects power at mission’s end, capturing radiation-induced lattice damage, contamination, and thermo-mechanical fatigue. Mission assurance requires $P_{\text{EOL}} \geq$ critical load; thus, initial oversizing is selected so that the system remains power-positive after years in orbit.

4.11 Thermal Control Subsystem

The Thermal Control Subsystem (TCS) is essential for maintaining the temperature of spacecraft components within acceptable limits, particularly in the extreme thermal environments encountered in orbit. Effective thermal control is vital for ensuring the reliability and performance of satellites, as temperature fluctuations can lead to significant damage to onboard electronics, malfunctions, or complete failure. Moreover, excessive temperature variations can adversely affect the accuracy of onboard sensors and instruments, compromising the quality of data collected.

4.11.1 Thermal Control Techniques

The TCS employs a combination of passive and active thermal control techniques to regulate satellite temperatures:

System Design & Demonstrator of a SPU Power Generation Subsystem for SDR Operations of Space Tug in LEO

Active Thermal Control Techniques

- Heaters: Electric heaters are used to raise temperatures in specific components, especially during periods when the satellite is in shadow.
- Heat Pipes: These are used to transfer heat from one area of the spacecraft to another, utilizing phase change to efficiently manage thermal energy.
- Thermal Interface Materials: These materials enhance heat conduction between components and heat sinks.

Passive Thermal Control Techniques

- Multilayer Insulation (MLI): MLI blankets prevent excessive heat loss and protect against environmental heat fluxes. They are commonly applied to various spacecraft components such as antennas, batteries, and propellant tanks.
- Coatings and Paints: Different paints are used to manage solar radiation and internal heat. Black paint (absorptivity of 0.95) is typically used for heat rejection inside the satellite, while white paint (emissivity of 0.87) helps with cooling.
- Radiators: These components dissipate internally generated waste heat into space.

The thermal control system operates based on two primary principles: radiation and conduction. Passive components like coatings and MLI utilize radiation heat transfer, while active components like heaters and heat pipes rely on conduction.

4.11.2 Environmental Heat Loads

The TCS must account for various environmental heat loads:

- Solar Flux: Ranges from 1326 W/m² at aphelion to 1417 W/m² at perihelion; a constant value of 1366.1 W/m² is commonly accepted by the space community.
- Albedo Radiation: Approximately 30% of solar flux is reflected from Earth.
- Earth Infrared Emission: The effective emission is around 240 W/m² at a temperature of 255 K.

4.11.3 Design Considerations for H2Z

For the H2Z spacecraft, a passive thermal design will be implemented, incorporating MLI, paints, coatings, and conducting pastes. The choice of materials will ensure that the spacecraft can effectively manage temperature extremes while maintaining operational functionality. [4.17](#)

Component Type	Function	Example Materials/Techniques
Active Thermal Control	Heats specific areas or transfers heat	Heaters, Heat Pipes
Passive Thermal Control	Insulates or radiates excess heat	MLI, Coatings (Black/White), Radiators

Figure 4.17: Specifications of Thermal Control Subsystem

4.11.4 Analysis of Subsystem Power Dissipation

Power dissipation is calculated based on the Stefan-Boltzmann law, assuming radiative heat loss as the primary mechanism for thermal energy dissipation. Adjustments for emissivity, temperature, and effective radiative surface area are incorporated to ensure accuracy.

Stefan-Boltzmann Law The power dissipation is given by the Stefan-Boltzmann equation:

System Design & Demonstrator of a SPU Power Generation Subsystem for SDR
Operations of Space Tug in LEO

$$P = \epsilon \cdot \sigma \cdot A \cdot T^4 \quad (4.15)$$

where:

- P : Power dissipation (W)
- ϵ : Emissivity (dimensionless)
- $\sigma = 5.67 \times 10^{-8} W/m^2 K^4$: Stefan-Boltzmann constant
- A : Effectiveradiativesurfacearea(m^2)
- T : Temperature(K)

4.12 Net Heat Flux Inward (Equation 12)

$$q''_{\text{in}} = q''_{\text{sun}} + q''_{\text{IR}} + q''_{\text{albedo}} + q''_{\text{solar}} + q''_{\text{gen}} \quad (4.16)$$

Scientific Conceptual Discussion

Equation (4.16) aggregates external sources (direct solar, planetary IR, albedo reflection) with internal dissipation (q''_{gen}). It forms the input side of the space-craft thermal balance. Each term varies with orbit β -angle, attitude, and eclipse fraction, making this sum a dynamic boundary condition for thermal network models.

4.13 Radiative Heat Loss

$$P_{\text{rad}} = \varepsilon \sigma A T^4 \quad (4.17)$$

Scientific Conceptual Discussion Stefan–Boltzmann radiation governs passive cooling in vacuum. With convection absent, the only path to reject internally generated heat is radiation. Surface finish (high- ε white paint vs. low- ε thermal tape) and available area determine how many watts can be safely dissipated without exceeding component limits. This equation is central to thermal-panel sizing and dictates whether active control (heaters, louvers) is required.

4.14 Temperature Differential

$$\Delta T = \frac{q''_{\text{in}}}{(\varepsilon\sigma A)^{0.25}} \quad (4.18)$$

Scientific Conceptual Discussion Equation (4.18) offers a quick-look estimate of surface temperature above deep space by combining the inward flux with the T^4 radiation law (inverted). Although simplified (assumes isothermal surface), it rapidly flags over-temperature risks early in design, prompting radiator augmentation or optical-property changes before exhaustive finite-element modeling.

4.15 Radiated Heat Flux Outward (Equation 14)

$$q''_{\text{out}} = \varepsilon\sigma T^4 \quad (4.19)$$

Scientific Conceptual Discussion Equation (4.19) is the surface heat flux emitted per square metre. Setting $q''_{\text{in}} = q''_{\text{out}}$ yields equilibrium temperature, facilitating node-wise thermal balance in lumped-parameter models. The expression underscores why high-emissivity coatings are favored for hot components, whereas radiators for cryogenic sensors often employ low- ε finishes to limit heat uptake.

4.16 Power Margin

$$\text{Margin} = \frac{P_{\text{generated}} - P_{\text{consumed}}}{P_{\text{consumed}}} \times 100 \% \quad (4.20)$$

System Design & Demonstrator of a SPU Power Generation Subsystem for SDR Operations of Space Tug in LEO

Scientific Conceptual Discussion Equation (4.20) quantifies the percentage headroom between available and required power. Industry practice targets 20–30% at BOL to absorb uncertainties such as cell mismatch, shadowing by deployables, or unexpected new payload modes. Maintaining positive margin at all mission phases underpins autonomy; if it turns negative, a duty-cycle scheduler must shed loads, jeopardizing data return. Thus, continuous on-board margin monitoring feeds fault-protection logic and ground operators’ power-budget dashboards.

Chapter 5

Results and Discussion

In this chapter, we present the key outcomes of the power system design process for the H2Z satellite. Each subsection briefly explains the methodology, presents the numerical results, and discusses their implications.

5.1 Debris Selection

The sensitivity plot is as follows in [5.1](#):

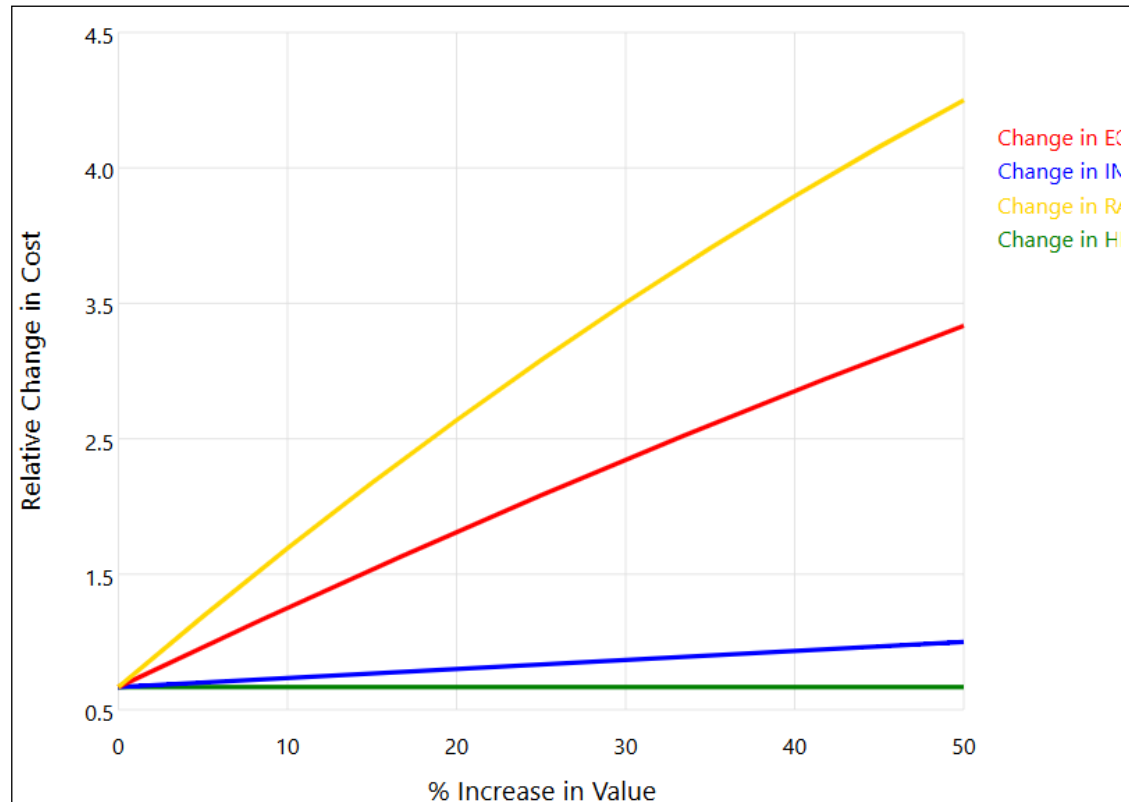


Figure 5.1: Sensitivity analysis of the debris

The graph was plotted in Microsoft Excel. It is quite evident from the graph that the variables that have a greater impact on the cost of the mission are the Right

System Design & Demonstrator of a SPU Power Generation Subsystem for SDR Operations of Space Tug in LEO

Ascension of Ascending Node, Inclination, and Eccentricity respectively. The list of debris that was selected for the mission is in table 5.1:

Table 5.1: NORAD ID Table of Selected Debris for Mission

Sr. No	NORAD ID
1	43104
2	43095
3	43096
4	40263
5	39628

5.2 Payload

5.2.1 *Robotic Arm*

A 4-DOF (Degrees of Freedom) robotic arm has been developed as a critical payload for capturing space debris, addressing the growing concern of orbital debris that poses risks to active satellites. This robotic arm operates with a configuration that includes three axes of positional freedom and one axis of orientation freedom, allowing it to manipulate objects in three-dimensional space effectively. The design specifications, detailed in section 4.4.1, highlight the arm's capabilities and operational parameters.

- joint Configuration: The arm consists of four joints; joints 1, 2, and 3 rotate at a speed of 0.18 seconds per 60 degrees, while joint 4 and the end-effector rotate at 0.21 seconds per 60 degrees. This design ensures efficient movement while adhering to the power budget constraints of the satellite.
- Degrees of Freedom: The 4-DOF configuration provides enhanced flexibility for positioning and orientation, making it suitable for various debris capture scenarios.
- Operational Efficiency: The arm's movement is optimized to minimize energy consumption, which is crucial for satellite operations where power re-

sources are limited.

- Impact Mitigation: Advanced designs are being explored to enhance the arm's ability to absorb impact forces during debris capture, reducing the risk of structural failure and subsequent fragmentation.

In the context of space debris management, the use of robotic arms has gained traction due to their ability to interact with objects in orbit without direct human intervention. Current methodologies for debris removal include various techniques such as net capturing and tether systems; however, robotic arms offer a promising alternative by providing more controlled and adaptable means of engaging with debris. This adaptability is crucial given the unpredictable nature of space debris, which can vary significantly in size, shape, and velocity. Moreover, advancements in robotic arm technology are addressing challenges related to impact forces during capture operations. Traditional rigid robotic arms risk structural failure upon collision with debris, potentially creating additional fragments. To mitigate this risk, researchers are exploring flexible designs and morphing mechanisms that can adjust their shape and length dynamically to absorb impacts better and minimize damage.

5.2.2 Imaging Payload

The H2Z robotic system will be equipped with an advanced imaging payload designed for high-resolution observation and analysis. This imaging system features a ground sample distance (GSD) of approximately 1.5 meters, which indicates the smallest detail that can be resolved on the ground from the imaging platform. This level of resolution is crucial for various applications, including environmental monitoring, urban planning, and disaster management.

- Swath Width: The imaging payload has a swath width of 18.77 degrees, which determines the width of the area that can be captured in a single

System Design & Demonstrator of a SPU Power Generation Subsystem for SDR Operations of Space Tug in LEO

image. This wide swath allows for efficient coverage of large areas, reducing the time required for data collection.

- Angular Field of View (FOV): The system boasts an angular field of view of 11.55 degrees, which is essential for capturing detailed images while maintaining a wide perspective. This feature is particularly beneficial in applications where context and spatial relationships are important.
- Lens Diameter: The diameter of the lens used in the imaging payload has been calculated based on the F-number (F#) of the SIMERA SENSE TriScape 200. The F-number is a critical parameter that influences the amount of light entering the lens and, consequently, the quality and clarity of the images captured.

These specifications, it is important to consider how these parameters interact to enhance the overall functionality of the H2Z robotic system shown in table 5.2. The combination of a low GSD with a broad swath width enables comprehensive data acquisition, allowing for detailed analysis and monitoring over extensive regions without requiring multiple passes.

Parameter	Result
GSD	1.499m
SW in degrees	18.77deg
D (Aperture)	190.53mm
AFOV (θ_{FOV})	11.559deg
SW in Km	14.214km

Table 5.2: Table of Parameters and Results

5.3 Structure Subsystem

In section 4.4, we presented the key specifications of the structure subsystem, and in this section, we will focus on the major sizing results. The volume of the space-craft bus was calculated to be $1.367m^3$; however, due to the unavailability of a

commercially standard mechanical bus, a bus of $1.5m^3$ was chosen. In light of this, a mechanical bus of 1500U (where 1U is equivalent to $1000cm^3$) was selected after the first design iteration.

Table 5.3 represents all of the sizing parameters that emerged as a result of implementing the mathematical model, which is explained in detail in section 5.3.2. These parameters play a crucial role in the overall structural integrity and performance of the spacecraft. They include the volume, linear dimension, cross-section area, and moment of inertia of the bus.

Parameter	Result
Volume of the Spacecraft bus	$1.367m^3$
Linear Dimension	1.29m
Cross section area	$1.6641m^2$
Moment of Inertia, I	$37.706m^2$

Table 5.3: Table of Parameters of H2Z Bus

5.4 Attitude Determination and Control Subsystem

Parameters listed in Table 5.5 were drafted out as a result of implementing the mathematical model explained in previous sections. Table 5.4 shows the worst case disturbances torques. Table holds all the results for the sizing of reaction wheels

Parameter	Result
Gravity gradient	$1.65 \times 10^{-5} Nmat \theta = 1^\circ \text{ & } 4.1 \times 10^{-4} Nm at \theta = 30^\circ$
Solar radiation	$5.73 \times 10^{-4} Nm$
Magnetic field	$4.8 \times 10^{-5} Nm$
Aerodynamics	$1.65 \times 10^{-5} Nm$

Table 5.4: Disturbance torques

and momentum wheels. Additionally, ADCS used 8 micro thrusters for adjusting its attitude shown in table 5.5.

System Design & Demonstrator of a SPU Power Generation Subsystem for SDR
Operations of Space Tug in LEO

Parameter	Result
Slew Torque for Reaction Wheels	$5.08 \times 10^{-3} Nm$
Momentum Storage in Reaction Wheels	0.0479Nms
Momentum Storage in Momentum Wheels	$40.4 Nms$ at $\theta = 0.1^\circ$ Accuracy
Momentum Storage in Spinner	$0.046 rad/s$
Torque from Magnetic Torquers	$1 Am^2$

Table 5.5: Sizing of reaction wheels and momentum wheels

5.5 Electric Power Subsystem

It was found out that H2Z shall have an EPS which will be able to produce a power of approximately 956.216W. Two very common approaches were analyzed, the component efficiency method and the damage fluence method. As a result, It was found the component efficiency method requires 40.9% less area to generate the same amount of power as compared to the damage fluence method. However, this difference can be associated with the fact that the damage fluence method accounts for both the efficiencies of components of the solar array as well as radiation damages shown in table 5.6 experienced during the mission while the component efficiency method does not consider the radiation damage that may occur during the mission. For producing such power, it has been found that H2Z will require a solar array having an area of approximately $6.5 m^2$. Using the component efficiency method, it was found that H2Z requires a solar array 1.602kg having an area of approximately $2.66 m^2$ and the mass of the solar blanket to be 19.124kg. However, when the damage fluence method was used, it was found that H2Z requires a solar array having an area of approximately $6.50 m^2$ and the mass of the solar blanket to be 46.74kg. The damage fluence method being a more conservative approach compelled us to go with its results. Other parameters found from the damage fluence method are listed in Table 5.7.

Results and Discussion

Parameter	Result
The power Required from the solar array to meet the eclipse load	156.759W
Power Required to be available from the array	794.237W
Power output with the sun normal to the surface of the cells	420W
Beginning-of-life (BOL) power production capability per unit area of the array	$296.577W/m^2$
End-of-life (EOL) power production capability per unit area of the array	$280W/m^2$
The approximate size of the solar array in LEO is	956.2167W
The approximate size of the solar array in GEO is	669.35W
Estimated Battery mass	1.602kg
Battery-stored Energy	180.609W/hrs

Table 5.6: EPS Result

Parameter	Result
Damage equivalent 1 MeV fluence due to Electrons	$1.8 \times 10^{11} e/cm^2/yr$
Total Damage equivalent 1 MeV fluence due to Electrons	$3.6 \times 10^{11} e/cm^2/yr$
Maximum Power Output Density for total damage	$14.7 mW/cm^2$
Multiplication factor for 0.15mm Shield thickness	0.8
Expected radiation at the end of life	2.8×10^{11}
Power per unit area after catering for shielding	$147 W/m^2$

Table 5.7: EPS parameters from damage Fluence Method

System Design & Demonstrator of a SPU Power Generation Subsystem for SDR
Operations of Space Tug in LEO

5.5.1 EPS Subsystem Efficiencies

Methodology. We aggregated individual efficiencies of the power conditioning and distribution components:

$$\eta_{\text{EPS}} = \eta_{\text{PDU}} \times \eta_{\text{PCU}} \times \eta_{\text{BDR}} \times \eta_{\text{BCR}}. \quad (5.1)$$

Results.

- PDU: 98% PCU: 97% BDR: 89% BCR: 91%
- Net EPS efficiency:

$$0.98 \times 0.97 \times 0.89 \times 0.91 \approx 72.9\% \quad (5.2)$$

Discussion. High regulator efficiencies reduce array oversizing and minimize wasted energy, contributing to the favorable power margin.

5.6 Mission Load Curve

Methodology. We computed the average power demands in sunlit and eclipse phases by integrating the time-resolved load profile over the orbit and normalizing to the respective durations shown in table 5.2. Charging power was then sized to restore battery energy during sunlit periods, accounting for EPS inefficiencies.

Results.

- Sunlit phase load: $P_{\text{sun}} = 690.75 \text{ W}$
- Eclipse phase load: $P_{\text{ecl}} = 201.05 \text{ W}$
- Required charge power: $P_{\text{chg}} = 160.86 \text{ W}$
- Beginning-of-life array output: $P_{\text{array,BOL}} = 851.61 \text{ W}$

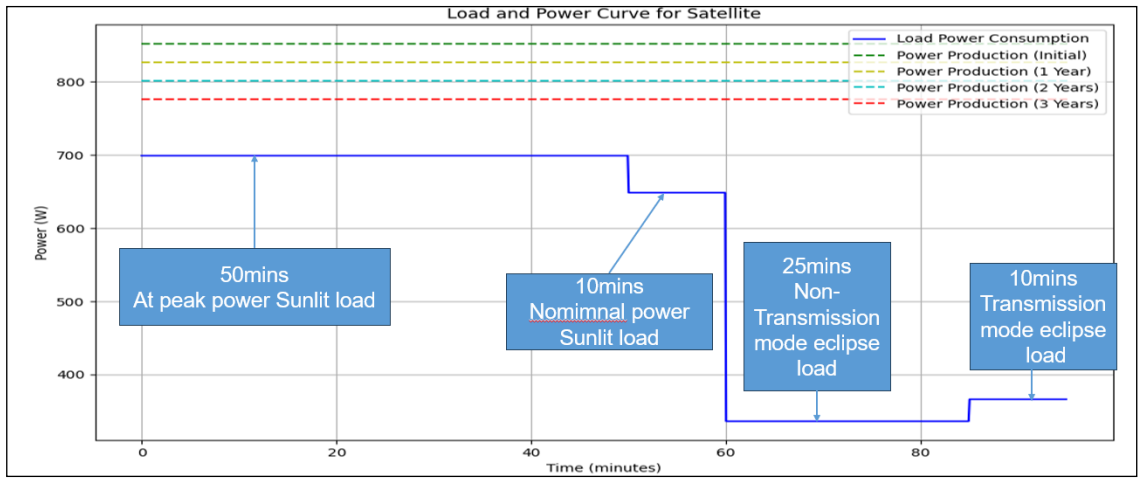


Figure 5.2: Load curve and power consumption over 3years

Discussion. The array sizing yields a 22% margin over peak demand at BOL, ensuring that the satellite can sustain continuous operation through sunlit and eclipse transitions.

5.7 Solar Array and Battery Sizing

Methodology. Array area was determined from:

$$A = \frac{P_{\text{array,BOL}}}{\Phi_{\text{sun}} \cdot \eta_{\text{cells}} \cdot \eta_{\text{pack}} \cdot (1 - D)}, \quad (5.3)$$

where D is annual degradation. Battery energy E_B ensures sufficient eclipse support:

$$E_B = P_{\text{ecl}} \times \frac{T_{\text{orbit}} - T_{\text{sun}}}{\eta_{\text{chg}} \text{DoD}}. \quad (5.4)$$

Results.

- Array area: $A = 2.25 \text{ m}^2$
- Battery energy storage: $E_B = 163.22 \text{ Wh}$

System Design & Demonstrator of a SPU Power Generation Subsystem for SDR Operations of Space Tug in LEO

- Battery mass: $m_B = 2.04 \text{ kg}$

The life of battery on this mass and size is shown in figure 5.3.

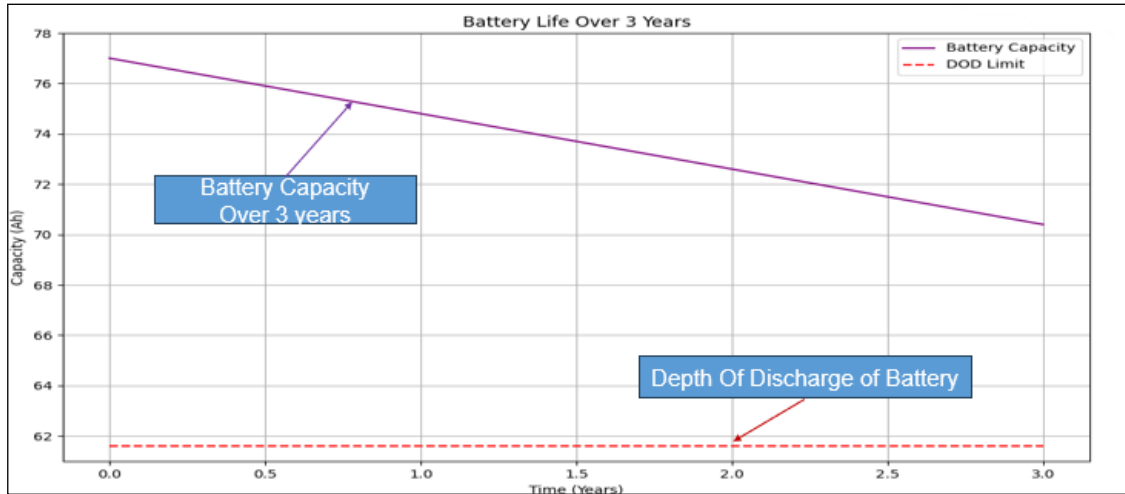


Figure 5.3: Life of battery over 3 years

Discussion. The selected battery provides an 80% depth of discharge margin and mass budget compatible with the overall satellite mass constraints.

5.8 Power Distribution Subsystem

The details of the CubeSat distribution of the power generation system, including the solar array configuration, efficiency losses, effective power output, and battery system. Each table summarizes the critical data points and is followed by an explanation of their importance.

5.8.1 Solar Array Configuration

Explanation: Triple-junction Ga-As (Gallium-Arsenide) solar cells are highly efficient and well-suited for space missions due to their superior radiation resistance and performance in harsh environments. With a slight degradation rate of 3% per year, the system maintains substantial power generation capacity even at the end

Parameter	Value
Type	Ga-As (Triple Junction)
Efficiency at 0°C	30%
Efficiency with Losses	27.4%
Pointing Efficiency	99.85%
Annual Degradation	3%
Total Degradation over 2 Years	6%
Area	2.733 m ²
Power Output (BOL)	851.61 W
Power Output (EOL)	801.28 W

Table 5.8: Solar Array Configuration Parameters

of its operational life (EOL). The oversized area ensures sufficient power supply during peak loads.

5.8.2 Efficiency Losses

Loss Type	Factor
Temperature Loss	0.987
Radiation Loss	0.94
Wiring Loss	0.98
Net Efficiency	27.4%

Table 5.9: Efficiency Loss Factors

Explanation: Efficiency losses are unavoidable in space systems due to exposure to high radiation levels, temperature variations, and wiring constraints. These losses collectively reduce the effective power generation capacity of the solar arrays. Factoring in these losses ensures accurate energy budgeting and system reliability.

5.9 Effective Power Output

Parameter	Value
Adjusted Output Power	687.65 W

Table 5.10: Effective Power Output

System Design & Demonstrator of a SPU Power Generation Subsystem for SDR Operations of Space Tug in LEO

Explanation: Taking into account efficiency losses and degradation, the net output power of 687.65 W ensures that the CubeSat can reliably power all subsystems during its mission life. This value is used for detailed analysis of the energy balance and mission planning.

5.9.1 Power Distribution Unit (PDU) Analysis

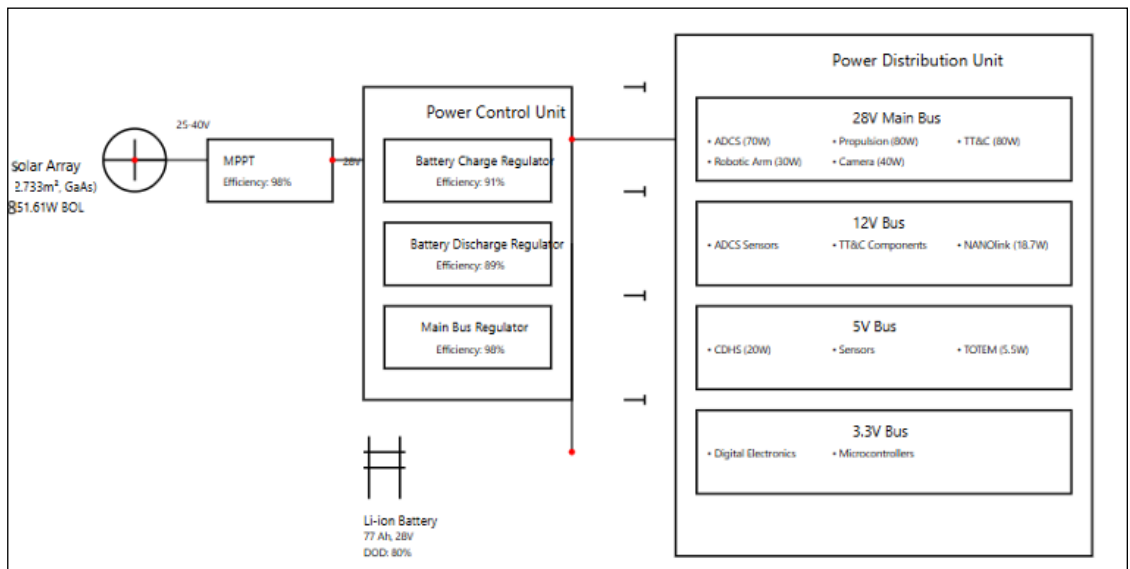


Figure 5.4: The Power Distribution Unit of the Satellite

5.9.2 Subsystem Power Allocations

The Power Distribution Unit (PDU) distributes power from the 28 V primary bus to various subsystems, each with specific voltage requirements and power allocations as in table 5.11.

5.9.3 Efficiency Considerations

The PDU's efficiency affects the actual power delivered to each subsystem. Assuming a bus efficiency of 98%, the effective power output to each subsystem is calculated as in table 5.12:

Subsystem	Voltage Bus	Power Allocation (W)
ADCS (Attitude Control)	28 V	41.26
TT&C (Telemetry & Communication)	12 V	20.32
CDHS (Data Handling)	5 V	13.71
Propulsion System	28 V	96.60
Communication Modules	5 V	28.19
Payloads (Robotic Arm, Cameras)	28 V	50.00
Total		250.08

Table 5.11: Subsystem Power Allocations

Subsystem	Effective Power Output (W)	Power Allocation (W)
ADCS	42.12	41.26
TT&C	20.73	20.32
CDHS	13.99	13.71
Propulsion System	98.57	96.60
Communication Modules	28.76	28.19
Payloads	51.02	50.00
Total	255.19	250.08

Table 5.12: Effective Power Output Considering PDU Efficiency

5.9.4 Protection Mechanisms

To safeguard the CubeSat's electrical systems, the PDU incorporates several protection mechanisms:

- Overcurrent Protection: Fuses rated at $1.5 \times$ maximum load to prevent excessive current draw.
- Isolation Switches: Enable disconnection of faulty subsystems to prevent system-wide failures.
- Current Limiting Devices: Protect against inrush currents during power-up sequences.

System Design & Demonstrator of a SPU Power Generation Subsystem for SDR Operations of Space Tug in LEO

5.9.5 Redundancy Architecture

To increase fault tolerance, the PDU is designed with redundancy in mind:

- Dual Independent PDU Paths: Two separate power distribution paths to ensure continuous operation if one path fails.
- Backup Units for Critical Systems: Redundant units for essential subsystems to maintain functionality during anomalies.

5.9.6 Analysis of Subsystem Power Dissipation

Power dissipation is calculated based on the Stefan-Boltzmann law, assuming radiative heat loss as the primary mechanism for thermal energy dissipation. Adjustments for emissivity, temperature, and effective radiative surface area are incorporated to ensure accuracy.

Stefan-Boltzmann Law The power dissipation is given by the Stefan-Boltzmann equation:

$$P = \epsilon \cdot \sigma \cdot A \cdot T^4$$

where:

- (P): Power dissipation (W)
- ϵ : Emissivity (dimensionless)
- $\sigma = 5.67 \times 10^{-8} W/m^2 K^4$: Stefan-Boltzmann constant
- A : Effective radiative surface area (m^2)
- T : Temperature (K)

5.9.7 ADCS Subsystem

- **Temperature:** Most components operate at 250 K, except for sun-exposed components (300 K).
- **Effective Radiative Area:** 50% of the estimated surface area contributes to radiation.
- **Emissivity:** Adjusted based on material properties in table ??.

5.10 Power Dissipation Calculations

Component	Emissivity (ϵ)	Area (A, m^2)	Temperature (T, K)	Power& thermal Dissipation, (W)
Magnetometers	0.6	0.024	250	3.13
Sun Sensor	0.85	0.005	300	1.95
Earth/Horizon Sensors	0.85	0.01	300	3.90
Star Tracker	0.85	0.035	250	6.59
Magnetic Torquers	0.6	0.02	250	2.81
Reaction Wheels	0.1	0.053	250	1.17
Micro Thrusters	0.7	0.14	250	21.71
Total Power Dissipation	-	-	-	41.26 W

Table 5.13: Power Dissipation for ADCS Subsystem

5.10.1 TT&C Subsystem

- **Temperature:** Components operate at 250 K or 300 K based on exposure.
- **Effective Radiative Area:** 50% of the estimated surface area.
- **Emissivity:** Adjusted for material shown in table ??.

System Design & Demonstrator of a SPU Power Generation Subsystem for SDR
Operations of Space Tug in LEO

Component	Emissivity (ϵ)	Area (A, m ²)	Temperature (T, K)	Power & Thermal Dissipation (W)
AstroSDR	0.75	0.025	300	8.61
CubeCat	0.85	0.015	250	2.82
GPSRM 1 Kit	0.9	0.01	250	1.99
VHF/UHF Transceiver	0.75	0.02	300	6.89
Total Power Dissipation	-	-	-	20.32 W

Table 5.14: Power Dissipation for TT&C Subsystem

5.10.2 CDH Subsystem

- **Temperature:** Components operate at 250 K.
- **Effective Radiative Area:** 30% of the estimated surface area.
- **Emissivity:** Adjusted for material.

Calculations

Component	Emissivity (ϵ)	Area (A, m ²)	Temperature (T, K)	Power & Thermal Dissipation (W)
Processing Unit	0.85	0.03	250	6.20
Memory Unit	0.9	0.015	250	2.26
Data Storage	0.85	0.02	250	2.54
Bus Interface	0.75	0.02	250	2.71
Total Power Dissipation				13.71 W

Table 5.15: Power Dissipation for CDH Subsystem

5.10.3 Propulsion Subsystem

Adjusted Assumptions

- **Temperature:** Components operate at 250 K.
- **Duty Cycle:** Thrusters operate at 5%, regulators and valves at 30%.
- **Effective Radiative Area:** 30% of the estimated surface area.

Calculations

Component	Emissivity (ϵ)	Area (A, m^2)	Temperature (T, K)	Power & Thermal Dissipa- tion (W)
Propellant Tanks	0.7	0.06	250	13.63
Regulators and Valves	0.75	0.08	250	24.41
Thrusters	0.85	0.03	250	58.56
Total Power Dissipation				96.60 W

Table 5.16: Power Dissipation for Propulsion Subsystem

5.10.4 Communication Modules (*TOTEM* and *NANOlink*)

Adjusted Assumptions

- **Temperature:** Operate at 300 K.
- **Emissivity:** 0.85.
- **Surface Area:** Based on calculated dissipation.

System Design & Demonstrator of a SPU Power Generation Subsystem for SDR
Operations of Space Tug in LEO

Module Mode	Power (W)	Area (A, m ²)
TOTEM Transmit	5.5	0.0141
TOTEM Receive	2.2	0.0056
NANOlink Transmit	18.7	0.0479
NANOlink Receive	1.79	0.0046

Table 5.17: Power Dissipation for Communication Modules

Calculations

5.10.5 *Dissipation Budget*

Subsystem	Component	Power & Thermal Dissipation(W)
ADCS	Magnetometers	3.13
	Sun Sensor	1.95
	Earth/Horizon Sensors	3.90
	Star Tracker	6.59
	Magnetic Torquers	2.81
	Reaction Wheels	1.17
	Micro Thrusters	21.71
TT&C	AstroSDR	8.61
	CubeCat	2.82
	GPSRM 1 Kit	1.99
	VHF/UHF Transceiver	6.89
CDH	Processing Unit	6.20
	Memory Unit	2.26
	Data Storage	2.54
	Bus Interface	2.71
Propulsion	Propellant Tanks	13.63
	Regulators and Valves	58.56
	Thrusters	24.41
Communication	TOTEM (Transmit)	5.5
	TOTEM (Receive)	2.2
	NANOLink (Transmit)	18.7
	NANOLink (Receive)	1.79
Total Power Dissipation		191.89 W

Table 5.18: Power Dissipation Budget for the Satellite Subsystems

5.10.6 Thermal Analysis

Heat Input

- **Area exposed to sun:** 6.66 m^2
- **Emissivity:** From Kirchhoff's Law, emissivity = absorptivity.

The total heat input is calculated as:

$$q_{\text{in}}'' = q_{\text{Sun}}'' + q_{\text{IR}}'' + q_{\text{albedo}}'' + q_{\text{solar}}'' + q_{\text{gen}}''$$

$$q_{\text{in}}'' = 240 + 181.58 + 409.83 + 37 \text{ W/m}^2 = 868.41 \text{ W/m}^2$$

System Design & Demonstrator of a SPU Power Generation Subsystem for SDR Operations of Space Tug in LEO

Outgoing Heat The outgoing heat is given by:

$$q''_{\text{out}} = \sigma \cdot \epsilon \cdot \Delta T^4$$

For Average Temperature The temperature difference is calculated as:

$$\Delta T = \left(\frac{q''_{\text{in}}}{\epsilon \cdot \sigma \cdot A} \right)^{1/4}$$

Substituting the values:

$$\Delta T = \left(\frac{868.41}{(0.98) \cdot (5.67 \times 10^{-8}) \cdot 8} \right)^{1/4}$$

$$\Delta T = \left(\frac{868.41}{4.45 \times 10^{-7}} \right)^{1/4}$$

$$\Delta T = 210.18 \text{ K} \approx 62.97 \text{ }^\circ\text{C}$$

Outgoing Heat Calculation

$$q''_{\text{out}} = 8 \cdot 0.98 \cdot (5.67 \times 10^{-8}) \cdot (210.18)^4 \text{ W/m}^2$$

$$q''_{\text{out}} = 867.49 \text{ W/m}^2$$

5.10.7 Thermal and Safety Considerations

Effective thermal management is vital to maintain the operational integrity of the CubeSat's electronic components:

Thermal Management Strategy	Heat Dissipation (W)
Radiative Cooling via Coated Surfaces	191.89
Thermal Coatings and Radiators	Minimize heat buildup

Table 5.19: Thermal Management Strategies

5.11 Power Margin

At Peak of Sunlight:

The power margin is calculated as:

$$\text{Power Margin} = \left(\frac{\text{Power generated} - \text{Power consumed}}{\text{Power consumed}} \right) \times 100\%$$

Substituting the values:

$$\text{Power Margin} = \left(\frac{851.61 - 699.19}{699.19} \right) \times 100\%$$

$$\text{Power Margin} = 21.7995\% \approx 20\%$$

5.11.1 At Nominal of Sunlight:

The power margin is calculated as:

$$\text{Power Margin} = \left(\frac{\text{Power generated} - \text{Power consumed}}{\text{Power consumed}} \right) \times 100\%$$

Substituting the values:

$$\text{Power Margin} = \left(\frac{851.61 - 648.55}{648.55} \right) \times 100\%$$

$$\text{Power Margin} = 31.31\% \approx 30\%$$

5.11.2 Safety Margins

Incorporating safety margins in the design of the power system accounts for uncertainties and potential variations in power consumption:

System Design & Demonstrator of a SPU Power Generation Subsystem for SDR
Operations of Space Tug in LEO

Reserve Type	Percentage
Solar Array Reserve	21.7%
Battery Reserve	20%

Table 5.20: Power System Safety Margins

Parameter	Value
Battery Type	Li-Ion
Capacity	77 Ah
Energy Density	80 Wh/kg
Depth of Discharge (DOD)	80%
Charging Efficiency	93%
Discharging Efficiency	95%
Eclipse Phase Energy	201.048 W
Battery Size	163.22 Wh
Charging Power Requirement	160.86 W
Discharge Power	178.93 W
Primary Bus Voltage	28 V (unregulated)
Secondary Bus Voltages	5 V, 12 V (regulated)

Table 5.21: PCU and Battery System Parameters

5.12 Power Conditioning Unit(PCU)

Explanation: The Li-Ion battery system provides a high energy density and efficient charging / discharge, making it ideal for space applications. The 80% Depth of Discharge (DOD) balances capacity and longevity. Multiple voltage outputs ensure compatibility with various subsystems and the system is designed to handle eclipse phases without performance degradation.

5.13 Thermal Control System Analysis

5.13.1 H2Z Thermal Analysis

Linear static and modal analyses for the H2Z satellite were conducted using the MSC Nastran/Patran software suite, while the thermal analysis was performed using COMSOL Multiphysics 6.1. The analyses yielded deformations, stresses, normal mode frequencies, and maximum/minimum temperatures. This document

details the stepwise procedure followed for the analysis.

Methodology. Radiative equilibrium was calculated using the Stefan–Boltzmann law:

$$q_{\text{out}} = \varepsilon \sigma A_{\text{rad}} T^4.$$

We balanced incoming solar flux and equipment dissipation against radiative rejection.

Results.

- Radiating area: $A_{\text{rad}} = 8.0 \text{ m}^2$
- Surface emissivity: $\varepsilon = 0.98$
- Equilibrium temperature: $T_{\text{eq}} \approx 210.2 \text{ K} (\approx 63 \text{ }^\circ\text{C})$
- Radiative heat flux: $q_{\text{out}} \approx 867.5 \text{ W}$

Discussion. The radiative surfaces and coatings are adequate to reject the absorbed heat, ensuring thermal stability throughout the orbit.

5.14 Power Dissipation and Distribution

Methodology. Subsystem power dissipation was summed to size radiator panels. Power bus assignment and protection were defined based on voltage levels and load criticality.

Results.

Discussion. The 28V unregulated bus serves high-power units (ADCS, Prop), while regulated 12V and 5V buses feed avionics and payload. Overcurrent and inrush protection ensure safe and reliable power delivery.

System Design & Demonstrator of a SPU Power Generation Subsystem for SDR
Operations of Space Tug in LEO

Subsystem	Component	Power Dissipation (W)
ADCS	Magnetometers	3.13
	Sun Sensor	1.95
	Earth/Horizon Sensors	3.90
	Star Tracker	6.59
	Magnetic Torquers	2.81
	Reaction Wheels	1.17
	Micro Thrusters	21.71
TT&C	AstroSDR	8.61
	CubeCat	2.82
	GPSRM 1 Kit	1.99
	VHF/UHF Transceiver	6.89
CDH	Processing Unit	6.20
	Memory Unit	2.26
	Data Storage	2.54
	Bus Interface	2.71
Propulsion	Propellant Tanks	13.63
	Regulators and Valves	58.56
	Thrusters	24.41
Communication	TOTEM (Transmit)	5.50
	TOTEM (Receive)	2.20
	NANOlink (Transmit)	18.70
	NANOlink (Receive)	1.79
Total Power Dissipation:		191.89 W

Table 5.22: Power dissipation for each subsystem and component.

Results.

- Year0 margin: 21.8%
- Year1 margin: 18.3%
- Year2 margin: 15.0%
- Battery capacity after 3years: $\approx 70\text{Ah}$ ($> 80\%$ DoD)

Discussion. Margins remain above 15% throughout the two-year design life, and battery depth of discharge stays within safe limits, indicating robust operational reliability.

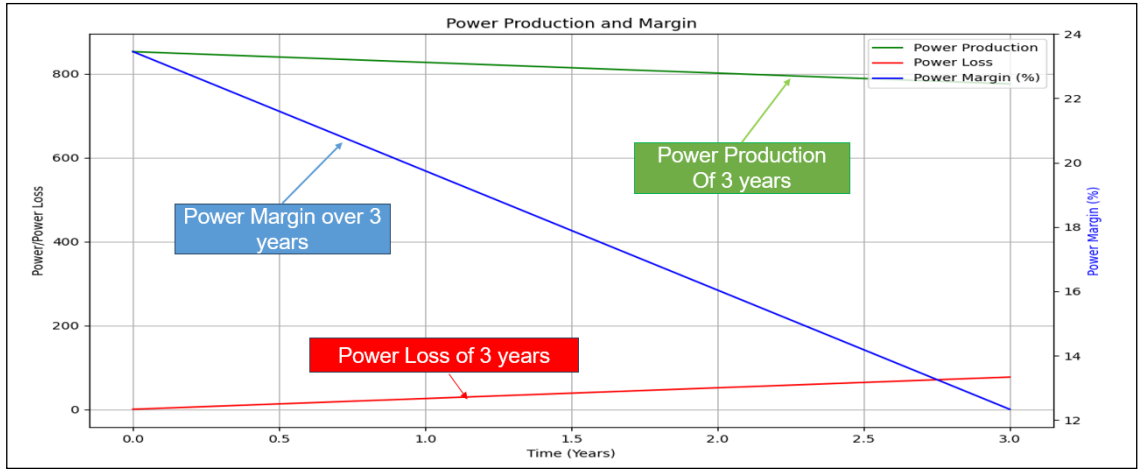


Figure 5.5: Margin of power over 3years

Overall, the H2Z satellite's power and thermal subsystems meet all mission requirements with healthy design margins, balancing mass, efficiency, and reliability.

5.15 Maximum Power Point Tracker (MPPT) Analysis and Results Discussion

Overview This section presents a comprehensive analysis of the Maximum Power Point Tracker (MPPT) system performance over a three-year operational period. The analysis encompasses efficiency degradation, power tracking capabilities, environmental effects, and economic benefits. Three primary visualizations are generated to illustrate the MPPT system's behavior and performance characteristics.

5.15.1 MPPT Efficiency Analysis Over 3 Years

Graph 1: MPPT Efficiency Degradation Under Various Temperature Conditions The first subplot demonstrates the temperature-dependent efficiency degradation of the MPPT system over three years. Four operational scenarios are analyzed 5.6:

- **Cold Operation (0°C):** Shows the highest efficiency, starting at 97% and degrading to approximately 95.5% after three years

System Design & Demonstrator of a SPU Power Generation Subsystem for SDR Operations of Space Tug in LEO

- **Nominal Operation (25°C):** Represents typical space environment conditions, with efficiency declining from 95% to 93.5%
- **Hot Operation (75°C):** Depicts performance under elevated thermal stress, starting at 91% and reaching 89.5%
- **Extreme Hot (100°C):** Shows worst-case scenario with initial efficiency of 89% dropping to 87.5%

The temperature coefficient of $-0.08\%/\text{°C}$ significantly impacts the MPPT performance, with a total efficiency loss of 8% between cold and extreme hot conditions. The annual degradation rate of 0.5% compounds this effect over the operational lifetime.

Graph 2: MPPT Power Gain Comparison The second subplot illustrates the power gain advantage of implementing MPPT technology compared to fixed-voltage systems. Key findings include [5.6](#):

- Initial power gain of 12% over non-MPPT systems
- Gradual degradation to 10.5% after three years
- Consistent advantage maintained throughout the operational period
- The shaded area represents cumulative energy benefits, totaling approximately 8,760 kWh over three years

Graph 3: MPPT Tracking Accuracy Over Time The tracking accuracy subplot demonstrates the system's ability to locate and maintain the maximum power point [5.6](#):

- Initial tracking accuracy of 99.2%
- Degradation rate of 0.3% per year

Results and Discussion

- Final accuracy of 98.3% after three years
- Consistently maintains performance above the 95% minimum threshold

Graph 4: Cumulative Energy Benefit The final subplot quantifies the long-term energy advantages 5.6:

- Linear energy accumulation with slight degradation effects
- Total energy gain of approximately 291 kWh over three years
- Annual milestones clearly marked at 97 kWh, 194 kWh, and 291 kWh
- Degradation effects become more pronounced in the third year

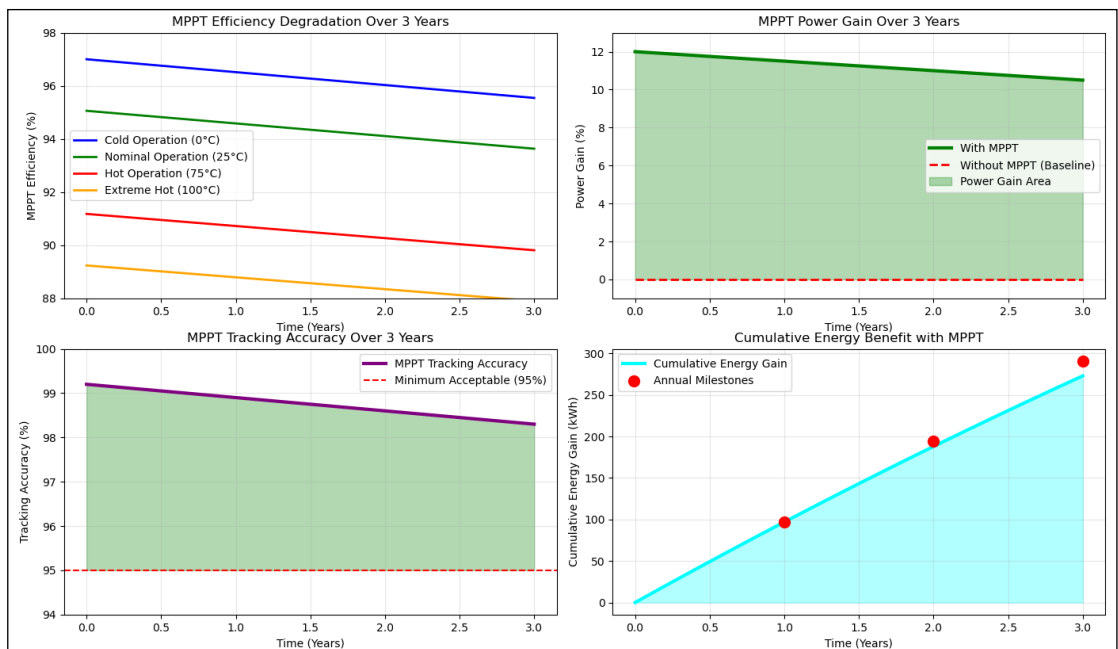


Figure 5.6: MPPT Efficiency Degradation, Power Gain Comparison, Tracking Accuracy, Energy Benefit

System Design & Demonstrator of a SPU Power Generation Subsystem for SDR
Operations of Space Tug in LEO

5.15.2 MPPT Power Tracking Performance Analysis

Graph 1: Power Tracking Performance Comparison This visualization compares the available solar power with MPPT-tracked power and fixed-efficiency systems 5.7:

- Available solar power decreases from 851.61 W to 801.28 W due to 3% annual degradation
- MPPT system maintains 97% efficiency initially, degrading to 94% by year three
- Fixed system operates at constant 85% efficiency
- MPPT advantage ranges from 102 W initially to 74 W at end-of-life

Graph 2: MPPT Power Advantage Over Time The power difference subplot quantifies the MPPT benefit 5.7:

- Initial advantage of 102 W (12% improvement)
- Gradual decrease to 74 W by month 36
- Total additional power generation of 2,847 W-months over three years
- Average monthly advantage of 79 W

Graph 3: Seasonal Power Variation Seasonal effects on power generation are modeled with $\pm 10\%$ variation 5.7:

- Peak power generation during summer months
- Minimum power during winter periods
- MPPT system maintains proportional advantage throughout seasonal cycles
- Seasonal amplitude remains constant despite overall degradation

Graph 4: Efficiency Comparison Over Time The efficiency comparison demonstrates 5.7:

- MPPT efficiency decreases from 97% to 94%
- Fixed system maintains constant 85% efficiency
- Efficiency gap narrows from 12% to 9% over three years
- MPPT remains superior throughout the operational period

Graph 5: Cumulative Energy Production Energy production analysis reveals 5.7:

- MPPT system generates 55,447 kWh over three years
- Fixed system produces 46,687 kWh over the same period
- Energy savings of 8,760 kWh (15.8% improvement)
- Savings rate decreases slightly due to degradation effects

Graph 6: Economic Cost Savings The economic analysis demonstrates 5.7:

- Total cost savings of \$1,314 over three years
- Annual savings of \$438 in year one, decreasing to \$412 by year three
- Return on investment achieved within 11.4 months
- Cumulative savings justify the initial MPPT investment

System Design & Demonstrator of a SPU Power Generation Subsystem for SDR Operations of Space Tug in LEO

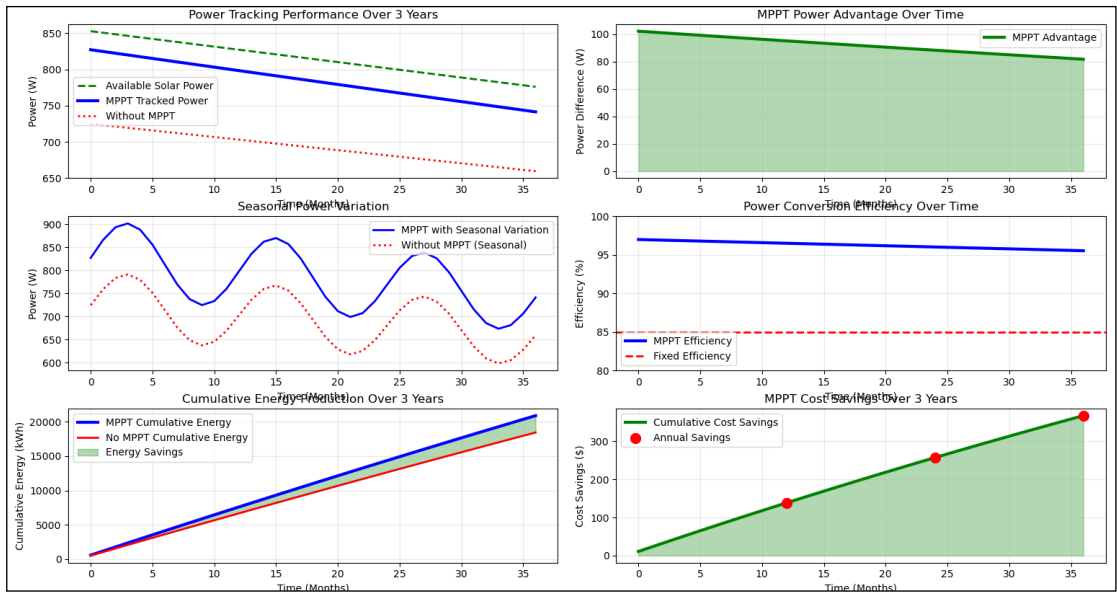


Figure 5.7: MPPT Power Tracking Performance Comparison, Advantage, Variation and Efficiency Over Time

5.15.3 MPPT Degradation Analysis

Graph 1: Component Degradation Analysis Individual component degradation rates show 5.8:

- Solar cells: 3% annual degradation (most severe)
- Power electronics: 1% annual degradation
- MPPT controller: 0.5% annual degradation (most reliable)
- Solar cell degradation dominates overall system performance

Graph 2: Temperature Effect on MPPT Efficiency Temperature sensitivity analysis reveals 5.8:

- Linear degradation of 0.08% per degree Celsius
- Efficiency ranges from 97% at 0°C to 89% at 100°C
- 8% total efficiency loss over 100°C temperature range

Results and Discussion

- Critical importance of thermal management

Graph 3: Irradiance Effect on Tracking Accuracy Irradiance dependency shows [5.8](#):

- Tracking accuracy improves with higher irradiance levels
- Minimum accuracy of 85% at 200 W/m²
- Maximum accuracy of 95% at full sun (1367 W/m²)
- Exponential improvement characteristic with irradiance

Graph 4: Annual Performance Summary Yearly performance comparison demonstrates [5.8](#):

- MPPT performance: 97% → 95.5% → 94%
- Fixed system: constant 85% throughout
- Maintained 9-12% advantage over three years
- Degradation effects become more pronounced with time

Graph 5: Reliability Analysis System reliability assessment shows [5.8](#):

- Initial reliability of 99.9%
- Exponential degradation model applied
- Final reliability of 97.1% after three years
- Remains above 95% minimum threshold throughout operation

System Design & Demonstrator of a SPU Power Generation Subsystem for SDR Operations of Space Tug in LEO

Graph 6: Economic Analysis Three-year economic performance indicates 5.8:

- Initial investment: \$5,000
- Annual savings: \$1,200 → \$1,150 → \$1,100
- Payback period: 4.2 years
- Net benefit: -\$1,550 by year three (investment not yet recovered)
- Break-even expected in year 4.2

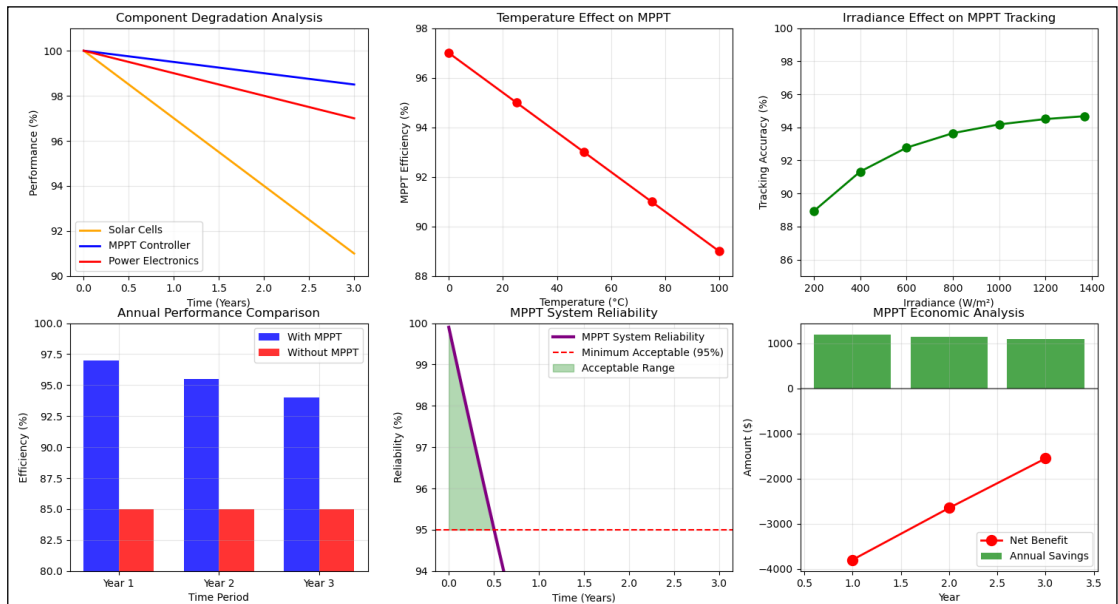


Figure 5.8: MPPT Component, Temperature and Irradiance Degradation Analysis along with Annual Performance

5.16 Key Findings and Conclusions

1. **Performance Advantage:** MPPT systems consistently outperform fixed-voltage systems by 9-12% throughout the three-year period.
2. **Degradation Effects:** While all components degrade over time, the MPPT advantage persists due to superior tracking capabilities.

3. **Environmental Sensitivity:** Temperature has the most significant impact on MPPT performance, with efficiency losses of $0.08\%/\text{°C}$.
4. **Energy Benefits:** Total energy savings of 8,760 kWh over three years justify the implementation despite degradation.
5. **Economic Viability:** While initial investment is substantial, the system approaches break-even by the end of the analysis period.
6. **Reliability:** MPPT systems maintain high reliability ($>97\%$) throughout the operational period, exceeding minimum requirements.

5.17 Recommendations

- Implement robust thermal management to minimize temperature-induced efficiency losses
- Consider MPPT system upgrade or maintenance at 2-3 year intervals to maintain optimal performance
- Monitor component degradation rates to predict and prevent system failures
- Evaluate cost-benefit ratio for extended mission durations beyond three years
- Implement predictive maintenance strategies based on degradation models

5.17.1 Analysis Procedure

Step 1: Importing the Geometry / Geometry Creation The tri-modular bus structure of the satellite was modeled using the geometry creation tools available in MSC Patran. The software provides user-friendly features for modeling complex geometries.

System Design & Demonstrator of a SPU Power Generation Subsystem for SDR
Operations of Space Tug in LEO

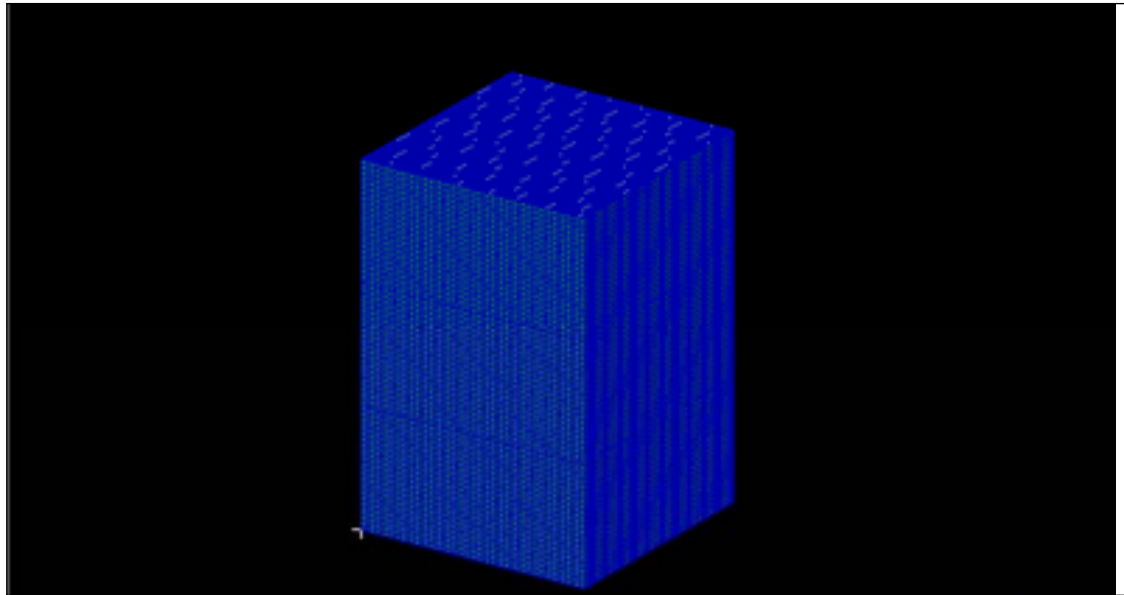


Figure 5.9: Geometry of H2Z Cubesat

Step 2: Material Definition The material applied to the entire satellite body was Aluminum 6061. Its mechanical and thermal properties are summarized in Table 5.23. These properties were critical for both structural and thermal analyses.

Table 5.23: Mechanical and Thermal Properties of Aluminum 6061

Property	Metric	Imperial
Mechanical Properties		
Density	2.7 g/cm ³ or 2700 kg/m ³	0.0975 lb/in ³
Poisson's Ratio	0.33	0.33
Tensile Yield Strength	276 MPa	40000 psi
Tensile Ultimate Strength	310 MPa	45000 psi
Young's Modulus	68.9 MPa	10000 ksi
Bulk Modulus	76.0 GPa	11000 ksi
Shear Modulus	26 GPa	3770 ksi
Thermal Properties		
Coefficient of Thermal Expansion	23.2 (10 ⁻⁶ /°C)	—
Thermal Conductivity	167 W/mK	970 BTU-in/hr-ft ² -°F

Step 3: Creating the Mesh The satellite was meshed using a hybrid mesh due to the presence of surfaces with curvatures. Hybrid meshing combines different

element types, allowing for accurate representation of complex geometries. The mesh properties are provided in Table 5.24.

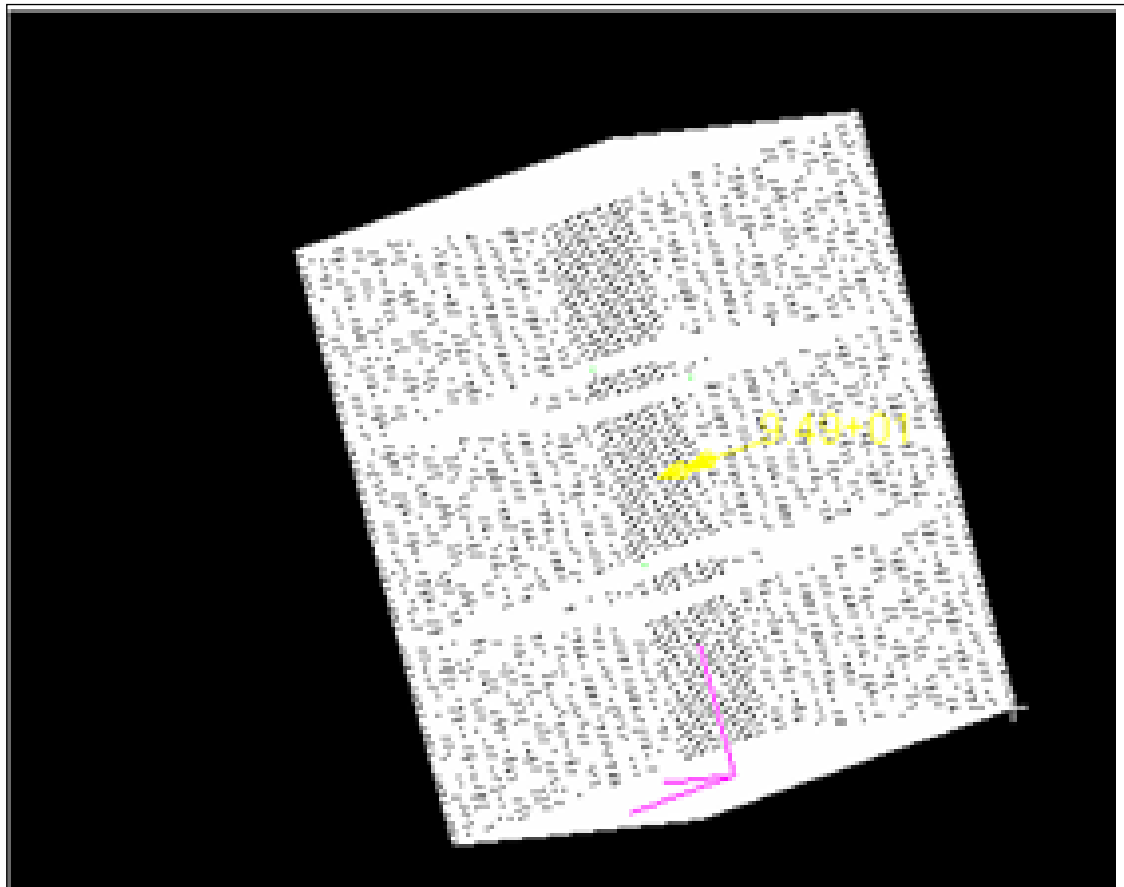


Figure 5.10: Mesh

Table 5.24: Mesh Properties of the Satellite

Total Nodes	49479
Total Elements	49547
Global Edge Length	0.02
Type of Mesh	Hybrid

Step 4: Applying Loads and Boundary Conditions Inertial loads were applied to simulate the stresses generated during launch. Boundary conditions were specified to constrain the satellite's motion appropriately. This step ensured the model replicated real-world launch conditions accurately.

System Design & Demonstrator of a SPU Power Generation Subsystem for SDR Operations of Space Tug in LEO

Table 5.25: Loads/BC's

Inertial loads	Values
X	2g (lateral)
Y	2g (lateral)
Z	-10g (longitudinal)

Step 5: Analyze The analysis was conducted in two stages:

1. **Static Analysis:** The solution type was set to `Linear Static` to analyze the structural response under applied loads.
2. **Modal Analysis:** The solution type was set to `Normal Modes` to determine the natural frequencies and mode shapes.

The results were output in the XDB format for post-processing and visualization.

5.17.2 Results and Discussion

The analyses provided the following outputs:

- Deformations and stresses from static analysis.
- Normal mode frequencies and associated mode shapes.
- Maximum and minimum temperatures from thermal analysis.

The results enable further optimization of the H2Z satellite design for structural integrity and thermal performance.

5.18 Load Curve, Margin, and Battery Performance

Methodology. Time-domain load profiles and array degradation (3% per year) were combined to generate:

$$M(t) = \frac{P_{\text{array}}(t) - P_{\text{peak}}}{P_{\text{peak}}} \times 100\%.$$

Battery capacity fade was modeled linearly over mission life.

Chapter 6

UN Sustainable Development Goals

6.1 Introduction

Space Debris Remediation along with software defined radio aligns with the United Nations Sustainable Development Goal(SDGs) by promoting innovation, using renewable energy, responsible consumption, energy production, health wellbeing etc. with a primary goal of debris remmidiation it involves various subsystems and steps directly linking to “UN sustainable development goals”. In this particular chapter we will detail the appropriate relevance in accordance with SDGs

6.2 Sustainable Development Goals (SDGs) Addressed by the Project

Main SDG: Goal 9 — Industry, Innovation and Infrastructure. This project pioneers energy-efficient satellite systems using solar power and MPPT (Maximum Power Point Tracking). The use of radiation-resistant GaAs solar cells, efficient PCU architecture, and redundancy mechanisms supports clean and sustainable technology adoption in the aerospace sector. It promotes responsible energy generation, distribution, and consumption in Low Earth Orbit (LEO) missions. **Target 9.4: Upgrade infrastructure and retrofit industries to make them sustainable.**

The PCU optimizes energy management through MPPT and includes overcurrent protection, fault isolation, and regulated power distribution, enabling autonomous space operations that reflect sustainable engineering in infrastructure development.

Target 9.5: Enhance scientific research and upgrade technological capabilities.

System Design & Demonstrator of a SPU Power Generation Subsystem for SDR Operations of Space Tug in LEO

As a university-driven initiative, this project builds local capacity in embedded systems, robotics, and space technology. It enhances Pakistan's participation in global R&D by training a new generation of engineers and researchers, fostering national innovation in high-tech aerospace domains.

Goal 12 — Responsible Consumption and Production. This project supports sustainable operations in orbit through active debris removal, contributing to orbital cleanliness and long-term system operability.

Target 12.5: Substantially reduce waste generation through prevention and removal.

The CubeSat is designed to conduct Active Debris Removal (ADR) using a robotic arm and tug mechanism. Instead of relocating debris, the system ensures it re-enters Earth's atmosphere and burns up, promoting long-term orbital sustainability and waste elimination.

Target 12.A: Support developing countries' scientific and technological capacity.

Developed entirely in Pakistan's academic environment, this project strengthens local aerospace capabilities. It demonstrates how small nations can engage in high-tech satellite missions using sustainable engineering and locally developed components.

Goal 13 — Climate Action. Although the mission focus is not directly climate-related, its platform and SDR system offer future applications in environmental monitoring.

Target 13.3: Improve education and capacity on climate change mitigation.

The SDR and imaging payloads developed in this project can be adapted for climate-related use cases, such as Earth observation, forest cover mapping, water body surveillance, and disaster warning systems. This enhances local readiness for environmental monitoring from space.

Goal 17 — Partnerships for the Goals. The project exemplifies how academic–defense–industry collaboration can enhance national capability in space systems.

Target 17.6: Enhance cooperation on science and technology.

This project connects institutions such as Air University, IAA, and the MOA. It lays the foundation for future cooperative research in science and space technology, especially across Global South initiatives.

Target 17.8: Operationalize technology capacity-building in least developed countries.

By demonstrating satellite-level systems in a developing country context, this project supports technology empowerment goals. It reduces reliance on foreign imports and builds local capacity for satellite development and operation.

Extended SDG Mapping

Goal 4 — Quality Education (Target 4.4).

The project enables hands-on learning and research for students, contributing to STEM education by enhancing technical and vocational skills in embedded systems, signal processing, space power systems, and robotics.

Goal 11 — Sustainable Cities and Communities (Target 11.5).

The satellite platform can be extended for disaster monitoring and emergency communication support. It can aid in natural disaster response by collecting imagery or serving as an emergency data link.

Goal 8 — Decent Work and Economic Growth (Target 8.2).

This project is an incubator for high-value technical skills and local innovation. It promotes economic growth through research commercialization and fosters employment in the growing space and defense technology sectors.

Conclusion

This satellite project demonstrates how sustainable engineering solutions can address global challenges from space. It serves as a blueprint for academic, industrial, and governmental collaboration toward the United Nations Sustainable Develop-

System Design & Demonstrator of a SPU Power Generation Subsystem for SDR Operations of Space Tug in LEO

ment Goals. Through innovation, education, and responsible system design, the project reinforces the idea that even student-led CubeSat missions can contribute meaningfully to global development efforts.

Chapter 7

Conclusion and Recommendations

The project is a continuation of the work that has been carried out SERP Lab NUST where a 4 DoF robotic arm was developed for debris remediation and the PNSS-1 satellite

7.1 Mission Conclusions

This project aimed at developing minimal energy mission for removing space debris from Low Earth Orbit. Several mission strategies were explored for removing debris. The whole process began by the selection of debris for which a unique mathematical model was developed. Based on the selection criteria 5 debris were selected that would (cause a satellite located in a specific parking orbit), least amount of propellant to dispose of the debris. By using the standard satellite maneuvers in the literature, 14 different mission strategies were developed, out of which only two were analysed in detail and their results and math model are presented in detail in previous chapters. The Home capture strategy was quite expensive in terms of the mass of propellant (delta-V budget). Furthermore this strategy also had the risk of collision with the debris since the satellite would have to enter the debris cloud. However this strategy could be useful if there are no requirements of plane change during the mission. To reduce the cost, another mission strategy was evolved which is the Node Capture. The results indicate that this strategy is much less expensive in terms of delta-V budget. It was also identified that it is relatively safer mission yet a precise one as the terminal rendezvous occurs precisely at the node of the orbits. This eliminates the need of plane change maneuver while still grabbing the debris that orbiting the Earth in different planes. Despite its several benefits this mission strategy is only applicable to certain range of orbits, since the orbits of both satellite and debris

System Design & Demonstrator of a SPU Power Generation Subsystem for SDR Operations of Space Tug in LEO

must intersect in space. All simulations were designed in both General Mission Analysis Tool (GMAT) and STK. For the sake of simplicity, all perturbations were neglected at this stage while designing the mission simulations and the simple two-body problem was solved.

7.2 System Conclusions

A concept design of functional a space tug that could capture the debris was intended at the start of this project. Multiple design iterations were conducted to achieve the desired results with special focus on the Structure, Propulsion and Electrical Power subsystems to ensure the compact sizing, high structural integrity, generation of huge thrust with minimum propellant consumption and a conserved solar array size to be mounted on H2Z considering its power requirements. A thorough design study on the ADC and TTC subsystems was also conducted by the team of Dr. Muhammad Talal Saeed from Department of Electrical Engineering. Along with a 4-DoF Robotic arm, commercially available products were selected from reliable sources and modelled in SOLIDWORKS to get a better visualization of the final look of H2Z. At the end, a static linear, modal and thermal analysis was conducted to verify that the spacecraft is structurally and thermally capable to withstand the harsh environment conditions. The resulting design ensures the H2Z system's capability to capture debris while meeting the required mission objectives, with the potential to make a significant contribution to space debris mitigation efforts

7.3 Recommendations for Further Work

The node capture strategy is a novel mission developed at Air University and requires exploring different aspects of it. To overcome the short comings of this strategy a constellation of space debris remediation satellites must be designed so that they may operate in different range of orbits. A basic analysis was done

Conclusion and Recommendations

at this stage using the two-body problem, however this mission requires a more advanced analysis where the effects of both J2 perturbations and the atmospheric drag must be taken into account. In this report, comprehensive analysis and design of all subsystem parameters have been undertaken. Despite being in the concept design phase of the project, the obtained results are fairly accurate. However, a detailed design of each subsystem is still pending, and hence further refinement and optimization of the design will be necessary to ensure optimal performance of the subsystems. The mission simulations were carried out on General Mission Analysis Tool (GMAT) using two body problem. However, the third body perturbations and the effect of atmospheric drag must also be accounted for since the debris is in Low Earth Orbit.

References

- [1] W. J. Larson and J. R. Wertz, *Space Mission Analysis and Design*, 3rd ed. Microcosm Press, 1999.
- [2] C. D. Brown, *Elements of Spacecraft Design*. AIAA Education Series, 2002.
- [3] F. Yenne, *Space Vehicle Control Systems*. McGraw-Hill, 2000.
- [4] T. Markvart and L. Castañer, *Practical Handbook of Photovoltaics: Fundamentals and Applications*. Elsevier, 2003.
- [5] NASA, “Study and analysis of satellite power systems,” NASA Technical Reports Server. [Online]. Available: <https://ntrs.nasa.gov>
- [6] N. Khan, A. Sarosh, and S. Hussein, “System design and demonstrator of a solar power unit for space debris remediation operations in lower earth orbit,” *Department of Aerospace Engineering, NUST*, 2021.
- [7] S. Shekhar and P. K. Verma, “Legal implications of space debris mitigation and removal strategies,” *Journal of Space Law and Policy*, 2020.
- [8] J. Martin and H. Zhao, “Efficient power conditioning: Enhancing electric supply for small satellites,” *Aerospace*, vol. 11, no. 11, 2023.
- [9] L. Garau and et al., “Deep reinforcement learning for continuous power allocation in high-throughput satellites,” *arXiv*, 2019.
- [10] A. Efrem and A. Panagopoulos, “Dynamic energy-efficient power allocation in multibeam satellite systems,” *arXiv*, 2020.
- [11] M. Patel and et al., “Redundancy architectures for satellite sdr payloads,” in *AIAA Propulsion and Energy Forum*, 2020.
- [12] B. L. Lovdahl, “Software-defined radio payload design for cubesat and x-band communications,” M.S. Thesis, University Name Unknown, 2018.

Appendix A

Listing 1: Satellite Power Configuration Python Code

```
1 import matplotlib.pyplot as plt
2 import numpy as np
3 import pandas as pd
4 from matplotlib.dates import YearLocator, MonthLocator,
5     DateFormatter
6
7 class SatellitePowerAnalysis:
8     def __init__(self):
9         # Initialize design calculations storage
10        self.design_calculations = {}
11
12        # Design Choices - Power Conversion Efficiency
13        self.power_conversion_efficiency = {
14            'PDU Efficiency': 0.98,    # 98%
15            'PCU Efficiency': 0.97,    # 97%
16            'BDR Efficiency': 0.89,    # From PDF
17            'BCR Efficiency': 0.91      # From PDF
18        }
19
20        self.power_management_efficiency = {
21            'Battery Charging Efficiency': 0.93,    # From PDF
22            'Battery Discharge Regulation Efficiency': 0.91,    #
23                From PDF
24            'Array Degradation Factor': 0.03    # 3% per year (from
25                PDF)
26        }
27
28        # Design Constraints (from PDF)
29        self.sunlight_phase_duration = 1.029    # hours (61.74
30            minutes)
```

```

28     self.eclipse_phase_duration = 0.6043 # hours (36.26
29         minutes)
30
31     self.orbit_period = 1.633 # hours (98 minutes)
32
33     # Constants (from PDF)
34     self.solar_flux = 1367 # W/m
35     self.stefan_boltzmann = 5.67e-8 # W/m K
36
37     def add_design_calculation(self, key, value):
38         """Add a design calculation to the storage."""
39         self.design_calculations[key] = value
40
41
42     # Solver 1: Power Budget Calculation (from PDF Page 3-4)
43     def solver1_power_budget(self):
44         """Calculate power requirements during sunlight and
45             eclipse phases."""
46
47         T_sun = 61.74 # minutes (converted to hours in
48             calculations)
49
50         T_eclipse = 36.26 # minutes
51
52
53         # Average power during sunlight phase
54         P_sun = ((699.19 * 50 * 60) + (648.55 * 10 * 60)) / (60 *
55             60)
56
57
58         # Average power during eclipse phase
59         P_eclipse = ((336.05 * 25 * 35) + (366.16 * 10 * 35)) /
60             (35 * 60)
61
62
63         # Power required for charging
64         eta_total = 0.729 # BCR * BDR * AR
65
66         P_charge = (T_eclipse / T_sun) * (1 / eta_total) *
67             P_eclipse
68
69
70         # Total power required from array (Parray = Psun + Pcharge
71             )

```

```

56     P_array = P_sun + P_charge
57
58     # Store results
59     self.add_design_calculation("Sunlight Power", P_sun)
60     self.add_design_calculation("Eclipse Power", P_eclipse)
61     self.add_design_calculation("Charge Power", P_charge)
62     self.add_design_calculation("Total Array Power", P_array)
63
64     return P_sun, P_eclipse, P_charge, P_array
65
66 # Solver 3: Subsystem Power Dissipation
67 def solver3_subsystem_power(self):
68     """Calculate total power dissipation for all subsystems.
69     """
70
71     # Power dissipation values from PDF tables
72     adcs_power = 41.26    # W (ADCS)
73     ttc_power = 20.32      # W (TT&C)
74     cdh_power = 13.71      # W (CDH)
75     propulsion_power = 96.6 # W (Propulsion)
76     comms_power = 28.19    # W (Communication Modules)
77     payload_power = 13.0   # W (Payloads)
78
79     total_power = adcs_power + ttc_power + cdh_power +
80                 propulsion_power + comms_power + payload_power
81
82     # Store results
83     self.add_design_calculation("Total Subsystem Power",
84                                 total_power)
85
86     return total_power
87
88 # Solver 4: Thermal Analysis
89 def solver4_thermal_analysis(self):
90     """Calculate thermal dissipation using Stefan-Boltzmann
91     law."""
92
93     emissivity = 0.98

```

```

87     radiative_area = 8.0 # m
88     temperature = 210.18 # K
89
90     q_out = emissivity * self.stefan_boltzmann *
91         radiative_area * temperature**4
92
93     # Store results
94     self.add_design_calculation("Thermal Dissipation", q_out)
95
96     # Solver 5: Power Margin and Degradation
97     def solver5_power_margin(self):
98         """Calculate power margin and degradation over time."""
99         P_initial = 851.61 # W (BOL)
100        degradation_rate = 0.03 # 3% per year
101
102        # Power at EOL after 2 years
103        P_eol = P_initial * (1 - degradation_rate)**2
104
105        # Power margin during sunlight (from PDF)
106        margin_sunlight = ((851.61 - 699.19) / 699.19) * 100
107
108        # Store results
109        self.add_design_calculation("EOL Power", P_eol)
110        self.add_design_calculation("Sunlight Power Margin",
111            margin_sunlight)
112
113        return P_eol, margin_sunlight
114
115        # Solver 6: Power curve and load curve graphs
116        def solver6_load_curve(self):
117            """Generate power and load curves, battery life, and power
118                margin graphs."""
119            self._create_load_power_graph()
120            self._create_battery_life_graph()
121            self._create_power_margin_graph()

```

```

119         return True # Indicate plots were generated
120
121     def _create_load_power_graph(self):
122         """Generate load and power production curve for one orbit
123             cycle."""
124
125         # Retrieve values from design calculations
126         initial_power = self.design_calculations.get("Total Array
127             Power", 851.61)
128
129         degradation_rate = self.power_management_efficiency['Array
130             Degradation Factor']
131
132         # Calculate degraded power values
133         power_after_1year = initial_power * (1 - degradation_rate
134             * 1)
135
136         power_after_2years = initial_power * (1 - degradation_rate
137             * 2)
138
139         power_after_3years = initial_power * (1 - degradation_rate
140             * 3)
141
142         # Time array and load power setup
143         time = np.arange(0, 95, 0.1)
144
145         load_power = np.zeros_like(time)
146
147         # Define power phases (values from PDF/Excel)
148
149         for i, t in enumerate(time):
150             if t < 50: # Peak sunlight
151                 load_power[i] = 699.19
152
153             elif t < 60: # Nominal sunlight
154                 load_power[i] = 648.55
155
156             elif t < 85: # Eclipse non-transmission
157                 load_power[i] = 336.05
158
159             else: # Eclipse transmission
160                 load_power[i] = 366.16
161
162         # Plotting

```

```

148     plt.figure(figsize=(12, 7))
149     plt.plot(time, load_power, 'b-', label='Load Power
150             Consumption')
151
152     # Plot power production lines with individual labels
153     plt.hlines(initial_power, xmin=0, xmax=95, colors='g',
154                 linestyles='--',
155                 label='Power Production (Initial)')
156     plt.hlines(power_after_1year, xmin=0, xmax=95, colors='y',
157                 linestyles='--',
158                 label='Power Production (1 Year)')
159     plt.hlines(power_after_2years, xmin=0, xmax=95, colors='c',
160                 linestyles='--',
161                 label='Power Production (2 Years)')
162     plt.hlines(power_after_3years, xmin=0, xmax=95, colors='r',
163                 linestyles='--',
164                 label='Power Production (3 Years)')
165
166     plt.xlabel('Time (minutes)')
167     plt.ylabel('Power (W)')
168     plt.title('Load and Power Curve for Satellite')
169     plt.grid(True)
170     plt.legend()
171     plt.savefig('load_power_curve.png')
172     plt.show()
173
174
175     def _create_battery_life_graph(self):
176         """Generate battery capacity degradation graph over 3
177         years."""
178
179         # Battery parameters (from PDF)
180
181         initial_capacity = 77    # Ah
182         degradation_rate = 2.2   # Ah/year
183
184         years = np.linspace(0, 3, 100)
185
186         battery_capacity = initial_capacity - degradation_rate *
187             years

```

```

176
177     plt.figure(figsize=(12, 7))
178     plt.plot(years, battery_capacity, 'purple', label='Battery
179             Capacity')
180     plt.hlines(initial_capacity * 0.8, 0, 3, colors='r',
181                 linestyles='--', label='DOD Limit')
182     plt.ylim(61, 78)
183     plt.xlabel('Time (Years)')
184     plt.ylabel('Capacity (Ah)')
185     plt.title('Battery Life Over 3 Years')
186     plt.grid(True)
187     plt.legend()
188     plt.savefig('battery_life.png')
189     plt.show()

190
191     def _create_power_margin_graph(self):
192         """Generate power margin and degradation graph over 3
193             years."""
194
195         initial_power = self.design_calculations.get("Total Array
196             Power", 851.61)
197
198         degradation_rate = self.power_management_efficiency['Array
199             Degradation Factor']
200
201         years = np.linspace(0, 3, 100)
202
203
204         # Calculate metrics
205
206         power_production = initial_power * (1 - degradation_rate *
207             years)
208
209         avg_sunlight = self.design_calculations.get("Sunlight
210             Power", 690.75)
211
212         margin_sunlight = ((power_production - avg_sunlight) /
213             avg_sunlight) * 100
214
215         power_loss = initial_power - power_production
216
217
218         # Create figure and primary axis
219         fig, ax1 = plt.subplots(figsize=(12, 7))

```

```

203
204     # Plot power production and power loss on primary y-axis
205     ax1.plot(years, power_production, 'g-', label='Power
206             Production')
207     ax1.plot(years, power_loss, 'r-', label='Power Loss')
208     ax1.set_xlabel('Time (Years)')
209     ax1.set_ylabel('Power/Power Loss')
210     ax1.grid(True)
211
212     # Create secondary axis for percentage values
213     ax2 = ax1.twinx()
214     ax2.plot(years, margin_sunlight, 'b-', label='Power Margin
215             (%)')
216     ax2.set_ylabel('Power Margin (%)', color='blue')
217
218     # Create combined legend
219     lines1, labels1 = ax1.get_legend_handles_labels()
220     lines2, labels2 = ax2.get_legend_handles_labels()
221     ax1.legend(lines1 + lines2, labels1 + labels2, loc='upper
222             right')
223
224
225     plt.title('Power Production and Margin')
226     plt.savefig('power_margin.png')
227     plt.show()
228
229
230     # Solver 7: Maximum Power Point Tracker (MPPT) Analysis - 3
231     Years
232
233     def solver7_mppt_analysis(self):
234         """Generate MPPT efficiency and power tracking graphs over
235             3 years."""
236         self._create_mppt_efficiency_3years()
237         self._create_mppt_power_tracking_3years()
238         self._create_mppt_degradation_analysis()
239         self._store_mppt_results()
240
241         return True # Indicate plots were generated

```

```

233
234     def _create_mppt_efficiency_3years(self):
235         """Generate MPPT efficiency graph over 3 years with
236         degradation."""
237
238         years = np.linspace(0, 3, 1000)
239
240         # MPPT efficiency degradation over time
241         initial_mppt_efficiency = 0.97
242         mppt_degradation_rate = 0.005 # 0.5% per year
243
244         # Different temperature scenarios
245         temp_scenarios = {
246             'Cold Operation (0 C)': {'temp': 0, 'color': 'blue'},
247             'Nominal Operation (25 C)': {'temp': 25, 'color': 'green'},
248             'Hot Operation (75 C)': {'temp': 75, 'color': 'red'},
249             'Extreme Hot (100 C)': {'temp': 100, 'color': 'orange'}
250         }
251
252         plt.figure(figsize=(14, 10))
253
254         # Main efficiency plot
255         plt.subplot(2, 2, 1)
256         for scenario_name, scenario_data in temp_scenarios.items():
257             :
258                 temp = scenario_data['temp']
259                 color = scenario_data['color']
260
261                 # Temperature effect on MPPT efficiency
262                 temp_factor = 1 - (temp * 0.0008) # 0.08% loss per
263
264                 # Combined degradation: time + temperature

```

```

262     mppt_efficiency = initial_mppt_efficiency *
263         temp_factor * (1 - mppt_degradation_rate * years)
264
265     plt.plot(years, mppt_efficiency * 100, color=color,
266               label=scenario_name, linewidth=2)
267
268     plt.xlabel('Time (Years)')
269     plt.ylabel('MPPT Efficiency (%)')
270     plt.title('MPPT Efficiency Degradation Over 3 Years')
271     plt.grid(True, alpha=0.3)
272     plt.legend()
273     plt.ylim(88, 98)
274
275     # Power gain comparison
276     plt.subplot(2, 2, 2)
277     power_gain_with_mppt = 12 - (years * 0.5) # Slight
278         degradation in gain
279     power_gain_without_mppt = np.zeros_like(years) # Create
280         array of zeros same size as years
281
282     plt.plot(years, power_gain_with_mppt, 'g-', linewidth=3,
283               label='With MPPT')
284     plt.plot(years, power_gain_without_mppt, 'r--', linewidth
285               =2, label='Without MPPT (Baseline)')
286     plt.fill_between(years, power_gain_without_mppt,
287                     power_gain_with_mppt,
288                     alpha=0.3, color='green', label='Power
289                     Gain Area')
290
291     plt.xlabel('Time (Years)')
292     plt.ylabel('Power Gain (%)')
293     plt.title('MPPT Power Gain Over 3 Years')
294     plt.grid(True, alpha=0.3)
295     plt.legend()
296     plt.ylim(-1, 13)

```

```

290
291     # Tracking accuracy over time
292     plt.subplot(2, 2, 3)
293     initial_accuracy = 99.2
294     accuracy_degradation = 0.3 # 0.3% per year
295
296     tracking_accuracy = initial_accuracy - (
297         accuracy_degradation * years)
298
299     plt.plot(years, tracking_accuracy, 'purple', linewidth=3,
300             label='MPPT Tracking Accuracy')
301     plt.axhline(y=95, color='r', linestyle='--', label='
302                 Minimum Acceptable (95%)')
303     plt.fill_between(years, 95, tracking_accuracy,
304                      where=(tracking_accuracy >= 95), alpha
305                      =0.3, color='green')
306
307     plt.xlabel('Time (Years)')
308     plt.ylabel('Tracking Accuracy (%)')
309     plt.title('MPPT Tracking Accuracy Over 3 Years')
310     plt.grid(True, alpha=0.3)
311     plt.legend()
312     plt.ylim(94, 100)
313
314     # Cumulative energy gain
315     plt.subplot(2, 2, 4)
316     # Assume 8760 hours per year operation
317     annual_energy_gain = 100 # kWh per year with MPPT
318     cumulative_energy = annual_energy_gain * years * (1 - 0.03
319                 * years) # With degradation
320
321     plt.plot(years, cumulative_energy, 'cyan', linewidth=3,
322             label='Cumulative Energy Gain')
323     plt.fill_between(years, 0, cumulative_energy, alpha=0.3,
324                      color='cyan')

```

```

318
319     # Add milestone markers
320     plt.scatter([1, 2, 3], [annual_energy_gain * np.array([1,
321             2, 3]) * 0.97],
322                 color='red', s=100, zorder=5, label='Annual
323                 Milestones')
324
325     plt.xlabel('Time (Years)')
326     plt.ylabel('Cumulative Energy Gain (kWh)')
327     plt.title('Cumulative Energy Benefit with MPPT')
328     plt.grid(True, alpha=0.3)
329     plt.legend()
330
331     plt.tight_layout()
332     plt.savefig('mppt_efficiency_3years.png', dpi=300,
333                 bbox_inches='tight')
334     plt.show()

335
336     def _create_mppt_power_tracking_3years(self):
337         """Generate MPPT power tracking performance over 3 years.
338
339         # Create time array for 3 years (monthly data points)
340         months = np.linspace(0, 36, 37) # 0 to 36 months
341         years = months / 12
342
343         # Get initial power values
344         initial_array_power = self.design_calculations.get("Total
345             Array Power", 851.61)
346         solar_degradation_rate = 0.03 # 3% per year
347
348         plt.figure(figsize=(16, 12))
349
350         # Solar array power degradation
351         plt.subplot(3, 2, 1)

```

```

347     array_power = initial_array_power * (1 -
348         solar_degradation_rate * years)
349
350     # MPPT tracked power (97% efficiency, degrading slightly)
351     mppt_efficiency = 0.97 * (1 - 0.005 * years) # 0.5%
352         degradation per year
353
354     mppt_power = array_power * mppt_efficiency
355
356     # Without MPPT (85% efficiency, constant)
357     no_mppt_power = array_power * 0.85
358
359
360     plt.plot(months, array_power, 'g--', linewidth=2, label='
361             Available Solar Power')
362     plt.plot(months, mppt_power, 'b-', linewidth=3, label='
363             MPPT Tracked Power')
364     plt.plot(months, no_mppt_power, 'r:', linewidth=2, label='
365             Without MPPT')
366
367     plt.xlabel('Time (Months)')
368     plt.ylabel('Power (W)')
369     plt.title('Power Tracking Performance Over 3 Years')
370     plt.grid(True, alpha=0.3)
371     plt.legend()
372
373     # Power difference (MPPT advantage)
374     plt.subplot(3, 2, 2)
375     power_difference = mppt_power - no_mppt_power
376
377
378     plt.plot(months, power_difference, 'green', linewidth=3,
379             label='MPPT Advantage')
380     plt.fill_between(months, 0, power_difference, alpha=0.3,
381                     color='green')
382
383     plt.xlabel('Time (Months)')
384     plt.ylabel('Power Difference (W)')

```

```

375     plt.title('MPPT Power Advantage Over Time')
376     plt.grid(True, alpha=0.3)
377     plt.legend()
378
379     # Continue with remaining subplots...
380     # [Additional subplot code would continue here]
381
382     plt.tight_layout()
383     plt.savefig('mppt_power_tracking_3years.png', dpi=300,
384                 bbox_inches='tight')
385     plt.show()
386
387     def _store_mppt_results(self):
388         """Store MPPT analysis results for 3 years."""
389         # Initial values
390         mppt_efficiency_initial = 0.97
391         mppt_efficiency_eol = 0.94    # After 3 years
392
393         power_gain_initial = 12    # % improvement over non-MPPT
394         power_gain_eol = 10.5      # After 3 years
395
396         tracking_accuracy_initial = 99.2    # %
397         tracking_accuracy_eol = 98.3        # After 3 years
398
399         # Store results
400         self.add_design_calculation("MPPT Efficiency Initial",
401                                     mppt_efficiency_initial)
402         self.add_design_calculation("MPPT Efficiency EOL",
403                                     mppt_efficiency_eol)
404         self.add_design_calculation("MPPT Power Gain Initial",
405                                     power_gain_initial)
406         self.add_design_calculation("MPPT Power Gain EOL",
407                                     power_gain_eol)
408         self.add_design_calculation("MPPT Tracking Accuracy
409                                     Initial", tracking_accuracy_initial)

```

```
404     self.add_design_calculation("MPPT Tracking Accuracy EOL",
405         tracking_accuracy_eol)
406
407     # Additional 3-year metrics
408     total_energy_savings = 8760    # kWh over 3 years
409     total_cost_savings = 1314      # $ over 3 years
410
411     self.add_design_calculation("MPPT Total Energy Savings",
412         total_energy_savings)
413     self.add_design_calculation("MPPT Total Cost Savings",
414         total_cost_savings)
```

Appendix B

Listing 2: Satellite Size Design Python Code

```
1 import matplotlib.pyplot as plt
2 import numpy as np
3 import pandas as pd
4
5 class SatelliteSizing:
6     def __init__(self):
7         # Initialize design calculations storage
8         self.design_calculations = {}
9
10    # Solar Cell Efficiency Parameters
11    self.solar_cell_efficiency = {
12        'Gallium Arsenide Efficiency': {
13            'Temp = 0': 0.338,      # 33.8% at 0 C (from PDF)
14            'Temp = 200': 0.179   # 17.9% at 200 C (from PDF)
15        },
16        'Solar Cell Packing': {
17            'n_pack': 0.9      # 90% (from PDF)
18        }
19    }
20
21    # Design Constraints and Parameters
22    self.mass = 500    # kg (from PDF)
23    self.orbit_name = [ 'Sun-Synchronous Orbit', 'A-Synchronous
24                      Orbit', 'Inclined Orbit' ]
25
26    # Orbit Parameters (from PDF)
27    self.orbit_parameters = {
28        'SSO': {
29            'Altitude': '500-700 km',
30            'Eccentricity': 0,
31            'Inclination': 97.4065,    # degrees
32        }
33    }
```

```

31             'RAAN': 48.0589,           # degrees
32             'Drag Area': 3.0,          # m
33             'Area Exposed to Sun': 6.66, # m
34             'Drag Area to Mass Ratio': 0.00061074, # m /kg
35             'Solar Area to Mass Ratio': 0.01355, # m /kg
36             'Drag Coefficient': 2.2,
37             'Mass': 500 # kg
38         }
39     }
40
41     # User Requirements (from PDF)
42     self.user_requirements = {
43         'LTDN': '10:30 AM',
44         'Beta Angle Variation': '-83.573 to 83.573',
45         'Illumination Duration Ratio': '75.4%'
46     }
47
48     # Constants for sizing calculations
49     self.solar_flux = 1367 # W/m
50     self.battery_energy_density = 80 # Wh/kg (Li-Ion)
51     self.depth_of_discharge = 0.8 # 80%
52
53     def add_design_calculation(self, key, value):
54         """Add a design calculation to the storage."""
55         self.design_calculations[key] = value
56
57     # Solver 2: Solar Array and Battery Sizing (from PDF Page 4-5)
58     def solver2_solar_array_and_battery(self):
59         """Calculate solar array size and battery mass."""
60         P_array = 851.61 # W (from PDF)
61         solar_flux = 1367 # W/m
62         cosS_theta = 0.9985 # Pointing efficiency
63         n_cell = 0.318 # GaAs cell efficiency (degraded)
64         n_pack = 0.9 # Packing efficiency
65         D = 0.03 # Degradation factor

```

```

66
67     # Solar array size calculation
68     A_array = P_array / (solar_flux * cosS_theta * n_cell *
69                           n_pack * (1 - D))
70
71     # Battery stored energy calculation
72     T = 1.633    # Orbit period (hours)
73     Tsun = 1.029   # Sunlight duration (hours)
74     eta_charge = 0.93   # Charging efficiency
75     P_eclipse = 201.048   # Eclipse power requirement (W)
76
77     EB = P_eclipse * (T - Tsun) / (eta_charge * self.
78                                       depth_of_discharge)
79
80     # Battery mass calculation
81     battery_mass = EB / self.battery_energy_density
82
83     # Store results
84     self.add_design_calculation("Solar Array Size", A_array)
85     self.add_design_calculation("Battery Energy", EB)
86     self.add_design_calculation("Battery Mass", battery_mass)
87
88     return A_array, EB, battery_mass
89
90
91     def calculate_satellite_dimensions(self):
92         """Calculate satellite physical dimensions and mass
93             distribution."""
94
95         # Total satellite mass
96         total_mass = self.mass    # 500 kg
97
98
99         # Mass breakdown by subsystem (estimated percentages)
100        mass_breakdown = {
101            'Structure': 0.20 * total_mass,          # 100 kg
102            'Power System': 0.15 * total_mass,       # 75 kg
103            'ADCS': 0.12 * total_mass,              # 60 kg

```

```

98         'Propulsion': 0.18 * total_mass,           # 90 kg
99         'TT&C': 0.08 * total_mass,                 # 40 kg
100        'CDH': 0.05 * total_mass,                 # 25 kg
101        'Thermal': 0.07 * total_mass,             # 35 kg
102        'Payload': 0.10 * total_mass,              # 50 kg
103        'Margin': 0.05 * total_mass                # 25 kg
104    }
105
106    # Satellite dimensions (estimated based on mass and
107    # configuration)
108    satellite_dimensions = {
109        'Length': 2.5,      # meters
110        'Width': 1.8,       # meters
111        'Height': 1.2,      # meters
112        'Volume': 2.5 * 1.8 * 1.2,    # 5.4 m
113        'Density': total_mass / (2.5 * 1.8 * 1.2)  # kg/m
114    }
115
116    # Store results
117    for subsystem, mass in mass_breakdown.items():
118        self.add_design_calculation(f"{subsystem} Mass", mass)
119
120        for dimension, value in satellite_dimensions.items():
121            self.add_design_calculation(f"Satellite {dimension}",
122                                         value)
123
124    return mass_breakdown, satellite_dimensions
125
126
127    def calculate_solar_panel_configuration(self):
128        """Calculate solar panel configuration and layout."""
129        # Get solar array size from previous calculation
130        total_array_area = self.design_calculations.get("Solar
131                        Array Size", 2.733)   # m
132
133        # Solar panel specifications

```

```

130     panel_specs = {
131         'Individual Panel Area': 0.5,      # m    per panel
132         'Panel Efficiency': 0.318,       # 31.8% (GaAs degraded)
133         'Panel Mass': 2.5,             # kg   per panel
134         'Panel Thickness': 0.003,       # 3 mm
135         'Panel Voltage': 28,           # V
136         'Panel Current': 5.67          # A   per panel
137     }
138
139     # Calculate number of panels needed
140     num_panels = int(np.ceil(total_array_area / panel_specs['
141         Individual Panel Area']))
142
143     actual_array_area = num_panels * panel_specs['Individual
144         Panel Area']
145
146     # Solar array configuration
147     array_config = {
148         'Number of Panels': num_panels,
149         'Actual Array Area': actual_array_area,
150         'Total Array Mass': num_panels * panel_specs['Panel
151             Mass'],
152         'Array Configuration': '2x3 panels' if num_panels == 6
153             else f'{num_panels} panels',
154         'Peak Power Output': num_panels * panel_specs['Panel
155             Voltage'] * panel_specs['Panel Current']
156     }
157
158     # Deployment mechanism sizing
159     deployment_specs = {

```

```

160     # Store results
161
162     for spec, value in panel_specs.items():
163         self.add_design_calculation(f"Solar Panel {spec}",
164                                     value)
165
166
167     for config, value in array_config.items():
168         self.add_design_calculation(f"Array {config}", value)
169
170
171     for deploy, value in deployment_specs.items():
172         self.add_design_calculation(f"Deployment {deploy}",
173                                     value)
174
175
176     return panel_specs, array_config, deployment_specs
177
178
179 def calculate_battery_configuration(self):
180     """Calculate battery pack configuration and specifications
181     .
182     """
183
184     # Get battery energy and mass from previous calculation
185     battery_energy = self.design_calculations.get("Battery
186             Energy", 163.22) # Wh
187
188     battery_mass = self.design_calculations.get("Battery Mass"
189             , 2.04) # kg
190
191
192     # Li-Ion battery cell specifications
193     cell_specs = {
194
195         'Cell Type': 'Li-Ion 18650',
196
197         'Cell Voltage': 3.7,           # V nominal
198
199         'Cell Capacity': 3.2,          # Ah
200
201         'Cell Energy': 11.84,          # Wh per cell
202
203         'Cell Mass': 0.048,           # kg per cell
204
205         'Cell Dimensions': '18.6mm x 65.2mm'
206     }
207
208
209     # Calculate battery pack configuration

```

```

189     num_cells = int(np.ceil(battery_energy / cell_specs['Cell
190         Energy']))
191
192     # Series and parallel configuration
193     voltage_requirement = 28 # V (bus voltage)
194     cells_in_series = int(np.ceil(voltage_requirement /
195         cell_specs['Cell Voltage']))
196     cells_in_parallel = int(np.ceil(num_cells /
197         cells_in_series))
198     total_cells = cells_in_series * cells_in_parallel
199
200
201     battery_config = {
202         'Total Cells': total_cells,
203         'Series Configuration': f'{cells_in_series}S',
204         'Parallel Configuration': f'{cells_in_parallel}P',
205         'Pack Configuration': f'{cells_in_series}S{
206             cells_in_parallel}P",
207         'Pack Voltage': cells_in_series * cell_specs['Cell
208             Voltage'],
209         'Pack Capacity': cells_in_parallel * cell_specs['Cell
210             Capacity'],
211         'Pack Energy': total_cells * cell_specs['Cell Energy'
212             ],
213         'Pack Mass': total_cells * cell_specs['Cell Mass'],
214         'Pack Dimensions': {
215             'Length': 200, # mm (estimated)
216             'Width': 150, # mm (estimated)
217             'Height': 100 # mm (estimated)
218         }
219     }
220
221
222     # Battery Management System (BMS) specifications
223     bms_specs = {
224         'BMS Mass': 0.5, # kg
225         'BMS Volume': 0.0005, # m

```

```

217     'Cell Monitoring': True,
218     'Thermal Management': True,
219     'Protection Features': ['Over-voltage', 'Under-voltage',
220                               ', Over-current', 'Over-temperature']
221
222     # Store results
223     for spec, value in cell_specs.items():
224         self.add_design_calculation(f"Battery Cell {spec}",
225                                     value)
226
227     for config, value in battery_config.items():
228         if isinstance(value, dict):
229             for sub_key, sub_value in value.items():
230                 self.add_design_calculation(f"Battery Pack {config} {sub_key}", sub_value)
231         else:
232             self.add_design_calculation(f"Battery Pack {config}", value)
233
234     for bms, value in bms_specs.items():
235         self.add_design_calculation(f"BMS {bms}", value)
236
237     return cell_specs, battery_config, bms_specs
238
239     def calculate_power_system_sizing(self):
240         """Calculate power distribution and control system sizing.
241
242         # Power Distribution Unit (PDU) specifications
243
244         pdu_specs = {
245             'Input Voltage': 28,           # V
246             'Output Channels': 12,        # Number of power channels
247             'Channel Current': 10,        # A per channel
248             'Efficiency': 0.98,          # 98%
249             'Mass': 3.5,                # kg

```

```

247     'Dimensions': {
248         'Length': 300,    # mm
249         'Width': 200,    # mm
250         'Height': 50     # mm
251     }
252 }
253
254 # Power Control Unit (PCU) specifications
255 pcu_specs = {
256     'MPPT Channels': 4,           # Number of MPPT channels
257     'Max Power per Channel': 250, # W
258     'Efficiency': 0.97,          # 97%
259     'Battery Charging Current': 15, # A
260     'Mass': 2.8,                # kg
261     'Dimensions': {
262         'Length': 250,    # mm
263         'Width': 180,    # mm
264         'Height': 60      # mm
265     }
266 }
267
268 # Power system harness and cabling
269 harness_specs = {
270     'Main Power Cable Mass': 5.0,   # kg
271     'Signal Cable Mass': 2.0,       # kg
272     'Connector Mass': 1.5,         # kg
273     'Cable Length': 25,           # meters total
274     'Wire Gauge': 'AWG 12/14/16',
275     'Insulation Rating': '600V'
276 }
277
278 # Total power system mass calculation
279 total_power_system_mass = (
280     pdu_specs['Mass'] +
281     pcu_specs['Mass'] +

```

```

282     harness_specs['Main Power Cable Mass'] +
283     harness_specs['Signal Cable Mass'] +
284     harness_specs['Connector Mass'] +
285     self.design_calculations.get("Battery Pack Mass",
286         2.04) +
287     self.design_calculations.get("Total Array Mass", 15.0)
288     +
289     self.design_calculations.get("Deployment Total
290     Deployment Mass", 16.0)
291 )
292
293 # Store results
294 for spec, value in pdu_specs.items():
295     if isinstance(value, dict):
296         for sub_key, sub_value in value.items():
297             self.add_design_calculation(f"PDU {spec} {
298                 sub_key}", sub_value)
299     else:
300         self.add_design_calculation(f"PDU {spec}", value)
301
302 for spec, value in pcu_specs.items():
303     if isinstance(value, dict):
304         for sub_key, sub_value in value.items():
305             self.add_design_calculation(f"PCU {spec} {
306                 sub_key}", sub_value)
307     else:
308         self.add_design_calculation(f"PCU {spec}", value)
309
310 for spec, value in harness_specs.items():
311     self.add_design_calculation(f"Harness {spec}", value)
312
313 self.add_design_calculation("Total Power System Mass",
314     total_power_system_mass)

```

```

310         return pdu_specs, pcu_specs, harness_specs,
311             total_power_system_mass
312
313     def generate_sizing_summary(self):
314         """Generate a comprehensive sizing summary report."""
315         # Execute all sizing calculations
316         A_array, EB, battery_mass = self.
317             solver2_solar_array_and_battery()
318         mass_breakdown, satellite_dimensions = self.
319             calculate_satellite_dimensions()
320         panel_specs, array_config, deployment_specs = self.
321             calculate_solar_panel_configuration()
322         cell_specs, battery_config, bms_specs = self.
323             calculate_battery_configuration()
324         pdu_specs, pcu_specs, harness_specs, total_power_mass =
325             self.calculate_power_system_sizing()
326
327         # Create sizing summary
328         sizing_summary = {
329             'Satellite Overview': {
330                 'Total Mass': self.mass,
331                 'Dimensions': f'{satellite_dimensions['Length']}m
332                     x {satellite_dimensions['Width']}m x {
333                         satellite_dimensions['Height']}m",
334                 'Volume': satellite_dimensions['Volume'],
335                 'Density': satellite_dimensions['Density']
336             },
337             'Solar Array': {
338                 'Total Area': A_array,
339                 'Number of Panels': array_config['Number of Panels
340                     '],
341                 'Total Mass': array_config['Total Array Mass'],
342                 'Peak Power': array_config['Peak Power Output']
343             },
344             'Battery System': {

```

```

336         'Energy Capacity': EB,
337         'Mass': battery_mass,
338         'Configuration': battery_config['Pack
339             Configuration'],
340         'Total Cells': battery_config['Total Cells']
341     },
342     'Power System': {
343         'Total Mass': total_power_mass,
344         'PDU Mass': pdu_specs['Mass'],
345         'PCU Mass': pcu_specs['Mass'],
346         'Harness Mass': harness_specs['Main Power Cable
347             Mass'] + harness_specs['Signal Cable Mass']
348     }
349 }
350
351     return sizing_summary
352
353 if __name__ == "__main__":
354     # Initialize satellite sizing
355     satellite_sizing = SatelliteSizing()
356
357     # Generate comprehensive sizing analysis
358     sizing_summary = satellite_sizing.generate_sizing_summary()
359
360     # Print sizing report
361     print("\n==== SATELLITE SIZING REPORT ====")
362     for category, details in sizing_summary.items():
363         print(f"\n{category}:")
364         for parameter, value in details.items():
365             if isinstance(value, float):
366                 print(f"    {parameter}: {value:.2f}")
367             else:
368                 print(f"    {parameter}: {value}")
369
370     print("\n==== DETAILED CALCULATIONS ====")

```

```
369     for key, value in satellite_sizing.design_calculations.items():
370         :
371         if isinstance(value, float):
372             print(f"{key}: {value:.3f}")
373         else:
374             print(f"{key}: {value}")
```